



Marco Antonio Guimarães Auad Barroca

**Computational perspectives on anyon
interferometry**

Dissertação de Mestrado

Dissertation presented to the Programa de Pós-graduação em Física da PUC-Rio in partial fulfillment of the requirements for the degree of Mestre em Física.

Advisor: Prof. Thiago Barbosa dos Santos Guerreiro

Rio de Janeiro
May 2020



Marco Antonio Guimarães Auad Barroca

**Computational perspectives on anyon
interferometry**

Dissertation presented to the Programa de Pós-graduação em Física da PUC-Rio in partial fulfillment of the requirements for the degree of Mestre em Física. Approved by the Examination Committee.

Prof. Thiago Barbosa dos Santos Guerreiro

Advisor

Departamento de Física – PUC-Rio

Prof. George Svetlichny

Departamento de Matemática – PUC-Rio

Prof. Guilherme Penello Temporão

Departamento de Engenharia Elétrica – PUC-Rio

Prof. Lucianno Augusto Coddato Antunes e Defaveri

Departamento de Física – PUC-Rio

Rio de Janeiro, May 8th, 2020

All rights reserved.

Marco Antonio Guimarães Auad Barroca

The author graduated in Physics from PUC-Rio (Pontifícia Universidade Católica do Rio de Janeiro) in 2017. Developed research on the fields of non-equilibrium physics and statistical physics during the undergraduate course at PUC-Rio. Participated in international schools for astronomy and quantum information ministered by CBPF (Centro Brasileiro de Pesquisas Físicas) and UFF (Universidade Federal Fluminense) respectively.

Bibliographic data

Barroca, Marco Antonio Guimarães Auad

Computational perspectives on anyon interferometry / Marco Antonio Guimarães Auad Barroca; advisor: Thiago Barbosa dos Santos Guerreiro. – Rio de Janeiro: PUC-Rio, Departamento de Física, 2020.

v., 103 f: il. color. ; 30 cm

Dissertação (mestrado) - Pontifícia Universidade Católica do Rio de Janeiro, Departamento de Física.

Inclui bibliografia

1. Física – Teses. 2. Anyon;. 3. Interferometria;. 4. Topologia;. 5. Computação Quântica;. 6. Metrologia Quântica.. I. Guerreiro, Thiago Barbosa dos Santos. II. Pontifícia Universidade Católica do Rio de Janeiro. Departamento de Física. III. Título.

CDD: 530

To my parents, for their support
and encouragement.

Acknowledgments

To my advisor Professor Thiago Guerreiro for the stimulus and partnership to carry out this work.

To Allan Tosta, Ernesto Galvão and Daniel Brod for the important discussions and collaboration on fermionic and bosonic anyons.

To CAPES and PUC-Rio, for the aids granted, without which this work would not have been accomplished.

This study was financed in part by the Coordenação de Aperfeiçoamento de Pessoal de Nível Superior - Brasil (CAPES) - Finance Code 001.

Abstract

Barroca, Marco Antonio Guimarães Auad; Guerreiro, Thiago Barbosa dos Santos (Advisor). **Computational perspectives on anyon interferometry**. Rio de Janeiro, 2020. 103p. Dissertação de Mestrado – Departamento de Física, Pontifícia Universidade Católica do Rio de Janeiro.

Interferometry has been used to study a variety of physical effects, from the early experiments of Michelson and Morley that provided evidence to special relativity to the more recent gravity-wave detection devices used by the Laser Interferometer Gravitational-Wave Observatory (LIGO) experiment. The purpose of this thesis is to understand how one can exploit anyons and its unique characteristics to build interferometers, and understand whether there are immediate advantages in doing so. Anyons are two-dimensional quasiparticles known for their unusual fractional statistics and applications in quantum computing models. To study their usefulness in the context of interferometry, we present a quantum computational approach to interference experiments. Next we give an introduction to anyon models and how they can be used to perform universal quantum computing. We propose a quantum circuit which implements a certain type of interferometer, and how it can be realized in different anyon models. Finally, we discuss a quantum computing model based on linear optics with fermionic anyons that would enable the creation of a logical version of our interferometer in terms of a physical interferometer.

Keywords

Anyon; Interferometry; Topology; Quantum Computation; Quantum Metrology.

Resumo

Barroca, Marco Antonio Guimarães Auad; Guerreiro, Thiago Barbosa dos Santos. **Perspectivas computacionais em interferometria de anyons**. Rio de Janeiro, 2020. 103p. Dissertação de Mestrado – Departamento de Física, Pontifícia Universidade Católica do Rio de Janeiro.

Interferometria tem sido utilizada para estudar uma variedade de efeitos físicos, desde os experimentos iniciais de Michelson e Morley que forneceram evidências para a teoria da relatividade restrita até os aparelhos de detecção de ondas gravitacionais utilizado no Laser Interferometer Gravitational-Wave Observatory (LIGO). O Propósito dessa dissertação é entender como explorar anyons e suas características únicas para construir interferômetros. Anyons são quasipartículas bi-dimensionais conhecidas por apresentarem estatística fracionária e possuem aplicações em modelos de computação quântica. Para estudar sua utilidade no contexto de interferometria nós apresentamos uma perspectiva de computação quântica para experimentos de interferência. Em seguida, introduzimos modelos anyônicos e suas aplicações em computação quântica universal. Propomos um circuito quântico que implementa um certo tipo de interferômetro, e como realizá-lo em diferentes modelos anyônicos. Finalmente, discutimos um modelo de computação quântica baseado em ótica linear de anyons fermiônicos que permitiria a criação de uma versão lógica do nosso interferômetro em termos de um interferômetro físico.

Palavras-chave

Anyon; Interferometria; Topologia; Computação Quântica; Metrologia Quântica.

Table of contents

1	Introduction	15
2	Interferometry and Quantum Information	18
2.1	Bosons	18
2.2	Fermions	28
2.3	The circuit approach	34
3	Anyons and quantum computers	45
3.1	Abelian Anyons	47
3.2	Non-Abelian Anyons	53
3.3	Computation and Fibonacci Anyons	58
4	Anyon interferometry	67
4.1	Linear optics and operator representation	67
4.2	Linear optics for fermionic anyons	68
4.3	Bosonic anyons and the Hong-Ou-Mandel Effect	71
4.4	Computing with fermionic anyons	74
4.5	NOON-like interferometer	78
5	Conclusions and future work	90
6	References	92
7	Appendix A: Code used to implement quantum circuits	96

List of figures

Figure 2.1	Schematic of an MZI. The beam comes from a source and enters the first beamsplitter (BS), the split beams are reflected by mirrors on each arm. Finally they go through the second BS and head to the detectors.	19
Figure 2.2	Diagram summing the probability amplitudes for the Hong-Ou Mandel Effect. Note that reflections give a relative phase.	21
Figure 2.3	General diagram of preparing a NOON state. We unitarily transform N single particle states to an entangled state, apply a phase θ , and make a measurement which collapses the wave-function to one of the detectors	23
Figure 2.4	Phasor diagram for coherent, NOON and classical states.	25
Figure 2.5	Ramsey interferometer for a 2-level system. Each $\pi/2$ pulse creates excited states $ e\rangle$ from the ground state $ g\rangle$. In the picture no interference pattern is formed as all output states are excited.	29
Figure 2.6	Diagram comparing Ramsey interferometry on the Bloch sphere with the MZI. The two arms on the MZI are analogous to the excited and ground states on the Ramsey interferometer. The highlighted area represents a squeezed state, just as in the MZI one can work with squeezed states to reduce the variance for the relevant quantities.	30
Figure 2.7	Diagram for a Non-local interferometer. Four beams from four different sources travel through two of the four beamsplitters before reaching the detectors. They pick up a phase in two of the four arms.	31
Figure 2.8	Plot of probability as function of phase for a two particle input in a Non-Local interferometer.	33
Figure 2.9	The CNOT gate. It takes two qubits, a target and a control and executes the above operation on the computational basis $ 00\rangle, 01\rangle, 10\rangle$ and $ 11\rangle$. On the table the second qubit is the target and the first is the control.	34
Figure 2.10	Representation of a Hadamard gate on state $ 0\rangle$	35
Figure 2.11	Quantum circuit implementing a logical beamsplitter.	35
Figure 2.12	Quantum circuit implementing a NOON-like interferometer. The phase shift gate simply adds a phase θ to the state $ 1\rangle$. At the end we have a detector for each qubit. In quantum circuit notation these are normally replaced by measurement operators.	36
Figure 2.13	Both pictures taken from the IBM website [22] (a) Layout of the chip (b) Topology of the chip. Each circle represents a qubit. A line connecting them tells that we can apply two qubit operations directly on both of them.	38
(a)		38
(b)		38
Figure 2.14	Mapping of the qubits on the chip topology. Our virtual qubit 0 was mapped to the chip's physical qubit 2, while the rest were distributed among the other physical qubits. Each circle represents a qubit. A line connecting them, tells that we can directly apply two-qubit operations on them.	39

Figure 2.15	Both pictures plotted on Qiskit. (a) Another circuit based on our NOON-like interferometer but now the CNOTs are cascaded. (b) Circuit that corresponds to the NOON-like interferometer. In both figures $\theta = \pi/10$ and $N = 5$. N classical bits are also created alongside the qubits for the measurements to be recorded on.	40
(a)		40
(b)		40
Figure 2.16	Simulated, experimental and theoretical results of the circuit for two qubits. Probabilities are calculated for one period in steps of $\pi/8$ for θ . Simulated results are given by the QASM Simulator on a classical computer and experimental results are given by the IBM Q 5 Yorktown.	41
Figure 2.17	Simulated, experimental and theoretical results of the circuit for three qubits. Probabilities are calculated for one period in steps of $\pi/12$ for θ . Simulated results are given by the QASM Simulator on a classical computer and experimental results are given by the IBM Q 5 Yorktown.	41
Figure 2.18	Simulated, experimental and theoretical results of the circuit for five qubits. Probabilities are calculated for one period in steps of $\pi/20$ for θ . Simulated results are given by the QASM Simulator on a classical computer and experimental results are given by the IBM Q 5 Yorktown.	42
Figure 2.19	Simulated, measured and mitigated results of the circuit for three qubits and $\theta = \pi/12$. Mitigating the measurement errors gives us no gain.	43
Figure 3.1	Diagram illustrating the 2D Aharonov-Bohm Effect in the unbound and bound cases. The particle follows the red path in the direction of the arrow around a solenoid represented by the cylinder. In both cases the topological phase is the same. It is independent of the path taken.	46
Figure 3.2	Braiding group element. Each colored dot represents a particle. Counterclockwise exchange of the blue and red particles.	49
Figure 3.3	A braiding can be deformed and still be the same element. While braiding (a) and (b) are the same, braiding (c) is another element altogether	49
Figure 3.4	Concatenating braids. Braiding (d) is done by concatenating (c), (b) and (a) in that order	50
Figure 3.5	Yang-Baxter relation. (a) and (b) are the group generators σ_1 and σ_2 respectively. (c) is a graphical representation of the relation $\sigma_1\sigma_2\sigma_1 = \sigma_2\sigma_1\sigma_2$	52

- Figure 3.6 Figure and values taken from Bonesteel et al. [30]. (a) A braiding that injects one anyon from one qubit into another qubit. It approximates the identity to a distance of $\epsilon = 1.5 \times 10^{-3}$. The products of σ_1 and σ_2 represent the correspondent unitary operation and are products of matrices R and $F^{-1}RF$ respectively in accordance to equation (3-43). (b) A braiding that approximates a NOT gate with error distance $\epsilon = 8.5 \times 10^{-4}$. (c) A braiding that approximates a CNOT gate utilizing braidings a and b. First it injects two particles from the control qubit into the target, then it executes a NOT-gate and finally it ejects the particles back to the control qubit. The errors distance from a real CNOT-gate are $\epsilon = 1.8 \times 10^{-3}$ and $\epsilon = 1.2 \times 10^{-3}$ when the total label of the six anyon system is 1 or γ , respectively. it is important to note that one could reduce the error distances even further by utilizing the Solovay-Kitaev algorithm on braidings (a) and (b). 65
- Figure 3.7 Braiding that approximates a Hadamard gate with error distance of $\epsilon = 3 \times 10^{-3}$. σ_1 and σ_2 are the braiding matrices for our model shown previously. Braiding and values taken from Field et al.[34] 65
- Figure 4.1 General unitary one-qubit gate built from phase-shifters and beamsplitters on the fermionic anyons computational model. On the left we have the two modes that anyons can occupy and on the right the qubit $|\psi\rangle$ before and after general unitary U . The parameters α , β , γ and δ can be chosen so as to create a general unitary. 76
- Figure 4.2 Unitary 2-qubit gate built from beamsplitters on the fermionic anyons computational model. On the left we have the four modes that anyons can occupy, which is equivalent to two qubits. 77
- Figure 4.3 New beamsplitter $LBS(\theta)$ for N qubits with $C^2(\theta)$ taking the place of the CNOTs and the Hadamard in a different qubit. 80
- Figure 4.4 This figure summarizes the argument we used to generalize the action of $LBS(\pi/2)$ on the basis states for N qubits. We begin with an arbitrary state filled randomly with 1s and 0s and execute the operations to recreate the $LBS(\pi/2)$. Equations (4-53) tell us how to use $C^2(\pi/2)$ and the action of the Hadamard was explained on section 2.3. The states depicted are just for illustration purposes. 83
- Figure 4.5 New interferometer for N qubits and phase ϕ . $C^2(\pi/2)$ takes the place of the CNOTs. N classical bits are also generated to record the measurements at the end. 84
- Figure 4.6 Simulated, experimental and theoretical results of the new circuit for two qubits. Probabilities are calculated for one period in steps of $\pi/8$ for θ . 86
- Figure 4.7 Simulated, experimental and theoretical results of the new circuit for three qubits. Probabilities are calculated for one period in steps of $\pi/12$ for θ . 86
- Figure 4.8 Simulated, experimental and theoretical results of the new circuit for five qubits. Probabilities are calculated for one period in steps of $\pi/20$ for θ . 87
- Figure 4.9 The gates used in our NOON-like interferometer for two qubits written in terms of beamsplitters and phase-shifters. We assign colors to each setup in order to be more compact. 88

Figure 4.10 The NOON-like interferometer for two qubits written in terms of beamsplitters and phase-shifters using the previously defined color code. Note the detectors at the end to act as measurements.

89

List of symbols

MZI – Mach-Zender Interferometer

BS – Beamsplitter

LIGO – Laser Interferometer Gravitational-wave observatory

RI – Ramsey Interferometer

HBTI – Hanbury Brown-Twiss Interferometer

LBS – Logical Beamsplitter

There is no such thing as a new idea. It is impossible. We simply take a lot of old ideas and put them into a sort of mental kaleidoscope.

Mark Twain, *Mark Twain's Own Autobiography: The Chapters from the North American Review.*

1

Introduction

Interferometry has cemented itself in modern physics as one of the most important methods of acquiring information from optical setups. It has left its mark in history by confirming special relativity with the fabled "failed experiment" of Michelson and Morley [1] and continues to have relevance to this day, being utilized by the Laser Interferometer Gravitational-wave Observatory (LIGO) to search for evidences of gravitational waves predicted by General Relativity [2].

The idea behind such experiments is that a phenomenon that is of interest causes a phase shift between beams of photons, atoms or even electrons, which in turn will lead to an interference pattern being formed. This pattern can then be detected and analyzed to better understand the original phenomenon. It is especially useful in cases where we are searching for minuscule effects that can be amplified by studying the interference pattern. The LIGO experiment is one of such cases.

The LIGO experiment plays an important role because it is the first one to reach the famous *standard quantum limit*. The phase difference ϕ it detects between the interferometer arms is affected by the uncertainty $\Delta\phi \propto 1/\sqrt{\langle N \rangle}$ where $\langle N \rangle$ is the mean number of photons in the interferometer. This is known as the *shot noise* and is the dominant source of noise for experiments in gravitational wave detection [2].

Fortunately, the shot noise is not a lower bound for interferometry. By exploiting squeezed states one can theoretically reach a scaling of $1/\langle N \rangle$ while increasing the uncertainty ΔN , which is known as the Heisenberg limit. There have been a number of attempts to create setups that can reach such limit the most common of which utilize the concept of NOON states [3]. Unfortunately this becomes non-trivial for high number of photons.

Enter anyons, differently from photons which are by definition bosons (particles with integer spin), these 2D quasi-particles have *fractional spin*. The immediate consequence of this is that particle exchange will produce an arbitrary complex phase in the system's wave-function whereas with the exchange of photons the wave-function would not change at all. In more extreme cases anyons can even execute non-trivial unitary operations on the wave-function [4].

In this thesis we seek to understand if there are any benefits that can be gained from using these fractional spin particles for interferometry. Ideally we

want to create a setup for anyons that is capable of reaching the Heisenberg limit.

To do so we take a different approach to interferometry and present it as a program on a quantum computer. As anyons have remarkable applications in quantum information [5], if we have a computer model that relies on anyons for its operation we are able to reproduce our program on it and consequently create an anyon interferometer.

This approach pays off because it allowed us to create a NOON-like interferometer that is scalable and capable of creating GHZ states, which means we can increase the number of particles/qubits by increasing the size of the setup and the amount of operations. It also gives us the opportunity to execute it on any universal quantum computer which we are able to do thanks to IBM's Qiskit software development kit and quantum computers available for public use.

By looking at quantum computer models involving anyons we encountered two optimal candidates to implement our interferometer. The first one describes the simplest universal quantum computer involving anyons known as Fibonacci anyons [6]. The second one uses fermionic anyon linear optics to perform universal quantum computation. This model is particularly interesting because it relies only on linear optical elements, such as beamsplitters and phase-shifters [7]. This way we can build a physical interferometer capable of doing NOON-like interferometry in the logical space. We then exhibit our NOON-like interferometer in both models.

This document is structured as follows:

In Chapter 2 we present a review on interferometry and how particle statistics, bosonic or fermionic, can affect the results helping us define an optimal setup to work on. We introduce concepts and tools that help us analyze interferometry setups such as phase resolution, NOON states and, the Heisenberg limit and the Jordan-Schwinger map. Finally, we present an approach to interferometry in the context of quantum information and a NOON-like interferometer that can be reproduced in any quantum computer. We also analyze this interferometer on real quantum devices with the help of the Qiskit software development kit and IBM's quantum computers.

In Chapter 3 we present a review on anyons in a context that is relevant to quantum information. We go through the differences between abelian and non-abelian anyon models, how to define an anyon model and present a simple model that has direct applications in quantum information, Fibonacci anyons. Ultimately we present our NOON-like interferometer for Fibonacci anyons.

Chapter 4 unites the topics discussed previously and presents a new

computational model based on linear optics for fermionic anyons created by Tosta et al. [7]. We use it to suggest a new NOON-like interferometer in a setup that relies only on anyonic beamsplitters and phase-shifters. To demonstrate the effectiveness of this new interferometer we implement it on IBM's quantum computer with the help of Qiskit as was done on Chapter 2.

Finally, in Chapter 5 we review the thesis, present our conclusions and discuss possible future work related to the interferometer here presented.

2

Interferometry and Quantum Information

In this chapter we discuss interferometry phenomena for general particle statistics, in particular bosonic and fermionic. We deal with different quantum states in the photon number basis and present a quantum circuit approach that illustrates some of the ideas we will discuss throughout the thesis.

2.1

Bosons

Bosonic statistics can be grasped by looking at the commutation relations between creation and annihilation operators of a boson field:

$$[a_i^\dagger, a_j^\dagger] = [a_i, a_j] = 0 \quad (2-1a)$$

$$[a_i, a_j^\dagger] = a_i a_j^\dagger - a_j^\dagger a_i = \delta_{ij}, \quad (2-1b)$$

where i and j represent different modes of the field and δ_{ij} is the Kronecker-delta [8]. From these relations one can see that there are no restrictions as to how many particles one can have in the same quantum state and that Bosons are symmetric under exchange of particles. This means that if we exchange two bosons the total system wave-funtion acquires phase $+1$. We will soon see how this can affect interferometry.

2.1.1

Mach-Zehnder Interferometer

The Mach-Zehnder interferometer (MZI) is an apparatus first proposed by Ludwig Mach and Ludwig Zehnder for the purpose of measuring relative phase shifts between two beams of light originating from a common source [9]. It has the following protocol: The beam enters the first beamsplitter (BS), the outputs are then reflected by mirrors on each arm, which finally go through a second BS reaching two detectors. The beamsplitter is a device that will split the beam of light into two different paths. We can see a diagram of it on figure 2.1.

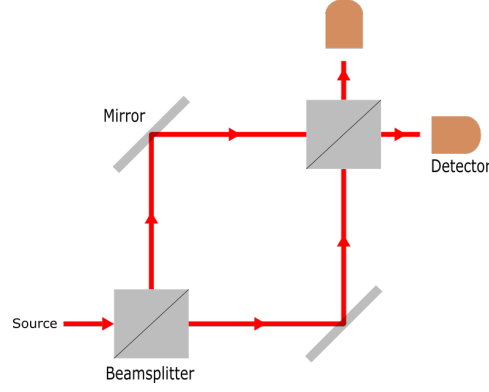


Figure 2.1: Schematic of an MZI. The beam comes from a source and enters the first beamsplitter (BS), the split beams are reflected by mirrors on each arm. Finally they go through the second BS and head to the detectors.

It is interesting to consider the action of the MZI in a one-particle wave function; for that we need to understand how the BS acts on one-particle states.

Upon entering the first BS, disregarding any losses, the creation operators in modes i and j transform according to:

$$a_i^\dagger \rightarrow \sqrt{T}a_i^\dagger + i\sqrt{1-T}a_j^\dagger \quad (2-2a)$$

$$a_j^\dagger \rightarrow \sqrt{T}a_j^\dagger + i\sqrt{1-T}a_i^\dagger. \quad (2-2b)$$

Taking the complex conjugate of the above gives us the annihilation operators:

$$a_i \rightarrow \sqrt{T}a_i - i\sqrt{1-T}a_j \quad (2-3a)$$

$$a_j \rightarrow \sqrt{T}a_j - i\sqrt{1-T}a_i, \quad (2-3b)$$

where T is the transmission coefficient of the BS and $1 - T = R$ the reflection coefficient.

A single particle state ($|1\rangle|0\rangle = a_i^\dagger|0\rangle|0\rangle$ in mode i or $|0\rangle|1\rangle = a_j^\dagger|0\rangle|0\rangle$ in mode j) would then be transformed as:

$$|1\rangle|0\rangle \rightarrow \sqrt{T}|1\rangle|0\rangle + i\sqrt{1-T}|0\rangle|1\rangle \quad (2-4a)$$

$$|0\rangle|1\rangle \rightarrow \sqrt{T}|0\rangle|1\rangle + i\sqrt{1-T}|1\rangle|0\rangle. \quad (2-4b)$$

The interferometer is composed of two BSs, meaning that the operation described previously will occur twice. Directly applying two BSs for a single

particle state results in:

$$|1\rangle|0\rangle \rightarrow \sqrt{T}|1\rangle|0\rangle + i\sqrt{1-T}|0\rangle|1\rangle \rightarrow (2T-1)|1\rangle|0\rangle + 2i\sqrt{T-T^2}|0\rangle|1\rangle \quad (2-5a)$$

$$|0\rangle|1\rangle \rightarrow \sqrt{T}|0\rangle|1\rangle + i\sqrt{1-T}|1\rangle|0\rangle \rightarrow 2i\sqrt{T-T^2}|1\rangle|0\rangle + (2T-1)|0\rangle|1\rangle. \quad (2-5b)$$

Note that for $T = 1/2$ we have $|0\rangle|1\rangle \rightarrow |1\rangle|0\rangle$.

We can add a relative phase $e^{i\theta}$ between the interferometer arms so that an interference pattern appears. Normally this phase would be physically created by an effect we are interested in studying with the device as we will soon mention.

With a relative phase the equation above becomes

$$|1\rangle|0\rangle \rightarrow \sqrt{T}|1\rangle|0\rangle + ie^{i\theta}\sqrt{1-T}|0\rangle|1\rangle \rightarrow \quad (2-6a)$$

$$\rightarrow (T(1+e^{i\theta})-e^{i\theta})|1\rangle|0\rangle + i\sqrt{T-T^2}(1+e^{i\theta})|0\rangle|1\rangle$$

$$|0\rangle|1\rangle \rightarrow \sqrt{T}|0\rangle|1\rangle + ie^{i\theta}\sqrt{1-T}|1\rangle|0\rangle \rightarrow \quad (2-6b)$$

$$\rightarrow i\sqrt{T-T^2}(1+e^{i\theta})|1\rangle|0\rangle + (T(1+e^{i\theta})-e^{i\theta})|0\rangle|1\rangle.$$

For $T = 1/2$ the probabilities of detection for input $|1\rangle|0\rangle$ are given by:

$$P(1,0) = \left|\frac{1}{2}(1-e^{i\theta})\right|^2 = \frac{1}{2}(1-\cos\theta), \quad (2-7a)$$

$$P(0,1) = \left|\frac{1}{2}i(1+e^{i\theta})\right|^2 = \frac{1}{2}(1+\cos\theta). \quad (2-7b)$$

We can also extended this to two-particle states such as $|1\rangle|1\rangle$ with each boson sent to a different input and analyse the effects of a MZI on it. After going through the first BS:

$$|1\rangle|1\rangle \rightarrow i\sqrt{T}\sqrt{1-T}|2\rangle|0\rangle + i\sqrt{T}\sqrt{1-T}|0\rangle|2\rangle + T|1\rangle|1\rangle - (1-T)|1\rangle|1\rangle. \quad (2-8)$$

Note that the state $|1\rangle|1\rangle$ cancels for $T = 1/2$ due to equations (2-1a) and (2-1b); this is the Hong-Ou-Mandel Effect first presented in 1987 [10]. Every time a boson goes through a BS it has two possible outcomes, either reflection (R) or transmission (T). When two bosons are input in each port of a BS logically there are now four possible outcomes TT, RR, TR, RT. The final state is given by the sum of probability amplitudes for all four possibilities with the condition that reflection gives a relative phase of $\pi/2$, as can be seen on figure 2.2.

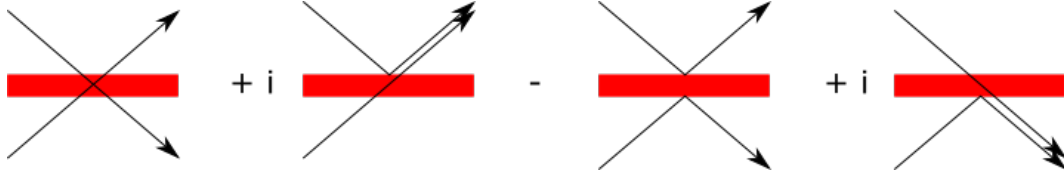


Figure 2.2: Diagram summing the probability amplitudes for the Hong-Ou Mandel Effect. Note that reflections give a relative phase.

This is an example of boson "bunching", identical bosons must have symmetric wave functions. Soon we will see how that contrasts with different statistics, such as the fermionic.

Going back to the interferometer, applying the second BS to equation (2-8) and making $T = 1/2$ the state now reads:

$$|1\rangle|1\rangle \rightarrow \frac{1}{2}|2\rangle|0\rangle + \frac{1}{2}|0\rangle|2\rangle \rightarrow |1\rangle|1\rangle. \quad (2-9)$$

We can then add the relative phase:

$$\begin{aligned} |1\rangle|1\rangle &\rightarrow \frac{1}{2}|2\rangle|0\rangle + \frac{1}{2}e^{2i\theta}|0\rangle|2\rangle \rightarrow \\ &\rightarrow \frac{1}{2\sqrt{2}}(1 - e^{2i\theta})|2\rangle|0\rangle + i\frac{1}{2}(1 + e^{2i\theta})|1\rangle|1\rangle - \frac{1}{2\sqrt{2}}(1 - e^{2i\theta})|0\rangle|2\rangle. \end{aligned} \quad (2-10)$$

It stands to reason that if we increase the number of inputs to two particles so would the relative phase increase to $e^{i2\theta}$. This comes from the fact that N and θ are conjugate variables, so phase displacements are given by $e^{iN\theta}$.

Finally, the probabilities are given by:

$$P(2, 0) = \left| \frac{1}{2\sqrt{2}}(1 - e^{2i\theta}) \right|^2 = \frac{1}{4}(1 - \cos 2\theta), \quad (2-11a)$$

$$P(0, 2) = \left| \frac{1}{2\sqrt{2}}(1 - e^{2i\theta}) \right|^2 = \frac{1}{4}(1 - \cos 2\theta), \quad (2-11b)$$

$$P(1, 1) = \left| \frac{1}{2}i(1 + e^{2i\theta}) \right|^2 = \frac{1}{2}(1 + \cos 2\theta). \quad (2-11c)$$

Note that the probabilities depend on the relative phase between the arms on both cases mentioned and that in the two-particle case it oscillates twice as fast with respect to the one-particle.

Ultimately this shows us how the interference pattern relates to the phase, $\theta = m\frac{\pi}{2}$ for integer m means destructive interference and $\theta = (2m + 1)\frac{\pi}{4}$ means constructive interference, while probabilities are distributed across the quantum states. It is reasonable to expect that this might allow us to have twice as much phase resolution.

Also interesting is the fact that the probabilities depend on the number of particles. This can be used as a resource to obtain better phase resolutions in interferometry and as we will see, this idea leads to the notion of the so-called Heisenberg Limit.

Any phenomena that creates a relative phase could be studied with interferometers. Some examples are Gravity wave detection, flow visualization in aerodynamics and plasma physics [11, 12, 13].

2.1.2

Phase resolution

One could ask how precise an interferometer can be, meaning, what would be the smallest detectable phase for a given setup? This leads us to the concept of phase resolution.

We can get an idea about such limit by looking at the Heisenberg uncertainty principle. From its energy-time form it is possible to obtain a relation between the number operator and phase variation. We assume a wave of N photons and frequency ω and by direct substitution using the relations $\Delta E = \hbar \Delta N \omega$ and $\Delta t = \Delta \theta / \omega$ We can get the the number-phase form of the relation:

$$\Delta E \Delta t \geq \frac{\hbar}{2} \implies \Delta N \Delta \theta \geq \frac{1}{2}. \quad (2-12)$$

Observe that the optimal phase resolution $\Delta \theta$ occurs when the above inequality is saturated. Note again that the same relation implies $\Delta \theta \geq \frac{1}{2\Delta N}$, meaning it is possible to improve our resolving power even further by increasing the uncertainty in N .

An interesting fact is that we can express ΔN as a function of the mean number of particles $\langle N \rangle$, which is the expected value of the number operator, thus obtaining a bound on the phase resolution in terms of how many particles are used in the measurement. There is a minimum amount of bosons necessary to achieve a specific phase resolution $\Delta \theta$.

One noteworthy example is the Laser Interferometer Gravitational-Wave Observatory (LIGO) as it is one of the only experiments limited by quantum mechanics [11]. LIGO works with laser beams, which are represented by a coherent state. This means two things, the phase-number uncertainty is saturated and the photon number distribution is Poissonian. Hence, $\Delta N = \sqrt{\langle N \rangle}$ [14]. So we get:

$$\Delta \theta = \frac{1}{2\Delta N} = \frac{1}{2\sqrt{\langle N \rangle}}. \quad (2-13)$$

As mentioned before, we could optimize this by increasing the uncertainty in N . One way to do this is prepare what is called a NOON state. For N particles it reads:

$$|\psi\rangle = \frac{|N\rangle_{a_i}|0\rangle_{a_j} + e^{iN\theta}|0\rangle_{a_i}|N\rangle_{a_j}}{\sqrt{2}}. \quad (2-14)$$

This is called a NOON state because we can form the word "NOON" by taking the 0s as Os. Note that the phase now depends on N as well. This is a sort of generalization of the two-photon example discussed earlier with the Hong-Ou-Mandel Effect. A general process to produce and check a NOON state is given by figure 2.3.

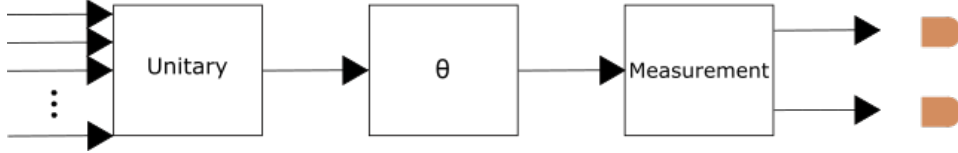


Figure 2.3: General diagram of preparing a NOON state. We unitarily transform N single particle states to an entangled state, apply a phase θ , and make a measurement which collapses the wave-function to one of the detectors

Consider now an observable O . Having enough resolution to measure it simply means that the signal is greater than the uncertainty. Say we measure O for zero phase and for an arbitrarily small phase, $\Delta\theta$. To be able to resolve the small phase we must have:

$$O(\Delta\theta) - O(0) \geq \Delta O(\theta). \quad (2-15)$$

In the limit $\Delta\theta \rightarrow 0$ this becomes:

$$\Delta\theta \geq \frac{\Delta O}{\left| \frac{\delta O}{\delta \theta} \right|}. \quad (2-16)$$

Assume then that O is given by:

$$O = |N\rangle_{a_i}|0\rangle_{a_j}\langle 0|_{a_i}\langle N|_{a_j} + |0\rangle_{a_i}|N\rangle_{a_j}\langle N|_{a_i}\langle 0|_{a_j}. \quad (2-17)$$

To simplify our calculations we may assign logical values to the following states $|N\rangle_{a_i}|0\rangle_{a_j} = |\mathbf{0}\rangle$ and $|0\rangle_{a_i}|N\rangle_{a_j} = |\mathbf{1}\rangle$. This is equivalent to turning $|\psi\rangle$ in a superposition of orthogonal states and O in the Pauli matrix σ_x :

$$|\psi\rangle = \frac{|\mathbf{0}\rangle + e^{iN\theta}|\mathbf{1}\rangle}{\sqrt{2}}, \quad (2-18a)$$

$$O = |\mathbf{0}\rangle\langle\mathbf{1}| + |\mathbf{1}\rangle\langle\mathbf{0}| = \sigma_x. \quad (2-18b)$$

One can note that $|\psi\rangle$ now represents a logical qubit. The form presented above is a superposition of two logic values with equal probability amplitudes, which differs from a classical bit that is assigned one of the values, either 0 or 1 [15].

The expected values are then:

$$\langle O \rangle = \langle \psi | (|0\rangle\langle 1| + |1\rangle\langle 0|) | \psi \rangle = \langle \psi | \sigma_x | \psi \rangle = \cos N\theta, \quad (2-19a)$$

$$\langle O^2 \rangle = \langle \psi | \sigma_x^2 | \psi \rangle = 1. \quad (2-19b)$$

The uncertainty becomes:

$$\Delta O = \sqrt{\langle O^2 \rangle - \langle O \rangle^2} = \sin N\theta. \quad (2-20)$$

Finally the phase variation reads:

$$\Delta\theta = \frac{\Delta O}{\left| \frac{\partial \langle O \rangle}{\partial \theta} \right|} = \frac{\sin N\theta}{N \sin N\theta} = \frac{1}{N}. \quad (2-21)$$

For consistency we check that the uncertainty principle still holds. Expected values for the number operator N_i are:

$$\langle N_i \rangle = \langle \psi | N_i | \psi \rangle = \frac{N}{2}, \quad (2-22a)$$

$$\langle N_i^2 \rangle = \langle \psi | N_i^2 | \psi \rangle = \frac{N^2}{2}. \quad (2-22b)$$

Then the uncertainty is:

$$\Delta N_i = \sqrt{\langle N_i^2 \rangle - \langle N_i \rangle^2} = \frac{N}{2}, \quad (2-23)$$

and the Uncertainty principle still holds,

$$\Delta N_i \Delta\theta = \frac{1}{2}. \quad (2-24)$$

for N_j the results are the same.

As previously mentioned the resolving power increased with the particle count in both the LIGO example and the NOON state, but it is still important to make distinctions about the states discussed above. The coherent state and the NOON state both saturate the uncertainty principle but the latter also minimizes phase variations. It is one example of a squeezed state as one of the uncertainties has been "squeezed" while the other "expanded". Unfortunately preparing such a state in an interferometer is non-trivial for $N > 2$ [16]. However we will soon discuss how NOON state interferometry can be seen as a particular example of a quantum algorithm. We will present a single unitary in the form of a quantum circuit that produces and analyzes NOON-like states. A phasor diagram that summarizes the idea of squeezed states can be found on figure 2.4

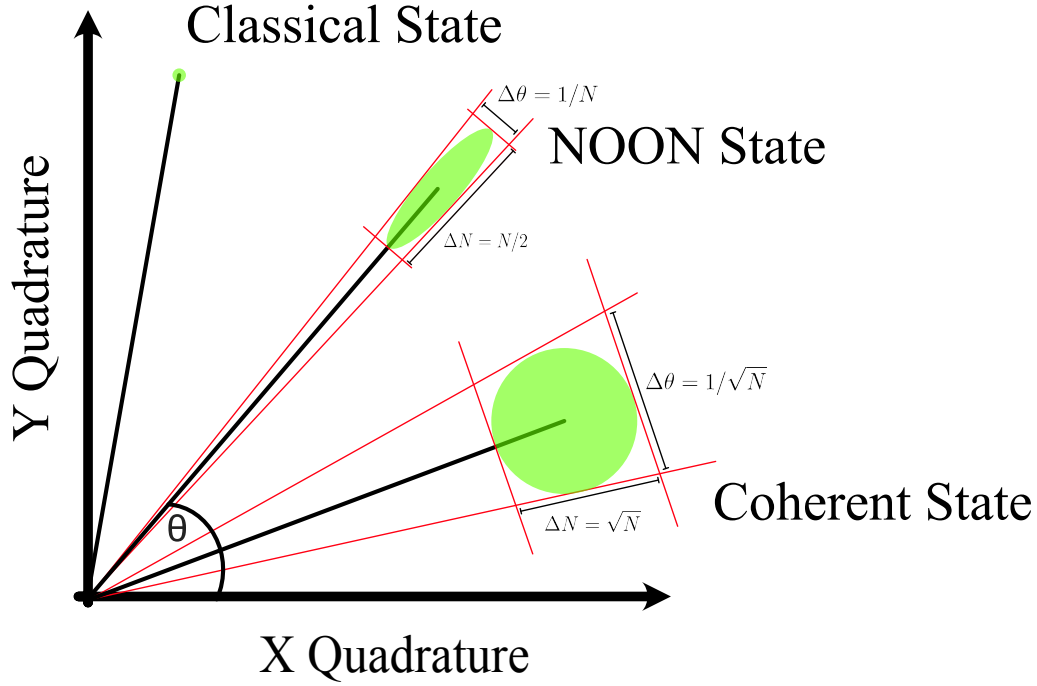


Figure 2.4: Phasor diagram for coherent, NOON and classical states.

2.1.3

Jordan-Schwinger map

Let us now consider the action of an interferometer on the number operator $N = N_i + N_j = a_i^\dagger a_i + a_j^\dagger a_j$. An MZI acts in the following way:

$$N_i^{in} = a_i^\dagger a_i \rightarrow N_i^{out} = \left(\frac{1 - \cos \theta}{2} \right) a_i^\dagger a_i + \left(\frac{1 + \cos \theta}{2} \right) a_j^\dagger a_j - \frac{1}{2} \sin \theta (a_i^\dagger a_j + a_j^\dagger a_i), \quad (2-25a)$$

$$N_j^{in} = a_j^\dagger a_j \rightarrow N_j^{out} = \left(\frac{1 - \cos \theta}{2} \right) a_j^\dagger a_j + \left(\frac{1 + \cos \theta}{2} \right) a_i^\dagger a_i - \frac{1}{2} \sin \theta (a_j^\dagger a_i + a_i^\dagger a_j). \quad (2-25b)$$

Where N^{in} is the number of particles before the MZI and N^{out} after. The number operator represents the number of particles in a system and is a conserved quantity in linear optical schemes. In a composite system it can be easily separated into one operator for each mode to check particle number per mode. In our case this translates to having operators N_i and N_j . However, there are two operators we are mostly interested in, N and $N_i - N_j$. The total number operator N , transforms as:

$$N^{in} = a_i^\dagger a_i + a_j^\dagger a_j \rightarrow N^{out} = N_i^{out} + N_j^{out} = a_i^\dagger a_i + a_j^\dagger a_j = N^{in}, \quad (2-26)$$

This means N is conserved as expected. The interferometer doesn't create or annihilate particles.

Moreover the difference between N_i and N_j reads:

$$(N_i - N_j)^{\text{out}} = \cos \theta (N_i - N_j)^{\text{in}} - \sin \theta (a_i^\dagger a_j + a_j^\dagger a_i)^{\text{in}}. \quad (2-27)$$

Despite N being conserved note that $N_i - N_j$ need not follow suit. From the equation above, it would only do so with $\theta = 2m\pi$ for integer m .

From the previous equation we can take the two new operators $N_i - N_j$ and $a_i^\dagger a_j + a_j^\dagger a_i$ and notice a curious relation. We begin by calculating the commutation relation:

$$[(a_i^\dagger a_j + a_j^\dagger a_i), (N_i - N_j)] = 2i(a_i^\dagger a_j - a_j^\dagger a_i). \quad (2-28)$$

This result gives the idea that we can define the following operators:

$$J_x = \frac{1}{2}(a_i^\dagger a_j + a_j^\dagger a_i), \quad (2-29a)$$

$$J_y = \frac{i}{2}(a_i a_j^\dagger - a_i^\dagger a_j), \quad (2-29b)$$

$$J_z = \frac{1}{2}(N_i - N_j). \quad (2-29c)$$

These are remarkably similar to angular momentum operators as their commutators follow the same algebra and commute with $J^2 = \frac{N}{2} \left(\frac{N}{2} + 1 \right)$, which is actually a conserved quantity.

We then construct the map and shed a new light on what it is that an interferometer does. From equations (2-27) and (2-26) we infer the MZI transforms the J operators according to:

$$\begin{pmatrix} J'_x \\ J'_y \\ J'_z \end{pmatrix} = \begin{pmatrix} \cos \theta & 0 & \sin \theta \\ 0 & 1 & 0 \\ -\sin \theta & 0 & \cos \theta \end{pmatrix} \begin{pmatrix} J_x \\ J_y \\ J_z \end{pmatrix}. \quad (2-30)$$

This means that an interferometer is nothing more than a rotation in an angular momentum space and the interference pattern we observe is given by the number operator difference $N_i - N_j = 2J_z$

We can also look back at our results for phase resolution. From equation (2-16) we take $O = J'_z$ and have that:

$$\Delta \theta \geq \frac{\Delta J'_z}{\left| \frac{\partial J'_z}{\partial \theta} \right|}. \quad (2-31)$$

From equation (2-30), we can construct:

$$\Delta J_z'^2(\theta) = \cos^2 \theta \Delta J_z^2 + \sin^2 \theta \Delta J_x^2 - 2 \cos \theta \sin \theta \text{Cov}(J_x, J_z), \quad (2-32)$$

with

$$\text{Cov}(A, B) = \frac{1}{2} \langle AB + BA \rangle - \langle A \rangle \langle B \rangle. \quad (2-33)$$

appearing in the second term due to error propagation. $\text{Cov}(A, B)$ stands for the covariance between operators A and B .

This result is interesting because it allows us to calculate the phase resolution by simply knowing the input quantum states and the relative phase. The phase resolution might be a function of θ , which implies an optimal operation point in the vicinity of the phase that minimizes $\Delta\theta$.

Consider now an example. Let us calculate the phase variation for state $|N\rangle_i |0\rangle_j$. First we need to calculate $\left| \frac{\partial \langle J'_z \rangle}{\partial \theta} \right|$. This is given by the matrix (2-30):

$$\langle J'_z \rangle = -\sin \theta \langle J_x \rangle + \cos \theta \langle J_z \rangle. \quad (2-34)$$

The expected values are:

$$\langle J_z \rangle = \frac{1}{2} (\langle N |_i \langle 0 |_j) (N_i - N_j) (|N \rangle_i |0 \rangle_j) = \frac{N}{2}, \quad (2-35a)$$

$$\langle J_x \rangle = \frac{1}{2} (\langle N |_i \langle 0 |_j) (a_i^\dagger a_j + a_j^\dagger a_i) (|N \rangle_i |0 \rangle_j) = 0. \quad (2-35b)$$

Then the modulus of the derivative is:

$$\left| \frac{\partial \langle J'_z \rangle}{\partial \theta} \right| = +\cos \theta \langle J_x \rangle + \sin \theta \langle J_z \rangle = \frac{N}{2} \sin \theta. \quad (2-36)$$

Second we need to calculate $\Delta J_z'^2$. The remaining expected values are:

$$\langle J_z'^2 \rangle = \frac{1}{4} (\langle N |_i \langle 0 |_j) (N_i - N_j)^2 (|N \rangle_i |0 \rangle_j) = \frac{N^2}{4}, \quad (2-37a)$$

$$\langle J_x'^2 \rangle = \frac{1}{4} (\langle N |_i \langle 0 |_j) (a_i^\dagger a_j + a_j^\dagger a_i)^2 (|N \rangle_i |0 \rangle_j) = \frac{N}{4}, \quad (2-37b)$$

$$\langle J_x J_z + J_z J_x \rangle = 0. \quad (2-37c)$$

The uncertainties then are:

$$\Delta J_z'^2 = \langle J_z'^2 \rangle - \langle J_z \rangle^2 = 0, \quad (2-38a)$$

$$\Delta J_x'^2 = \langle J_x'^2 \rangle - \langle J_x \rangle^2 = \frac{N}{4}. \quad (2-38b)$$

The covariance:

$$\text{Cov}(J_x, J_z) = \frac{1}{2} \langle J_x J_z + J_z J_x \rangle - \langle J_x \rangle \langle J_z \rangle = 0. \quad (2-39)$$

Then the variance becomes:

$$\Delta J_z'^2 = \frac{N}{4} \sin^2 \theta. \quad (2-40)$$

Finally, simply inputting the values in equation (2-31) gives:

$$\Delta\theta \geq \frac{\Delta J'_z}{\left| \frac{\partial J'_z}{\partial \theta} \right|} = \frac{\frac{\sqrt{N}}{2} \sin \theta}{\frac{N}{2} \sin \theta} = \frac{1}{\sqrt{N}}. \quad (2-41)$$

This is an important example as it shows how easier it becomes to calculate the uncertainties from the known input states. Previously one would need to calculate the action of the whole interferometer and the output states before proceeding with the calculation of the phase uncertainty, this way only the input states are needed.

2.2

Fermions

We now switch the discussion to fermions. First, it is important to note that they obey different statistics than bosons [8]:

$$\{a_i^\dagger, a_j^\dagger\} = \{a_i, a_j\} = 0, \quad (2-42a)$$

$$\{a_i, a_j^\dagger\} = a_i a_j^\dagger + a_j^\dagger a_i = \delta_{ij}. \quad (2-42b)$$

Going back to the NOON state, for bosons we know that if we prepare a state like that we would have a phase resolution proportional to $1/N$, equivalently the system would acquire relative phase $e^{iN\theta}$.

For fermions, any terms of the form $|N\rangle|0\rangle$ and $|0\rangle|N\rangle$, for $N \geq 1$ are excluded due to Pauli's exclusion principle [8]. (In fact any term with more than one fermion per mode would be excluded provided the particles have the same spin.) Even more relevant, terms of the type $|1\rangle|1\rangle$ are now anti-symmetric due to the new statistics. This means that particle exchanges now give the system's wave-function a global phase -1. We can go back to equations (2-4a) and (2-4b) and note that while we would have the same result for one fermionic particle in an MZI, equation (2-8) for two particles would become:

$$|1\rangle|1\rangle \rightarrow |1\rangle|1\rangle. \quad (2-43)$$

There is no relative phase in the output of a fermionic MZI, but a global one. Going through a second BS would simply yield the same result.

No relative phase means fermionic MZI yields no usable results because there would be no interference pattern to observe. We need then to look at new kinds of setups for measuring relative phase for fermion quantum states.

2.2.1

Ramsey interferometer

A Ramsey Interferometer (RI) works by preparing atoms in the ground state which will then suffer a $\pi/2$ pulse that takes them to an equal superposition of ground and excited states. After evolving freely for time t a second $\pi/2$ pulse is injected. Ideally the final states should all be excited but if there is a transition frequency mismatch $\omega \neq \omega_0$ the probability of finding an atom in an excited state is $\cos^2(\theta/2)$ for $\theta = (\omega - \omega_0)t$. This means that if a phase θ was applied between the pulses we should detect an interference pattern. On figure 2.5 we can see a diagram that describes this with no interference pattern present due to no frequency mismatch.

This device was first described in a 1950 research paper by Norman Ramsey [17], where he used magnetic resonance to measure transition frequencies of atoms between excited and ground states. We shall present the ideas from a publication by Demkowicz-Dobrzański et al. [18].

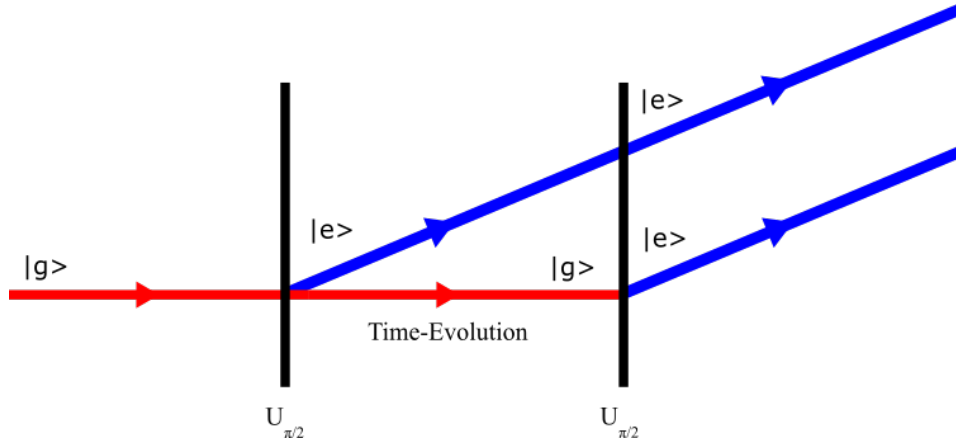


Figure 2.5: Ramsey interferometer for a 2-level system. Each $\pi/2$ pulse creates excited states $|e\rangle$ from the ground state $|g\rangle$. In the picture no interference pattern is formed as all output states are excited.

Our focus is on what something like a RI can do for fermions. We can think of two level atoms as $1/2$ spin particles where the direction of spin along the z component functions as the energy levels. In other words we are equating spin down to a ground state and spin up to an excited state ($|\uparrow\rangle = |g\rangle$ and $|\downarrow\rangle = |e\rangle$).

This way we can write the state evolution of an N atoms input through the interferometer using total spin operators:

$$J_i = \frac{1}{2} \sum_{k=0}^N \sigma_i^{(k)}, i = x, y, z. \quad (2-44)$$

Where $\sigma_i^{(k)}$ are Pauli matrices acting on the k -th particle.

Then the evolution is simply the $\pi/2$ pulses along a perpendicular axis with a phase θ on the spin orientation axis in between them.

$$|\psi\rangle^{out} = e^{-iJ_x\pi/2} e^{iJ_z\theta} e^{-iJ_x\pi/2} |\psi\rangle^{in}. \quad (2-45)$$

This is analogous to the evolution through a MZI. In more detail, J_z can be written as $J_z = 2(N_g - N_e)$, where N_g and N_e are the ground and excited state number operators. Then the difference between excited and ground states in the RI case is equivalent to the difference between outputs i and j in the MZI case.

To be more specific this resembles the example on subsection 2.1.3 of the state $|N\rangle_i |0\rangle_j$ going through a MZI. This means we can expect the same result to be obtained here. The phase resolution according to equation (2-41) will take the form:

$$\Delta\theta \geq \frac{1}{\sqrt{N}}. \quad (2-46)$$

This all means that a RI is simply a special case of a MZI and a viable alternative for interferometry with fermion-like statistics. In figure 2.6 we show the MZI side-by-side with its equivalent operations on the Bloch sphere.

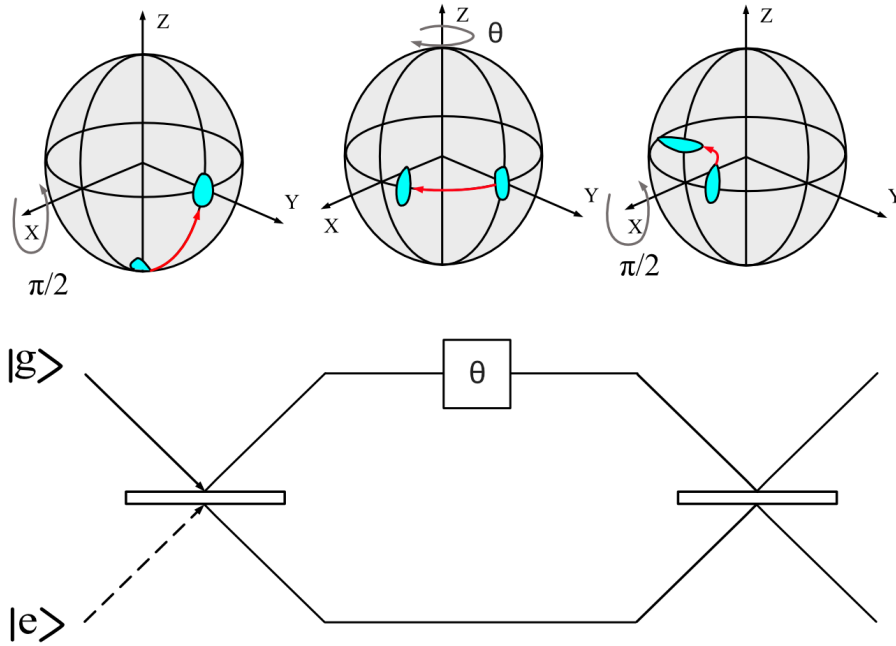


Figure 2.6: Diagram comparing Ramsey interferometry on the Bloch sphere with the MZI. The two arms on the MZI are analogous to the excited and ground states on the Ramsey interferometer. The highlighted area represents a squeezed state, just as in the MZI one can work with squeezed states to reduce the variance for the relevant quantities.

2.2.2

Non-local interferometers

Here we present a setup discussed by Dasenbrook et al [19] which generalizes the MZI. The interferometer in question produces and analyzes entanglement from single electron quantum states. It is known as a Hanbury Brown-Twiss Interferometer (HBTI).

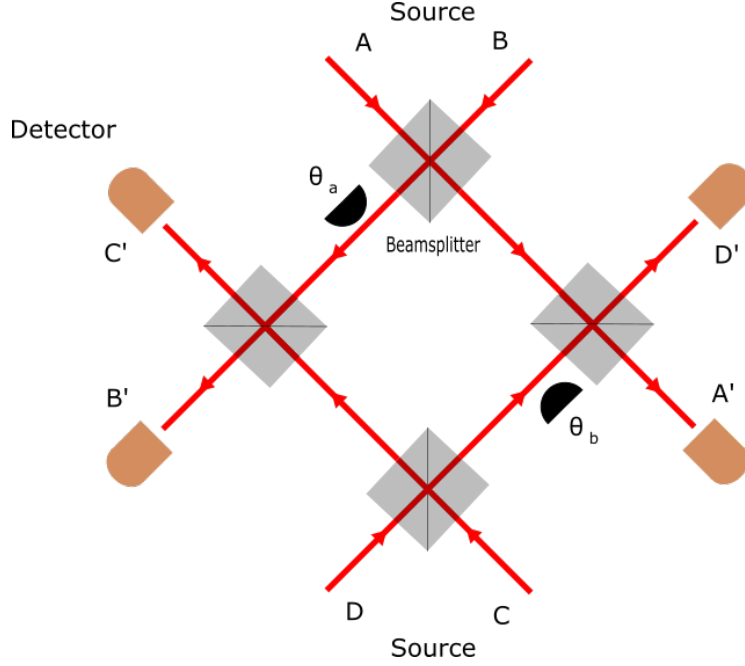


Figure 2.7: Diagram for a Non-local interferometer. Four beams from four different sources travel through two of the four beamsplitters before reaching the detectors. They pick up a phase in two of the four arms.

As shown in figure 2.7, it has four sources A, B, C and D and four outputs labeled A', B', C' and D'. Each beam goes through two BSs before reaching one of the four detectors. We also apply a phase θ_a and θ_b on two of the arms of the interferometer.

The feasibility of this setup is due to advancements in coherent single electron emitters and the possibility of using Edge channels created by the quantum Hall Effect as wave-guides for the electrons. The BSs are substituted for quantum point contacts as well and have 50:50 transmission rate [19].

The top BS implements the following transformation:

$$a_A^\dagger \rightarrow \frac{1}{\sqrt{2}}(a_{A'}^\dagger + a_{B'}^\dagger), \quad (2-47a)$$

$$a_B^\dagger \rightarrow \frac{1}{\sqrt{2}}(a_{A'}^\dagger - a_{B'}^\dagger). \quad (2-47b)$$

The same procedure happens for the bottom one with the appropriate indexes:

$$a_C^\dagger \rightarrow \frac{1}{\sqrt{2}}(a_{C'}^\dagger + a_{D'}^\dagger), \quad (2-48a)$$

$$a_D^\dagger \rightarrow \frac{1}{\sqrt{2}}(a_{C'}^\dagger - a_{D'}^\dagger). \quad (2-48b)$$

If we keep following the path from the top BS then one of the states acquires phase $e^{i\theta_a}$, and on the second BS the following happens:

$$\frac{1}{\sqrt{2}}(a_{A'}^\dagger + e^{i\theta_a} a_{B'}^\dagger) \rightarrow \frac{1}{2}(a_{A'}^\dagger + a_{D'}^\dagger + e^{i\theta_a} a_{B'}^\dagger + e^{i\theta_a} a_{C'}^\dagger), \quad (2-49a)$$

$$\frac{1}{\sqrt{2}}(a_{A'}^\dagger - e^{i\theta_a} a_{B'}^\dagger) \rightarrow \frac{1}{2}(a_{A'}^\dagger + a_{D'}^\dagger - e^{i\theta_a} a_{B'}^\dagger - e^{i\theta_a} a_{C'}^\dagger). \quad (2-49b)$$

And on the bottom path:

$$\frac{1}{\sqrt{2}}(a_{C'}^\dagger + e^{i\theta_b} a_{D'}^\dagger) \rightarrow \frac{1}{2}(a_{C'}^\dagger - a_{B'}^\dagger + e^{i\theta_b} a_{D'}^\dagger - e^{i\theta_b} a_{A'}^\dagger), \quad (2-50a)$$

$$\frac{1}{\sqrt{2}}(a_{C'}^\dagger - e^{i\theta_b} a_{D'}^\dagger) \rightarrow \frac{1}{2}(a_{C'}^\dagger - a_{B'}^\dagger - e^{i\theta_b} a_{D'}^\dagger + e^{i\theta_b} a_{A'}^\dagger). \quad (2-50b)$$

In summary the interferometer does the following to single electron states:

$$a_A^\dagger|0\rangle = |1, 0, 0, 0\rangle \rightarrow \frac{1}{2}(|1, 0, 0, 0\rangle + e^{i\theta_a}|0, 1, 0, 0\rangle + e^{i\theta_a}|0, 0, 1, 0\rangle + |0, 0, 0, 1\rangle), \quad (2-51a)$$

$$a_B^\dagger|0\rangle = |0, 1, 0, 0\rangle \rightarrow \frac{1}{2}(|1, 0, 0, 0\rangle - e^{i\theta_a}|0, 1, 0, 0\rangle - e^{i\theta_a}|0, 0, 1, 0\rangle + |0, 0, 0, 1\rangle), \quad (2-51b)$$

$$a_{C'}^\dagger|0\rangle = |0, 0, 1, 0\rangle \rightarrow \frac{1}{2}(-e^{i\theta_b}|1, 0, 0, 0\rangle - |0, 1, 0, 0\rangle + |0, 0, 1, 0\rangle + e^{i\theta_b}|0, 0, 0, 1\rangle), \quad (2-51c)$$

$$a_D^\dagger|0\rangle = |0, 0, 0, 1\rangle \rightarrow \frac{1}{2}(e^{i\theta_b}|1, 0, 0, 0\rangle - |0, 1, 0, 0\rangle + |0, 0, 1, 0\rangle - e^{i\theta_b}|0, 0, 0, 1\rangle).$$

Note now that we have a relative phase between pairs of states that would allow for the detection of an interference pattern, which is different from the fermionic MZI that only gives us a global phase.

More relevant is the state $a_A^\dagger a_C^\dagger |0\rangle$. It takes the following form:

$$\begin{aligned} a_A^\dagger a_C^\dagger |0\rangle &\rightarrow \frac{1}{2}(a_{A'}^\dagger + e^{i\theta_a} a_{B'}^\dagger)(a_{C'}^\dagger + e^{i\theta_b} a_{D'}^\dagger) |0\rangle \\ &\rightarrow \frac{1}{4}[a_{A'}^\dagger a_{C'}^\dagger (e^{i\theta} - 1) + a_{C'}^\dagger a_{D'}^\dagger (e^{i\theta} + 1) + \\ &\quad + a_{B'}^\dagger a_{A'}^\dagger (e^{i\theta} + 1) + a_{B'}^\dagger a_{D'}^\dagger (e^{i\theta} - 1) - \\ &\quad - 2e^{i\theta_a} a_{C'}^\dagger a_{B'}^\dagger + 2e^{i\theta_b} a_{A'}^\dagger a_{D'}^\dagger] |0\rangle. \end{aligned} \quad (2-52)$$

Where $\theta = \theta_a + \theta_b$. Note that the terms where two fermions reached the same output were eliminated due to Pauli's exclusion principle.

Now we can calculate the probabilities by simply doing the modulus squared of each coefficient:

$$P(A', C') = P(B', D') = \frac{1}{8}(1 - \cos \theta) \quad (2-53a)$$

$$P(C', D') = P(B', A') = \frac{1}{8}(1 + \cos \theta) \quad (2-53b)$$

$$P(C', B') = P(A', D') = \frac{1}{4} \quad (2-53c)$$

These are plotted in the figure 2.8:

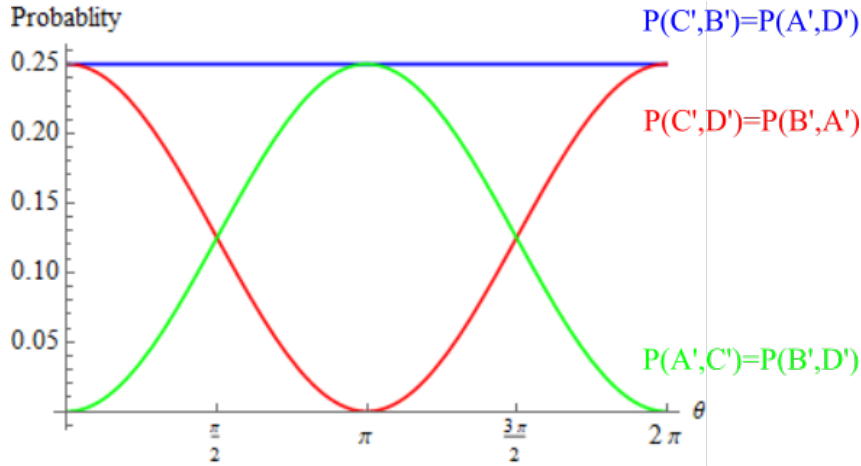


Figure 2.8: Plot of probability as function of phase for a two particle input in a Non-Local interferometer.

The calculation above can be extended for similar two electron states ($a_B^\dagger a_D^\dagger |0\rangle$, for instance), but we shall not repeat them here. Note as well that one can calculate the probabilities of each state from the equation above.

Furthermore it can be shown that the state above violates the CHSH inequality, which would prove that the state is in fact entangled. The correlator will be a function of the phases θ_a and θ_b and for a suitable choice it will violate the inequality. The calculation can be found at the source [19].

The conclusion that we want to draw though is that an interferometer of this kind is able produce constructive and destructive interference patterns dependent on the phases θ_a and θ_b , while also proving the entanglement of these states, despite the use of fermions. Fermionic statistics aren't an impediment to interferometry experiments.

2.3

The circuit approach

We can provide constructive examples of some of the concepts explored in the previous sections with the aid of the circuit approach to quantum computation. More specifically we can construct NOON state interferometers, which we discussed in this chapter, by presenting BSs and interferometers as quantum circuits and gates that represent a quantum computation.

A quantum circuit is a simple way to represent a quantum computation. Consider the CNOT gate in figure 2.9.

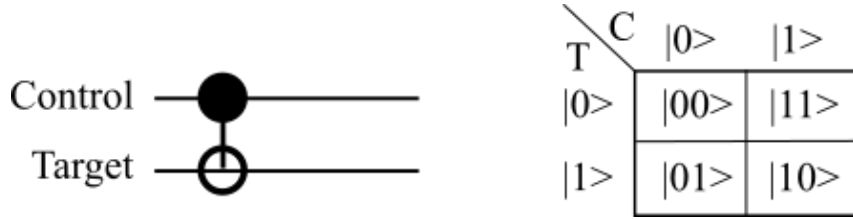


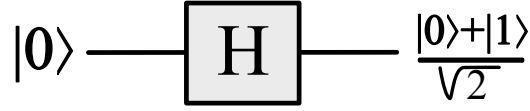
Figure 2.9: The CNOT gate. It takes two qubits, a target and a control and executes the above operation on the computational basis $|00\rangle, |01\rangle, |10\rangle$ and $|11\rangle$. On the table the second qubit is the target and the first is the control.

A CNOT is an operation involving two qubits, one target and one control. If the control has value $|1\rangle$ then the target flips values, otherwise if the control is $|0\rangle$ then the target is unchanged. This gate can be given the following representation as a matrix in the computational basis:

$$CNOT = \begin{pmatrix} 1 & 0 & 0 & 0 \\ 0 & 1 & 0 & 0 \\ 0 & 0 & 0 & 1 \\ 0 & 0 & 1 & 0 \end{pmatrix}. \quad (2-54)$$

Another interesting gate is the Hadamard gate. The Hadamard acts on a single qubit and transforms the basis states $|0\rangle$ and $|1\rangle$ to the superpositions $\frac{|0\rangle+|1\rangle}{\sqrt{2}}$ and $\frac{|0\rangle-|1\rangle}{\sqrt{2}}$. It can also be represented by the following matrix and figure 2.10:

$$H = \frac{1}{\sqrt{2}} \begin{pmatrix} 1 & 1 \\ 1 & -1 \end{pmatrix}. \quad (2-55)$$

Figure 2.10: Representation of a Hadamard gate on state $|0\rangle$

Now consider the following product states for N qubits:

$$|0\rangle = |00 \dots 0\rangle, \quad (2-56a)$$

$$|1\rangle = |11 \dots 1\rangle. \quad (2-56b)$$

A "logical BS" (LBS) would take this logical basis to what is known as GHZ states:

$$|0\rangle \rightarrow |GHZ_+\rangle = \frac{|0\rangle + |1\rangle}{\sqrt{2}}, \quad (2-57a)$$

$$|1\rangle \rightarrow |GHZ_-\rangle = \frac{|0\rangle - |1\rangle}{\sqrt{2}}. \quad (2-57b)$$

These states are interesting because they are "NOON-like" in a sense that using them for interferometry allows us to achieve the Heisenberg limit.

We can accomplish this operation by using the quantum circuit for N qubits in figure 2.11:

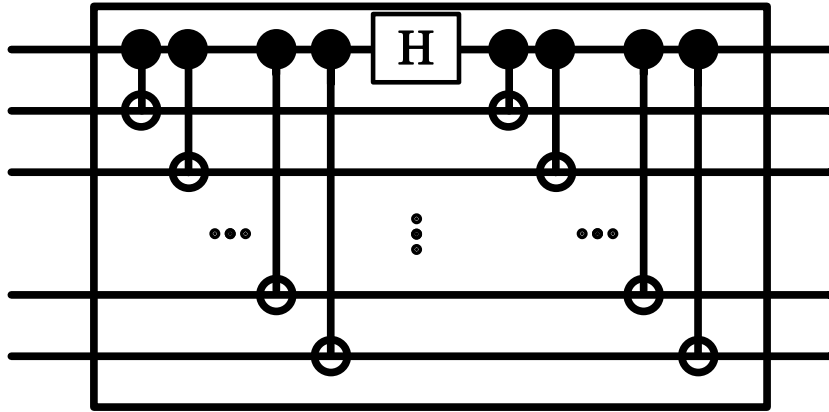


Figure 2.11: Quantum circuit implementing a logical beamsplitter.

It's possible to show the unitary matrix that represents this beamsplitter as well. For 2 qubits:

$$LBS = \frac{1}{\sqrt{2}} \begin{pmatrix} 1 & 0 & 0 & 1 \\ 0 & -1 & 1 & 0 \\ 0 & 1 & 1 & 0 \\ 1 & 0 & 0 & -1 \end{pmatrix}. \quad (2-58)$$

An interferometer is then implemented as a circuit in figure 2.12.

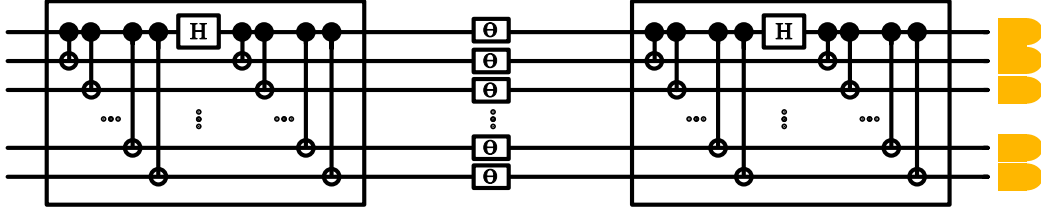


Figure 2.12: Quantum circuit implementing a NOON-like interferometer. The phase shift gate simply adds a phase θ to the state $|1\rangle$. At the end we have a detector for each qubit. In quantum circuit notation these are normally replaced by measurement operators.

The phase gates θ adds a phase so an interference pattern can be observed. For one qubit it has the following form:

$$\Theta = \begin{pmatrix} 1 & 0 \\ 0 & e^{i\theta} \end{pmatrix} \quad (2-59)$$

Note that if we applied two BSs without the phase we would simply recover the initial state

$$LBS \times SBS = I, \quad (2-60)$$

but, for phase θ we get:

$$(LBS)\Theta^N(LBS)|0\rangle = \frac{1 + e^{Ni\theta}}{2}|0\rangle + \frac{1 - e^{Ni\theta}}{2}|1\rangle, \quad (2-61a)$$

$$(LBS)\Theta^N(LBS)|1\rangle = \frac{1 + e^{Ni\theta}}{2}|1\rangle + \frac{1 - e^{Ni\theta}}{2}|0\rangle. \quad (2-61b)$$

Which gives the following probabilities for input $|0\rangle$:

$$P(|0\rangle) = \frac{1 + \cos N\theta}{2}, \quad (2-62a)$$

$$P(|1\rangle) = \frac{1 - \cos N\theta}{2}. \quad (2-62b)$$

Note that the probabilities are reversed for input $|1\rangle$ and that these results are similar to what you would expect for a NOON state in an interferometer. To see this remember the mapping we did in section 2.1.2: $|N\rangle_{a_i}|0\rangle_{a_j} = |0\rangle$ and $|0\rangle_{a_i}|N\rangle_{a_j} = |1\rangle$. This means we can reach the Heisenberg limit with this circuit.

Then it is possible to represent an interferometer as a program in a quantum computer and interferometry can be seen as a branch of quantum computation. This is specially interesting because it allows us to do scalable NOON-like interferometry, we can create NOON states for any N by increasing

the size of the circuit by adding qubits and operations. But not only that, we can simulate our interferometer in classical computers and also run it on real quantum devices, which is precisely what we do next.

2.3.1

Implementing the interferometer

We can leverage IBM's Quantum Computers and its SDK (Software Development Kit) known as Qiskit (Quantum Information Software Kit) [20] to implement our NOON-like interferometer. Qiskit allows us to code in the Python programming language and create a quantum circuit utilizing OpenQASM (Open Quantum Assembly Language) specs [21], it also provides access to different backends through an API (Application Programming Interface) to execute our computations. The backends are where our circuit is compiled and executed and what provides us the results of the computation. From the available ones we shall use only two.

The first is known as the QASM (Quantum Assembly Language) simulator which mimics the execution of the circuit through a real quantum computer and its measurements. It goes as far as being able to incorporate simulated custom and pre-configured noise models into the operation, but we won't be using this feature as we plan to run the same circuits on a real computer that is already susceptible to real noise.

The second one is a real device known as "IBM Q 5 Yorktown" on IBM's servers that we access through a freely available API. It is interesting to be able to run this circuit in a real computer because we can have a better understanding if such computation is feasible or not given today's quantum computational limits, be it in terms of the number of qubits or the reliability of logical operations. Concerning this specific device we are limited to only five qubit operations and its logical error rates are specified on IBM's website [22].

There are a number of factors to consider when choosing one of IBM's computers to run a circuit. Chief among them are the error rates of the logical operations; usually we want them to be as small as possible for the most critical operations, and also the topology of the computer itself; not all qubits share direct logical connections with each other for example. For the circuit we are discussing the IBM Q 5 Yorktown was the ideal choice because of its unique topology, it allows us to map a virtual qubit to a physical one that has a direct connection to all the others used in the computation. This is perfect for our NOON-like interferometer as all the control operations are concentrated on the first qubit. On figure 2.13 we can see the physical chip and graph of its topology.

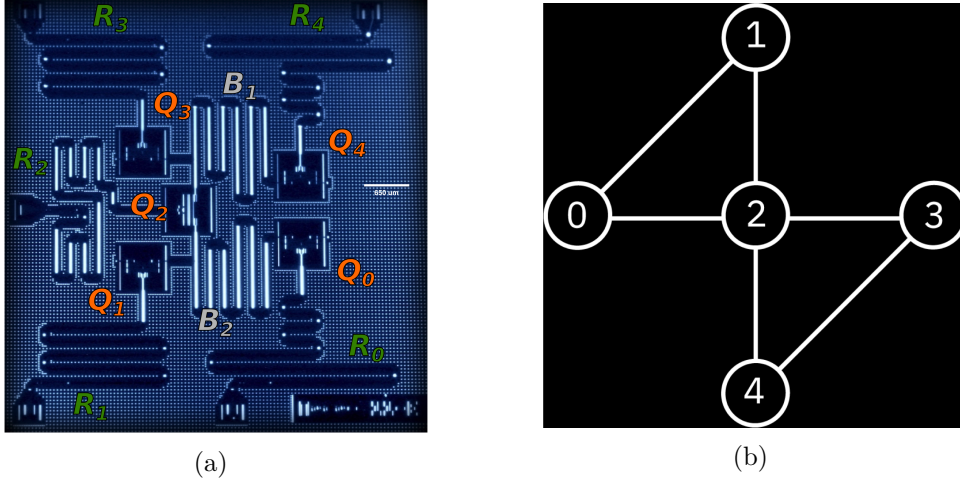


Figure 2.13: Both pictures taken from the IBM website [22] (a) Layout of the chip (b) Topology of the chip. Each circle represents a qubit. A line connecting them tells that we can apply two qubit operations directly on both of them.

This takes us to another problem when trying to execute our circuit on a real device. Real quantum computers can normally execute only a basic set of operations which we call a base, we say that a computer is then universal if from that base we can construct any unitary operation arbitrarily close to the desired logical operation [23]. IBM's computers utilize a specific base that consists of the following gates: $\mathcal{G} = \{U_1, U_2, U_3, CNOT, I\}$, where U_1 , U_2 and U_3 take the form:

$$U_3(\theta, \phi, \lambda) = \begin{pmatrix} \cos \frac{\theta}{2} & -e^{i\lambda} \sin \frac{\theta}{2} \\ e^{i\phi} \sin \frac{\theta}{2} & e^{i(\phi+\lambda)} \cos \frac{\theta}{2} \end{pmatrix}, \quad (2-63a)$$

$$U_3\left(\frac{\pi}{2}, \phi, \lambda\right) = U_2(\phi, \lambda) = \frac{1}{\sqrt{2}} \begin{pmatrix} 1 & -e^{i\lambda} \\ e^{i\phi} & e^{i(\phi+\lambda)} \end{pmatrix}, \quad (2-63b)$$

$$U_3(0, 0, \lambda) = U_1(\lambda) = \begin{pmatrix} 1 & 0 \\ 0 & e^{i\lambda} \end{pmatrix}. \quad (2-63c)$$

One can easily see that U_1 is simply the phase gate, U_2 is a generic gate that creates superpositions (The Hadamard is a specific implementation of U_2 for example) and that U_3 is just a general unitary. The problem that we face then is writing our circuit in a way that is optimal for IBM computers to understand. For that we have to not only consider the topology problem we mentioned earlier but the basis in which the computer operates as we want to use the least amount of gates possible so as to reduce the failure rate of the whole circuit, meaning, we would get less incorrect results after the execution.

Fortunately though, Qiskit already has a tool that does this very thing. Called Transpiler, it is responsible for doing the topology mapping of our

circuit to the chip and it can also write the circuit in the required basis while optimizing it into a form that uses the least amount of gates. It even allows for user input so we can suggest initial topology mappings. An example for a mapping of our circuit for five qubits can be seen on figure 2.14.

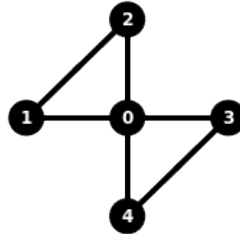


Figure 2.14: Mapping of the qubits on the chip topology. Our virtual qubit 0 was mapped to the chip's physical qubit 2, while the rest were distributed among the other physical qubits. Each circle represents a qubit. A line connecting them, tells that we can directly apply two-qubit operations on them.

With the Transpiler most of our problems are solved, we have a way to map our logical qubits onto the chips physical ones and we can already build our circuit on IBM's basis because our circuit only uses gates in said basis. As mentioned previously, the chip topology doesn't allow us to execute direct controlled operations between every qubit but, fortunately, one of the qubits has direct access to all the others. Taking this into consideration we take a look at our circuit realize that the controlled operations are all condensed on the first qubit, that's the reason we map it to the central qubit on the chip and why this topology is beneficial to us.

Before we proceed further it is useful to introduce another concept known as depth for comparing circuits. The size of a circuit is simply the amount of gates a circuit has, but depth has a more subtle meaning. It is the longest path from input to output on a circuit, we can think of each gate taking one unit of time to be executed for the purpose of this calculation. Consider figure 2.15 as an example, in figure (a) we can see that qubit $q161_3$ has a depth of twelve, There are ten operations in its line but the first controlled operation on it has to wait for previous two ones to complete, this adds up to twelve. On circuit (b) $q159_3$ has depth twenty but only six operation in its line, this is due to the fact that it also has to wait for previous operations on $q159_0$ to complete. So, circuit (a) has a lower depth of twelve while circuit (b) has a higher depth of

twenty. On the other hand, both circuits have the same size as they require twenty eight operations.

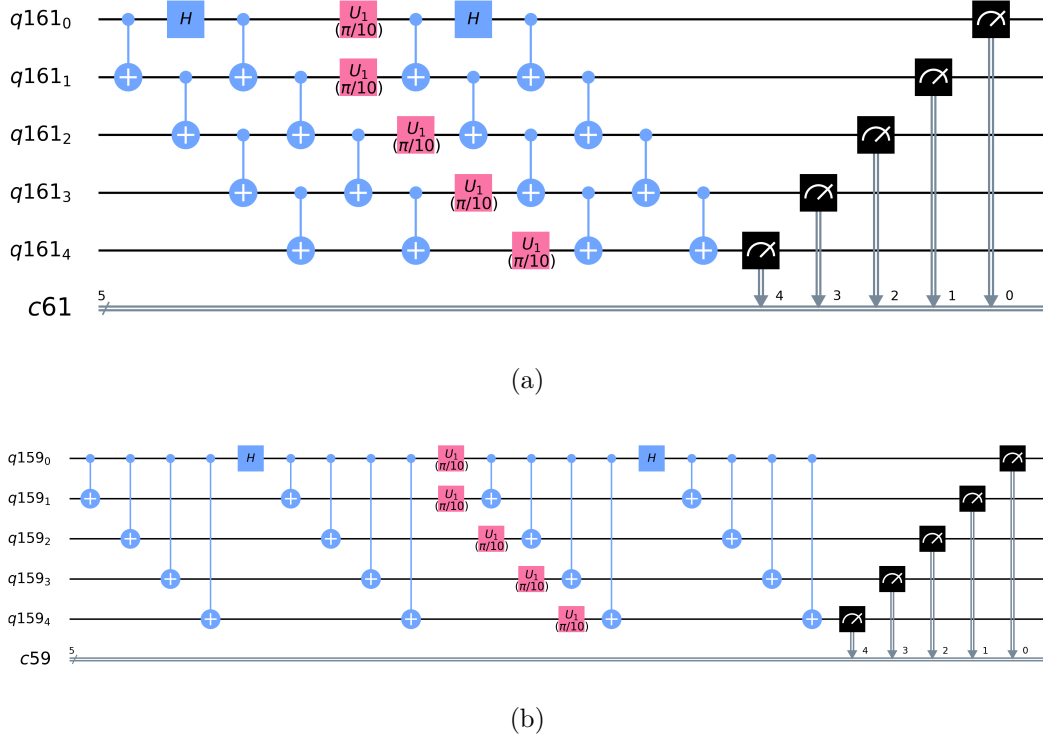


Figure 2.15: Both pictures plotted on Qiskit. (a) Another circuit based on our NOON-like interferometer but now the CNOTs are cascaded. (b) Circuit that corresponds to the NOON-like interferometer. In both figures $\theta = \pi/10$ and $N = 5$. N classical bits are also created alongside the qubits for the measurements to be recorded on.

Now we can then start executing the circuits for different values of θ and N . We begin by building a two qubit implementation of our Interferometer and realizing measurements on the two outputs. We start with only a small number of qubits because this allows us to create a smaller circuit that is less susceptible to errors and decoherence. It will later be increased to five qubits as that is the current limit of the computer we chose to work on. It is worthwhile to mention that with two qubits we have a depth of six, while for five the depth increases to twenty.

We will run the circuit multiple times and calculate the probabilities of obtaining the state $|00\rangle$ as a function of the phase θ in the interferometer utilizing both the QASM simulator and IBM Q 5 Yorktown. The theoretical prediction would be:

$$P(00) = \frac{\cos 2\theta + 1}{2}. \quad (2-64)$$

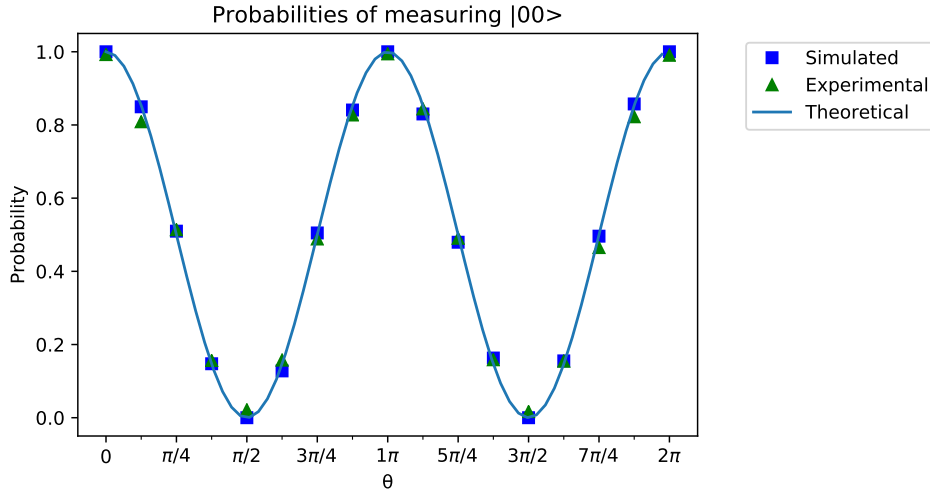


Figure 2.16: Simulated, experimental and theoretical results of the circuit for two qubits. Probabilities are calculated for one period in steps of $\pi/8$ for θ . Simulated results are given by the QASM Simulator on a classical computer and experimental results are given by the IBM Q 5 Yorktown.

As we can see the experimental results are appreciably close to the theoretical predictions and simulations. This gives us the hope that we can execute our circuit without encountering any major issues due to the error rates of the operations. The next step is to increase the number of qubits.

Let us now do $N = 3$. The theoretical prediction changes to:

$$P(000) = \frac{\cos 3\theta + 1}{2}. \quad (2-65)$$

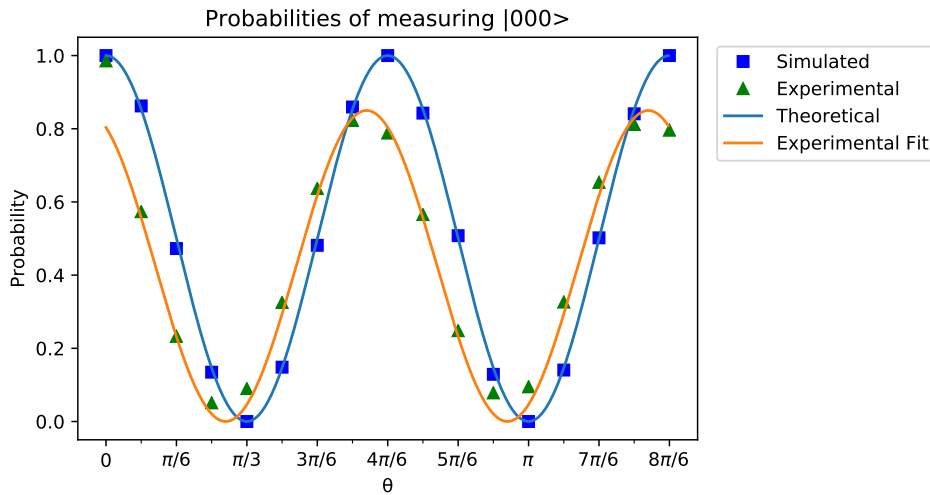


Figure 2.17: Simulated, experimental and theoretical results of the circuit for three qubits. Probabilities are calculated for one period in steps of $\pi/12$ for θ . Simulated results are given by the QASM Simulator on a classical computer and experimental results are given by the IBM Q 5 Yorktown.

It is clear that our experimental results get considerably worse, but are still somewhat similar to the expected results. The fitted function is of the form:

$$P'(000) = 0.85 \frac{\cos 3(\theta + 0.05\pi) + 1}{2}, \quad (2-66)$$

which means we had a decrease in amplitude and a small phase shift.

The depth for $N = 3$ is twelve, this gives us an idea that depth and precision might be correlated in this experiment. Most likely as depth (and with it, the time necessary to compute) increases our results get noisy due to decoherence effects on the chip. With that in mind we increase the number of qubits to the limit of the device.

Now for $N = 5$. The theoretical prediction changes to:

$$P(00000) = \frac{\cos 5\theta + 1}{2}. \quad (2-67)$$

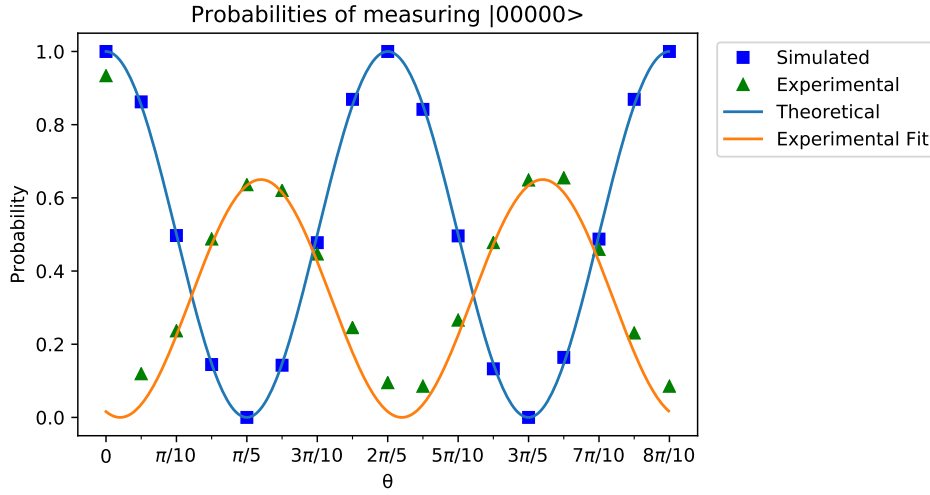


Figure 2.18: Simulated, experimental and theoretical results of the circuit for five qubits. Probabilities are calculated for one period in steps of $\pi/20$ for θ . Simulated results are given by the QASM Simulator on a classical computer and experimental results are given by the IBM Q 5 Yorktown.

The interference pattern visibility decreases appreciably. The fitted function is now of the form:

$$P'(00000) = 0.65 \frac{\cos 5(\theta + 0.18\pi) + 1}{2}, \quad (2-68)$$

which means we had an even greater decrease in amplitude and a larger phase shift.

As previously mentioned this is most likely due to the fact that errors accumulate as the depth increases. The noise becomes so high that the outputs are almost completely flipped due to the amount of bit flip and phase flip errors in the operations. At this point one might ask themselves where in

the computation the errors might be occurring. There are two possibilities, either the logical operations of the circuit are flawed or the measurements are inaccurate. There are no guarantees that the computer isn't executing the computation perfectly and the measurements are the ones introducing the noise.

Fortunately, there is a procedure to mitigate measurement errors described in the Qiskit textbook that we can utilize [24]. We won't go into the details here about the method, suffice it to say that we are simply creating a change of basis matrix that will take our results from the noisy measurement to the ideal measurement.

To do so we first have to calibrate our matrix by executing "empty" circuits. We input, one at a time, the logical basis states (For two qubits these would be $|00\rangle$, $|01\rangle$, $|10\rangle$ and $|11\rangle$) and execute measurements without doing any logical operation, which means the states are unchanged by the circuit and the results should be equal to the inputted states. This won't be true due to measurement errors, but we can execute those circuits multiple times to calculate how the basis vectors change on average to a noisy result.

With that in hand we have a change of basis matrix that takes us from the ideal results to the noisy ones. As the operation we want is the opposite we can simply invert that matrix to get a basis change from the noisy results to the ideal results, with measurement errors mitigated.

Let us then execute this method to mitigate measurement errors in our circuits. We shall only do so for $\theta = \pi/12$ and three qubits. Below is the histogram of probability per state:

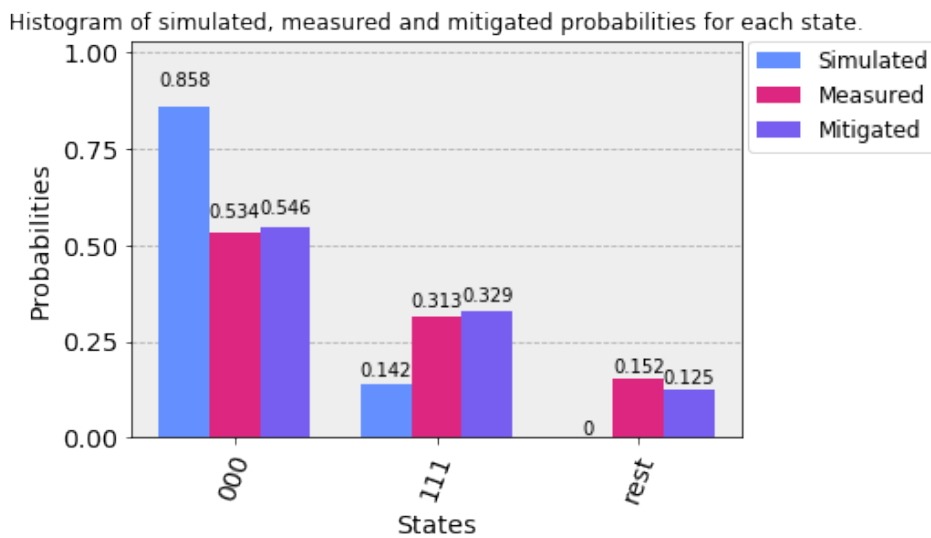


Figure 2.19: Simulated, measured and mitigated results of the circuit for three qubits and $\theta = \pi/12$. Mitigating the measurement errors gives us no gain.

As we can see mitigating the measurement errors gives no gain in precision which in turn implies that most of the errors occur during the logical operations.

What we can take from these results is that while theoretically feasible it is still not possible for current devices to execute our circuit with satisfactory precision for a high number of qubits. One could think to run error correcting codes to fix the bit and phase flip errors for our circuit, but the unfortunate reality is that we would not only need error rates below the current threshold but also increase the number of available qubits in the computer while reserving some just to execute error correction.

As an example, if we consider the Shor code for error correction we would need eight ancillary qubits per useful data qubit, which would make it impossible to execute in the available IBM computers. Let us say then that we want to fix just the bit flip errors, still we would need to do so with two ancillary qubits per data qubit [25]. The amount of necessary qubits to compute the circuit would triplicate just to fix bit flips, so currently we simply do not have the necessary overhead to correct the errors and the available devices are not fault tolerant enough to ignore the need for corrections.

On the upside, this approach to interferometry still gives us the flexibility of being easily adaptable to any universal quantum computer granted we can write our circuit in the required basis. This means that if a future device or computational model that is more resilient to errors is discovered we can possibly implement our circuit. Next we will study how we can implement this interferometer for a model based on quasi-particles with non-abelian exchange statistics, anyons, which have interesting applications in quantum information due to its stability and resilience against decoherence [5].

The reader can find excerpts of the code used in this section in Appendix A.

3

Anyons and quantum computers

In the previous chapter we discussed interferometry in the context of particles in three dimensions, bosons and fermions. Those particles have the property of being indistinguishable, every photon is the exact same. This leads to an interesting effect, exchange symmetry.

As we have mentioned before, if two bosons are exchanged (positions swapped) the physical system is the exact same as before as it acquires a global phase $+1$. For fermions something similar is true, under exchanges the new wavefunction for the system acquires a -1 global phase. These are consequences of each particle being described by Bose and Fermi-Dirac statistics respectively.

We will be interested in indistinguishable particles in two dimensions. These can have generalized statistics, which are neither bosonic, nor fermionic. We call such particles anyons and exchanges between them produce non-trivial effects on the system's wave-function. This opens up new theoretical possibilities, specifically in the field of fault tolerant quantum computation. We must also mention that anyons are experimentally feasible with the most recent notable realization involving the Quantum Hall Effect [15].

As a starting point we will discuss the Aharonov-Bohm effect as a physical model of anyon statistics.

3.0.1

The Aharonov-Bohm Effect

The effect was first proposed by Yakir Aharonov and David Bohm in 1959 [26]. It relates to a phase shift acquired by a particle when taken adiabatically around a solenoid. To better understand the effects of restricting ourselves to two dimensions we shall do a 2D analysis of the effect as presented by Preskill [15].

In the two dimensional case the solenoid is replaced by a point-like "flux tube" of magnetic flux Φ . Suppose then that an electric charge q completes a counterclockwise rotation around the "flux tube", Quantum mechanics predicts that the wave-function acquires a phase $e^{iq\Phi}$. This is the Aharonov-Bohm effect and the phase is known as a "topological phase", since it is invariant under continuous deformations of the path taken by the electric charge.

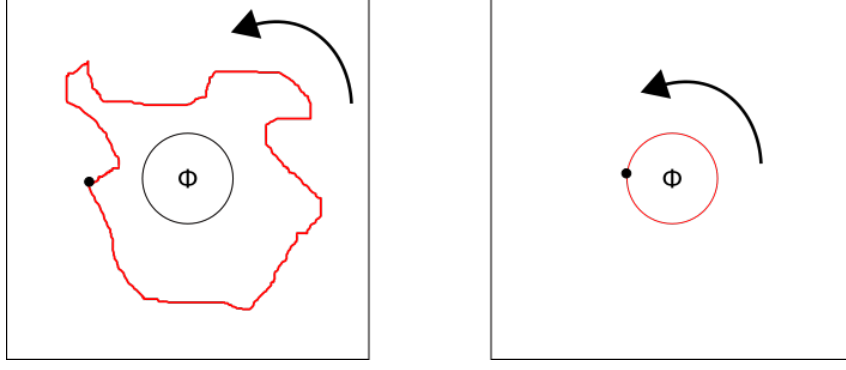


Figure 3.1: Diagram illustrating the 2D Aharonov-Bohm Effect in the unbound and bound cases. The particle follows the red path in the direction of the arrow around a solenoid represented by the cylinder. In both cases the topological phase is the same. It is independent of the path taken.

Now suppose that the charge and flux are bound together, meaning the electric charge q is now stuck to an impenetrable wall that contains flux Φ . This can be seen in figure 3.1. Rotating the charge around that wall by an angle of 2π is equivalent to the unitary transformation:

$$U(2\pi) = e^{-i2\pi J} = e^{iq\Phi}, \quad (3-1)$$

where J is the total angular momentum. The eigenvalues then become:

$$J = m - \frac{q\Phi}{2\pi}, \quad (3-2)$$

for integer m . We can then define $\theta = q\Phi \bmod 2\pi$, which means that eigenvalues of J are then shifted from integer values by $-\theta/2\pi$.

The above result is as expected. To understand why, consider an example: Imagine a particle orbiting around a solenoid in the $x - y$ plane. Its angular momentum around the rotation axis is quantized according to $l_z = m$. If a current is slowly turned on then an electric field on the plane takes the form $\vec{E}(\vec{r}) = -\frac{\hat{z} \times \vec{r} \Phi}{2\pi(x^2 + y^2)}$ according to Faraday's law. Then the change in angular momentum has to be of the form $\dot{l}_z = [\vec{r} \times (q\vec{E})]_z = -\frac{q\Phi}{2\pi}$, which means that changes in the angular momentum depend only on the flux Φ . So again, $l_z = m - \frac{q\Phi}{2\pi}$ which is the same quantized form obtained previously [4].

Consider now a composite system. Imagine two charged particles tightly bound to a solenoid, where we take the forces between the charges to be small perturbations, meaning $q \rightarrow 0$ for fixed $q\Phi$. In a manner analogous to equation (3-1) rotating both charges by an angle of 2π is equivalent to:

$$U(2\pi) = e^{-i4\pi J} = e^{2iq\Phi}. \quad (3-3)$$

Now the interesting takeaway is that in three dimensions θ is restricted to

0 and π . This comes from the property of the rotation group $SO(3)$, any closed path beginning at identity and ending at a 4π rotation can be contracted to a trivial path. So 4π rotations are the identity operation, which means that 2π rotations have $+1$ and -1 eigenvalues (bosons and fermions respectively). This however is not true for rotations in two dimensions $SO(2)$ [15] and, consequently, θ can assume any value.

From what we have seen on the previous chapter one can start to make a clear connection between spin number and the statistics of a particle. Bosons, which have integer spin, obey bosonic statistics and fermions, which have half-integer spin, obey fermionic statistics. Interestingly enough, we have just discussed particles in two dimensions that can have fractional spin dependent on the phase θ . What does that mean for their statistics and exchange symmetry?

Assume that we exchange two particle-flux composites around each other. This is equivalent to each particle being rotated by π around one of the fluxes Φ . Each one of the particles will then acquire a phase equivalent to half of a complete revolution. Adding together both phases we find that the wave-function that describes the system changes by $e^{i\frac{\theta}{2}+i\frac{\theta}{2}} = e^{i\theta} = e^{-i2\pi J}$. This means that, in this context, exchanging two objects is the same as rotating one by 2π . This implies that particles with fractional statistics have fractional spin.

3.1 Abelian Anyons

Particles that obey generalized statistics were first called anyons by Frank Wilczek in 1982 [27] precisely because exchanging them can give "any" phase. A simple way to summarize this and the idea discussed in the previous section is the following. Assume $|\psi_1\psi_2\psi_3...\psi_i\rangle$ is the wave function for a system of i anyons confined to two dimensions. A two-anyon system could then be described by $|\psi_1\psi_2\rangle$. Suppose then that we exchange both particles and now the system can be described by:

$$|\psi_2\psi_1\rangle = e^{i\theta}|\psi_1\psi_2\rangle, \quad (3-4)$$

where θ is the anyonic phase or topological phase from before. Note that we can recover bosonic and fermionic results by setting $\theta = 2n\pi$ and $\theta = (2n+1)\pi$ respectively for integer n .

As mentioned before we can closely link this to spin by doing $\theta = 2\pi s$ where s stands for the spin number of the particle:

$$e^{i\theta}|\psi_1\psi_2\rangle = e^{i2\pi s}|\psi_1\psi_2\rangle = (-1)^{2s}|\psi_1\psi_2\rangle, \quad (3-5)$$

where s has integer values for bosons and semi-integer for fermions, again recovering the known results for those statistics.

It is important to note as well that: (1) Charges in this context are labels assigned to each particle (2) Anyons are charged particles and its charges are locally conserved and (3) There are no long range interactions between anyons mediated by other particles.

Another point of interest is that one can take the permutation operators (+1 and -1) of bosons and fermions and see that they form the group known as the permutation group S_n , where n is the number of indistinguishable particles. On the other hand, anyonic permutation operator ($e^{i\theta}$) will form a more interesting group known as the Braid group B_n [28]. Going forward we will define it and see how it actually forms a mathematical group.

3.1.1

Braid Group

Before proceeding with definition it is worth to consider our motivations. We want to be able to calculate transition probabilities between quantum states by summing over particle histories, much like a Feynman path integral. So to connect this idea to a Braid group we must think of each braid as a way to represent every particle and their history and our path integral simply becomes an integral over every braid.

First let us consider a system of n indistinguishable particles confined to a 2D surface. Imagine that such surface also has n vacancies or holes that the particles can occupy. Particles cannot be outside of their holes and each hole only supports one particle, which means that every hole is occupied and particles can only be exchanged. This is equivalent to saying that these particles have a "hard-core interaction" and can't occupy the same space.

Normally, to calculate the probability amplitudes for this system we would consider the evolution of every particle through time over all the classical paths to achieve the final state and sum those histories while weighted by the phase e^{iS} , where S stands for the classical action.

To add to the previous statement, we also associate a particle and its history to a world line that will tell us its complete path from beginning to end. Each particle is then given a strand and permutations of particles will be defined as braids of those strands. This way we can define each braid as an element of our group. But to define a group we need to go further and also choose a group operation.

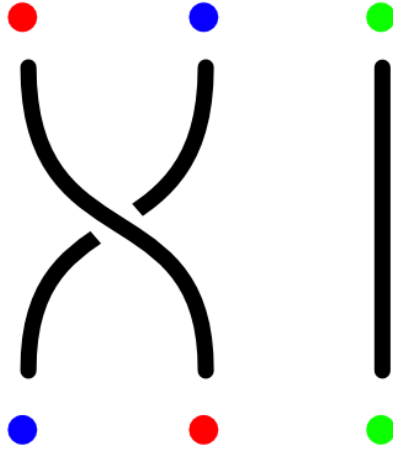


Figure 3.2: Braiding group element. Each colored dot represents a particle. Counterclockwise exchange of the blue and red particles.

First it is important to note what distinguishes elements in the group. Say we modify the exchange in figure 3.2 to a clockwise exchange as in figure 3.3 (c), we no longer have the same element, on the other hand we can push and pull strands to deform the braid and this wouldn't modify the braiding as in figure 3.3 (b). Now let us define an operation as simply the composition of braids. One can achieve any braid by simply concatenating various different elements as in figure 3.4.

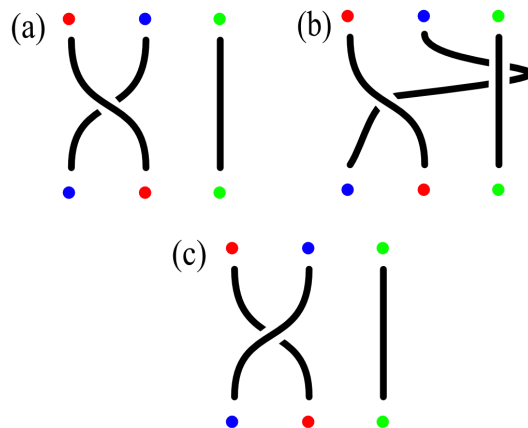


Figure 3.3: A braiding can be deformed and still be the same element. While braiding (a) and (b) are the same, braiding (c) is another element altogether

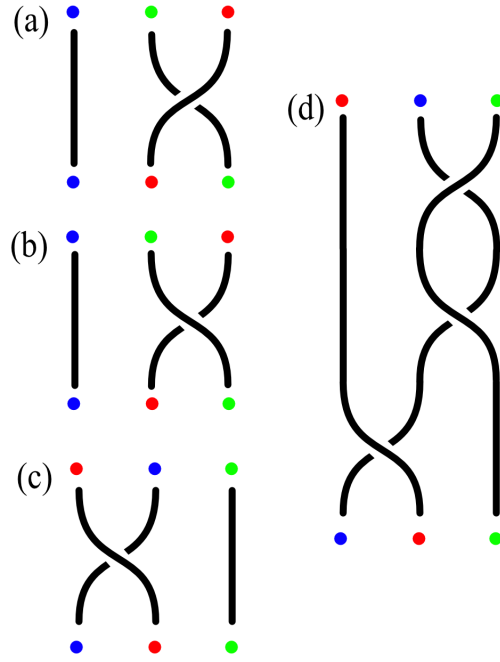


Figure 3.4: Concatenating braids. Braiding (d) is done by concatenating (c), (b) and (a) in that order

To make absolutely sure that this is, in fact, a group we must guarantee that it also satisfies what is known as the group axioms of which there are four:

- **Closure:** The result of the operation between two set elements must remain in the set. This is easily seen above when we defined the concatenation operation.
- **Associativity:** "Groupings" of the elements of the set shouldn't affect the outcome of an operation. This can be seen from figure 3.4. Note that $[(c) + (b)] + (a) = (c) + [(b) + (a)]$; where $+$ represents our group operation, not addition.
- **Identity element:** There is an element e in the set such that $e + a = a + e$ for every element a in the set. This is equivalent to a braiding with completely vertical strands where no exchange occurs.
- **Inverse element:** For each element a in the set there exists an element b in the set such that $a + b = b + a = e$. This is the braid that undoes another. In figure 3.3 note that (c) undoes (a) and vice-versa: $(a) + (c) = (c) + (a) = e$.

This forms an infinite group known as the Braid group B_n where n is the number of strands or particles. It is important to understand that with the properties above we can create this group from a set of generators that

have relations among them. First, consider that each strand/particle is ordered in a line with labeled positions, we then define operators σ_n that represents the counterclockwise exchange of the n -th particle with the $(n+1)$ -th particle. This way it is possible to create any braid by simply concatenating σ operators, which means we are simply doing successive exchanges.

The exchanges defined as the σ operators are the group generators. They can generate any element in the group if properly arranged. More interestingly these generators are constrained by two important relations. The first one is simply:

$$\sigma_i \sigma_j = \sigma_j \sigma_i, \quad |i - j| \geq 2. \quad (3-6)$$

This says that exchanges between non-neighbouring strands commute. Consider the example: σ_1 exchanges strands 1 and 2 while σ_3 exchanges strands 3 and 4. The order of these operations is irrelevant as one exchange does not affect the other, but the same could not be said about σ_1 and σ_2 .

The second, more important one, is:

$$\sigma_i \sigma_{i+1} \sigma_i = \sigma_{i+1} \sigma_i \sigma_{i+1}. \quad (3-7)$$

This is known as the Yang-Baxter relation and is shown on figure 3.5. It simply describes an exchange of particles adjacent to an in-between particle that leaves the middle one unchanged. For example: The relation $\sigma_1 \sigma_2 \sigma_1 = \sigma_2 \sigma_1 \sigma_2$ is true as both of those operations are exchanging particles 1 and 3 while leaving 2 in the original position.

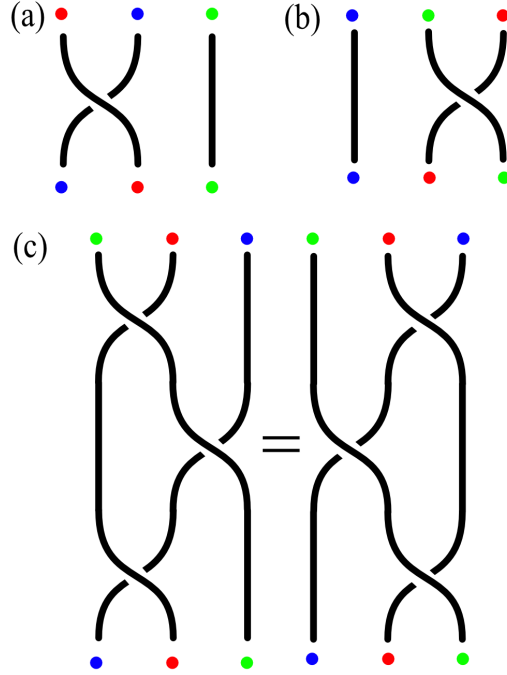


Figure 3.5: Yang-Baxter relation. (a) and (b) are the group generators σ_1 and σ_2 respectively. (c) is a graphical representation of the relation $\sigma_1 \sigma_2 \sigma_1 = \sigma_2 \sigma_1 \sigma_2$

What we have discussed above is the one dimensional braid group which we can see as a representation of the Hilbert space created by a system of anyons. We can go even further and state that, for abelian anyons, we can associate the generator of the braid group B_n with the anyonic phase like so: $\sigma_j = e^{i\theta_j}$.

We can also see that, due to the Yang-Baxter relations, $e^{i\theta_j} = e^{i\theta_{j+1}} = e^{i\theta}$ which should be expected. As the particles are indistinguishable it would make no sense for the exchange phase to be able to distinguish them. Observe as well that for $\theta = 0$ and $\theta = \pi$ we recover bosons and fermions but also something deeper. Bosons and fermions are in fact the representation of another one-dimensional group, but with generators $+1$ and -1 respectively, this is the permutation group S_n we mentioned before.

3.1.2

Particle Fusion

We mentioned before that anyons locally conserve their charge which motivates us to question what happens when we join anyons together to obtain new charges, we will call this operation fusion. We are specifically interested in how the statistics of the new system change. For abelian anyons the answer

becomes quite simple as the fused charge can be uniquely generated. We will show later how that might not always be the case.

Consider one system of two indistinguishable anyons, as previously seen, exchanging them with one another causes the system to pick up a phase $e^{i\theta}$. Now let us create a duplicate of the system and fuse the pairs of anyons on the original and the copy. We now have a new system of two composite anyons that we can then exchange but now the phase acquired upon exchange becomes $e^{i4\theta}$ as we have four exchanges of individual anyons with each contributing $e^{i\theta}$.

One can then generalize this relation and say that for a fusion of N indistinguishable abelian anyons with statistic operators $e^{i\theta}$ the new composite system will create a phase of $e^{iN^2\theta}$.

3.2

Non-Abelian Anyons

To talk about non-abelian anyons we first need to go back to our analogy with the Aharonov-Bohm effect. This time we will consider a non-abelian superconductor of two dimensions, in this conductor we will find fluxons (particles that carry a magnetic flux) and chargeons (particles that carry charge). This is a toy-model to better understand what are the consequences of working with Non-abelian effects.

Let us now consider a particular chargeon C . We say this state/chargeon has dimension $|C|$ and define a basis for it:

$$|C, i\rangle, \quad i = 1, 2, \dots |C|. \quad (3-8)$$

Now we move this chargeon through an enclosed path around a fluxon F . The resulting state is no longer the same, it changes accordingly:

$$|C, j\rangle \rightarrow \sum_{i=1}^{|C|} |C, i\rangle U_{ij}^C(F), \quad (3-9)$$

where $U_{ij}^C(F)$ is an unitary matrix that rotates the original state. Note that this is remarkably different from the previous case of abelian anyons. Previously our state would not change with the exception of the added phase, but now we have a completely new state.

For the definition of abelian anyons we focused on two things: (1) How we can exchange two particles and its effect on the system and (2) How we can fuse two particles and its effects on the charge and statistics of the composite system. We are going to call these two braiding rules and fusion rules respectively and will try to encounter similar relations for non-abelian anyons.

Before proceeding, we must be more precise with our definition of charge for anyons. Charge here is nothing more than a label, one particle will have a specific charge denoted by letters $\{a, b, c, \dots\}$, the set of possible charges will always be finite for us, charges are locally conserved, so it can only be changed by short-range interactions with other particles. We also have a special label, the identity label 1, which means absence of charge and, by definition, particle. Charge conjugation is an allowed operation and the conjugate charge of a is denoted by \bar{a} . Like we did in the previous section we can consider our particles ordered in a horizontal line each with their respective label/charge.

3.2.1

Fusion Rules

Let us now focus on the fusion rules. In the case of abelian anyons we mentioned that there is only one way to fuse particles. This is not the case for non-abelian anyons. A more general way to represent the fusion rules between two charged particles a and b is:

$$a \times b = \sum_c N_{ab}^c c. \quad (3-10)$$

For N_{ab}^c being a non negative integer that represent how many ways a and b can fuse into c and the sum being over the set of all possible charges c . The \times sign does not represent a tensor product and the sum on the right side is not a direct sum, this is an abstract relation that maps $(a, b; c)$ into N_{ab}^c . For abelian anyons we have that $N_{ab}^c = 0$ for all labels c except for one in which $N_{ab}^c = 1$. This means that there is only one possible way to fuse those particles. In other words applying this equation to fusing n abelian anyons with k abelian anyons of statistics $\theta = \frac{\pi}{m}$ for integer m :

$$a \times b = \theta \times \theta = \frac{n^2 \pi}{m} \times \frac{k^2 \pi}{m} = \frac{(n+k)^2 \pi}{m}. \quad (3-11)$$

As expected $N_{nk}^n = N_{nk}^k = 0$ and $N_{nk}^{n+k} = 1$. This is completely analogous to the way we presented fusions in the previous section. Two particles of statistics θ will fuse into a composite of statistic 4θ as is the case for $n = k = 1$.

The same is not true for non-abelian anyons ($\sum_c N_{ab}^c > 1$) and this is the fundamental way in which they differ. This notion might seem odd at first. How can two charges fuse in different ways? In reality this isn't much different from spin addition, for example two spin 1/2 particles can fuse into either a spin-0 or spin-1 particle.

To define an anyon model we have to set what our possible charges are and then define the fusion rules between them, the fusion rules we settle on

are what decide if our model is abelian or not. In order to clarify let us work with some examples.

For our first example consider a model with three different anyons with labels 0, $\frac{1}{2}$ and 1 where 0 stands for the identity charge. The fusion rules are as follows:

$$\frac{1}{2} \times \frac{1}{2} = 0N_{\frac{1}{2}\frac{1}{2}}^0 + \frac{1}{2}N_{\frac{1}{2}\frac{1}{2}}^{\frac{1}{2}} + 1N_{\frac{1}{2}\frac{1}{2}}^1 = 0 \cdot 1 + \frac{1}{2} \cdot 0 + 1 \cdot 1 = 0 + 1, \quad (3-12a)$$

$$\frac{1}{2} \times 1 = 0N_{\frac{1}{2}1}^0 + \frac{1}{2}N_{\frac{1}{2}1}^{\frac{1}{2}} + 1N_{\frac{1}{2}1}^1 = 0 \cdot 0 + \frac{1}{2} \cdot 1 + 1 \cdot 0 = \frac{1}{2}, \quad (3-12b)$$

$$1 \times 1 = 0N_{11}^0 + \frac{1}{2}N_{11}^{\frac{1}{2}} + 1N_{11}^1 = 0 \cdot 1 + \frac{1}{2} \cdot 0 + 1 \cdot 0 = 0. \quad (3-12c)$$

Note that this is remarkably similar to spin addition because these are also similar to decomposition rules for tensor products of SU(2) with the only difference being that 1 is the maximum "spin" (which is shown by $\frac{1}{2} \times 1 = \frac{1}{2}$ and $1 \times 1 = 0$). We have chosen not to write trivial fusion rules that involve the identity charge.

For another example consider a model with two possible charges, 1 and 2, where 1 is the identity charge and let us write the fusion rules:

$$1 \times 1 = 1N_{11}^1 + 2N_{11}^2 = 1 \cdot 1 + 2 \cdot 0 = 1, \quad (3-13a)$$

$$1 \times 2 = 1N_{12}^1 + 2N_{12}^2 = 1 \cdot 0 + 2 \cdot 1 = 2, \quad (3-13b)$$

$$2 \times 2 = 1N_{22}^1 + 2N_{22}^2 = 1 \cdot 1 + 2 \cdot 1 = 1 + 2. \quad (3-13c)$$

What this essentially means is that no particles fuse into no particle, one particle with no particle fuse into one particle, and one particle with one particle fuse into one particle or no particle. The only non-trivial rules is the last one as we have $N_{22}^1 = N_{22}^2 = 1$. We shall go back to these relations later as this model is of special interest.

What is more relevant is that one can take N_{ab}^c and construct an orthonormal basis for a Hilbert space V_{ab}^c called fusion space. We represent these states in such a way:

$$|ab; c, \mu\rangle, \quad \mu = 1, 2, \dots, N_{ab}^c, \quad (3-14)$$

where μ represents one of the allowed forms for the fusion. Note that the dimension of fusion space V_{ab}^c is given by how many way a and b can fuse into c (N_{ab}^c). It is also worth noting that there is a dual vector space V_c^{ab} that describe particle splitting.

As expected the basis elements will be orthogonal and the base is

complete:

$$\langle ab; c', \mu' | ab; c, \mu \rangle = \delta_c^{c'} \delta_\mu^{\mu'}, \quad (3-15a)$$

$$\sum_{c, \mu} |ab; c, \mu \rangle \langle ab; c, \mu| = I_{ab}. \quad (3-15b)$$

Where I_{ab} is the projector onto space $\bigoplus_c V_{ab}^c$. Note that equation (3-15a) represents particle c' splitting and refusing into c , which is only possible if $c' = c$ and $\mu = \mu'$. Also equation (3-15b) represents particles a and b fusing and re-splitting in every possible way.

Note that we can raise and lower indices by conjugating the labels, i.e $V_{ab}^c \cong V_{ab\bar{c}}^1$ to get isomorphic spaces, this is equivalent to fusing particles a , b and \bar{c} to get the identity charge.

This leads to interesting relations:

$$V_{a1}^a \cong V_{a\bar{a}}^1, \quad (3-16a)$$

$$V_{a1}^a \cong V_1^{a\bar{a}}. \quad (3-16b)$$

Equation (3-16a) gives us the only way we can fuse a particle with another to obtain 1 and equation (3-16b) tells us that when created in a vacuum particles have conjugate charges.

The most important result we can take from all this is the ability to ascertain if we are talking about abelian or non abelian anyons simply by looking at the fusion rules. Consider the following relation:

$$\dim \left(\bigoplus_c V_{ab}^c \right) = \sum_c N_{ab}^c \geq 2. \quad (3-17)$$

if the above holds for at least one ab pair, then we are talking about non-abelian anyons.

Before proceeding further we must note another property of fusions, associativity:

$$(a \times b) \times c = a \times (b \times c). \quad (3-18)$$

Physically this makes perfect sense. The total charge of a complete system is an intrinsic characteristic of itself so the order of fusions shouldn't affect the final charge.

To better understand this we can begin by decomposing the total fusion space in terms of fusions spaces of particle pairs:

$$V_{abc}^d \cong \bigoplus_e V_{ab}^e \otimes V_{ec}^d \cong \bigoplus_{e'} V_{ae'}^d \otimes V_{bc}^{e'}. \quad (3-19)$$

This is the same thing as describing V_{abc}^d in two different bases:

$$|(ab)c \rightarrow d; e, \mu\nu\rangle \equiv |ab; e, \mu\rangle \otimes |ec; d, \nu\rangle, \quad (3-20a)$$

$$|a(bc) \rightarrow d; e', \mu'\nu'\rangle \equiv |ae'; d, \nu'\rangle \otimes |bc; e', \mu'\rangle. \quad (3-20b)$$

We can then relate the two bases with a unitary transformation F :

$$F : |(ab)c \rightarrow d; e, \mu\nu\rangle = \sum_{e', \mu', \nu'} |a(bc) \rightarrow d; e', \mu'\nu'\rangle \left(F_{abc}^d\right)_{e\mu\nu}^{e'\mu'\nu'}. \quad (3-21)$$

Where $\left(F_{abc}^d\right)_{e\mu\nu}^{e'\mu'\nu'}$ is a unitary matrix which we simply call the F -matrix. Normally the F -matrix can be found by utilizing what is called as "The pentagon equation", we shall not delve on specifics about its calculation but it relies on the fact that one can do different series of basis changes to a system of four anyons and still obtain the same result [15].

3.2.2

Braiding Rules

As we have seen, exchanging particles in an anyon system has a non-trivial effect on the system's wavefunction. With abelian anyons we saw that exchanging two particles created a phase $e^{i\theta}$ in the original state according to the fractional statistics. For the non-abelian case we ended up with a new rotated state. This situation begs us to create more general rules that can describe both cases. These are called braiding rules.

When we exchange the positions of two particles a and b their total charge c remains unchanged, but the fusion space is no longer the same: The space V_{ab}^c now changes to V_{ba}^c . We can then create a map between the two fusion spaces:

$$R : |ba; c, \mu\rangle \rightarrow \sum_{\mu'} |ab; c, \mu'\rangle (R_{ab}^c)_{\mu}^{\mu'}. \quad (3-22)$$

Where $(R_{ab}^c)_{\mu}^{\mu'}$ is a unitary matrix that we call the R -matrix. Normally the R -matrix can be found utilizing the so-called "hexagon equation", but once again we will not go into the details of this derivation here but it relies on similar properties required for the pentagon equation. We utilize a three anyon system and execute two different sequences of basis changes and braidings that produce the same result [15]. Note that this relation is analogous to equation (3-9).

It is interesting to see what happens to this relation when we are dealing with abelian anyons. In that case there is only one possible way to fuse them, so the sum over μ' becomes one term. This also means $(R_{ab}^c)_{\mu}^{\mu'}$ is no longer a matrix, but a number we are already familiar with:

$$R : |ba; c, \mu\rangle \rightarrow |ab; c, \mu\rangle R_{ab}^c = |ab; c, \mu\rangle e^{i\theta}. \quad (3-23)$$

Next we discuss what is the simplest non-abelian anyon model capable of universal quantum computation. As we will see the F and R matrices play an important role.

3.3

Computation and Fibonacci Anyons

We are interested in the possibilities of creating a universal quantum computer with a suitable anyon model and Fibonacci anyons provide us with the simplest model capable of doing so. Quantum computation allows us to implement the NOON-like interferometer described in the previous chapter and, in particular, verify if there are any advantages in doing such metrology experiments with particles that obey anyonic statistics over more conventional approaches.

The literature is very extensive on this specific model [15, 29, 30, 31]. So for that reason we shall present a more reduced and direct approach focusing on introducing the model and its most important features. As a result most of the discussion below is based on the work of Nayak et al [6]

In our model there are two types of labels, 1 and γ , with 1 being the identity label. We end up with only one non-trivial fusion rule:

$$\gamma \times \gamma = 1 + \gamma. \quad (3-24)$$

This might seem familiar to the reader, it is the same model as in our second example in section 3.2.1. This model receives its name from the fact a system with n particles has a fusion space $V_{\gamma^n}^1$ of dimension $Fib(n)$, where $Fib(n)$ gives the n -th term of a Fibonacci sequence. To see this consider that our n anyons are ordered in a line each with its respective label and look at the dimension $N_{\gamma^n}^1$ of fusion space $V_{\gamma^n}^1$. If we progressively fuse every pair of particles note that if the first fusion yields trivial charge 1 then the remaining $n - 2$ can fuse in $N_{\gamma^{n-2}}^1$ ways and if the first fusion is nontrivial then the remaining labels can only fuse in $N_{\gamma^{n-1}}^1$ ways. This way we get the following recursive relation:

$$N_{\gamma^n}^1 = N_{\gamma^{n-1}}^1 + N_{\gamma^{n-2}}^1. \quad (3-25)$$

Note as well that $N_{\gamma}^1 = 0$ as if we only have one particle it can't change labels and that $N_{\gamma^2}^1 = 1$. This way we get:

$$\begin{aligned} n &= 1, 2, 3, 4, 5, 6, 7, 8, 9, \dots \\ N_{\gamma^n}^1 &= 0, 1, 1, 2, 3, 5, 8, 13, 21, \dots \end{aligned} \quad (3-26)$$

This means that the dimension of fusion space $V_{\gamma^n}^1$ grows in an equivalent way to a Fibonacci sequence, which grows, approximately, according to "the golden ratio" given by $\phi = \frac{1}{2}(1 + \sqrt{5}) \approx 1.618$. The quantity ϕ will also be called the quantum dimension d_γ for Fibonacci anyons as it tells us the rate at which the fusion space dimension increases.

To further define our model we need to find both the F-matrix and R-matrix. This is equivalent to understanding the basis changes between the possible fusion spaces and the effects braiding might have on our system. As mentioned before, normally one would need to solve both the pentagon equation and the hexagon equation, but we shall opt for a more straight forward approach.

At this point we introduce a new notation and start to write our states as $|(\bullet, \bullet)_1\rangle$ and $|(\bullet, \bullet)_\gamma\rangle$ where each dot represents a particle of charge γ , a parentheses a fusion and the sub-index the resulting label of the fusion. This notation is taken from Nayak et al. [6] but is also used extensively by other researchers.

Note that in this scheme if we add a third particle there are only three possible outcomes: $|((\bullet, \bullet)_1, \bullet)_\gamma\rangle$, $|((\bullet, \bullet)_\gamma, \bullet)_\gamma\rangle$ and $|((\bullet, \bullet)_\gamma, \bullet)_1\rangle$. Let us also write equation (3-21) for the F-matrix, in this new notation:

$$|(\bullet, (\bullet, \bullet)_i)_k\rangle = \sum_j [F_{\gamma\gamma\gamma}^k]_{ij} |((\bullet, \bullet)_j, \bullet)_k\rangle, \quad i, j, k = \{1, \gamma\}. \quad (3-27)$$

One should note here that the states above form bases on a 3D Hilbert space. In one basis the rightmost particles fuse first and in another the leftmost fuse first and both bases are connected via the F-matrix. If our particles are fusing to 1 then for Fibonacci anyons the following occurs according to the fusion rules:

$$|(\bullet, (\bullet, \bullet)_\gamma)_1\rangle = |(\bullet, \bullet)_\gamma, \bullet)_1\rangle. \quad (3-28)$$

As on both bases we have only a single state with total label 1. Which means that $F_{\gamma\gamma\gamma}^1$ is simply a 1x1 "matrix" of value 1. Not only that but as described by equation (3-27) $F_{\gamma\gamma\gamma}^\gamma$ has to take a two-by-two form because there are two states on both bases with total label γ .

To find the F-matrix let us consider the following example:

$$\begin{aligned} |(\bullet(\bullet, (\bullet, \bullet)_1)_\gamma)_1\rangle &= |((\bullet, \bullet)_1, (\bullet, \bullet)_1)_1\rangle \\ &= |(((\bullet, \bullet)_1, \bullet)_\gamma, \bullet)_1\rangle. \end{aligned} \quad (3-29)$$

This is simply the different ways we can fuse four particles and still have total charge 1, an example of associativity that we can find the same way we did

for example (3-28). Using equation (3-27) we can write the above example as:

$$\begin{aligned}
 |(\bullet(\bullet, (\bullet, \bullet)_1)_\gamma)_1\rangle &= F_{11}|(\bullet((\bullet, \bullet)_1, \bullet)_\gamma)_1\rangle + F_{1\gamma}|(\bullet((\bullet, \bullet)_\gamma, \bullet)_\gamma)_1\rangle = (3-30) \\
 &= F_{11}|((\bullet, (\bullet, \bullet)_1)_\gamma, \bullet)_1\rangle + F_{1\gamma}|((\bullet, (\bullet, \bullet)_\gamma)_\gamma, \bullet)_1\rangle = \\
 &= \sum_j (F_{11}F_{1j} + F_{1\gamma}F_{\gamma j})|((\bullet, \bullet)_j, \bullet)_\gamma, \bullet)_1\rangle.
 \end{aligned}$$

From that we conclude $F_{1\gamma}(F_{11} + F_{\gamma\gamma}) = 0$ and $F_{11}F_{11} + F_{1\gamma}F_{\gamma 1} = 1$. These are just two of the relations we can obtain from the pentagon equation we mentioned earlier which are called "consistency conditions" or "consistency identities". This also means that $F_{\gamma\gamma}^\gamma$ is non-trivial.

We will not solve for the remaining conditions but as mentioned before one can find the general equation in [15]. Using the other condition that the F-matrix must also be unitary we get the following form for Fibonacci anyons:

$$F_{\gamma\gamma}^\gamma = \begin{pmatrix} F_{11} & F_{1\gamma} \\ F_{\gamma 1} & F_{\gamma\gamma} \end{pmatrix} = \begin{pmatrix} \phi^{-1} & \sqrt{\phi^{-1}} \\ \sqrt{\phi^{-1}} & -\phi^{-1} \end{pmatrix}. \quad (3-31)$$

where ϕ is the golden ratio presented earlier.

The next step is to find the R-matrix. Normally those values would be determined by the aforementioned hexagon equation and the consistency identities that derive from it, we shall not be presenting it in full detail. For a brief explanation we can say that the hexagon equation relies on knowing the F-matrix first and ensuring that we can arrive at the same results by braiding in between two basis changes or changing base in between two braidings, this is equivalent to saying that $RFR = FRF$.

Let us write equation (3-22) in the new notation as well:

$$|(\bullet, \bullet)_i\rangle = [R_{\gamma\gamma}^i]_{ii}|(\bullet, \bullet)_i\rangle, \quad i = \{1, \gamma\}. \quad (3-32)$$

Note that the states on the left and on the right are not the same, the particles are now switched. The sum now disappears as there is only one way to fuse the particles for each charge. This means that, much like the F-matrix, the R-matrix is not only 2x2 but also block diagonal and there are only two 1x1 blocks, one where the total charge is 1 ($R^1 = [R_{\gamma\gamma}^1]_{11}$) and another for total charge γ ($R^\gamma = [R_{\gamma\gamma}^\gamma]_{\gamma\gamma}$).

Now we can apply the relation $RFR = FRF$ and get the following

equations:

$$R^1 F_{11} R^1 = F_{11} F_{11} + F_{1\gamma} R^1 F_{\gamma 1}, \quad (3-33a)$$

$$R^1 F_{1\gamma} R^\gamma = F_{11} F_{1\gamma} + F_{1\gamma} R^\gamma F_{\gamma\gamma}, \quad (3-33b)$$

$$R^\gamma F_{\gamma 1} R^1 = F_{\gamma 1} F_{11} + F_{\gamma\gamma} R^\gamma F_{\gamma 1}, \quad (3-33c)$$

$$R^\gamma F_{\gamma\gamma} R^\gamma = F_{\gamma 1} F_{1\gamma} + F_{\gamma\gamma} R^\gamma F_{\gamma\gamma}. \quad (3-33d)$$

Then using the F-matrix from before we find the two eigenvalues of the R-matrix:

$$R|(\bullet, \bullet)_1\rangle = e^{-4i\pi/5}|(\bullet, \bullet)_1\rangle, \quad (3-34a)$$

$$R|(\bullet, \bullet)_\gamma\rangle = -e^{-2i\pi/5}|(\bullet, \bullet)_\gamma\rangle. \quad (3-34b)$$

So the block diagonal form of the R-matrix in this basis is:

$$R = \begin{pmatrix} [R_{\gamma\gamma}^1]_{11} & [R_{\gamma\gamma}^1]_{1\gamma} \\ [R_{\gamma\gamma}^\gamma]_{\gamma 1} & [R_{\gamma\gamma}^\gamma]_{\gamma\gamma} \end{pmatrix} = \begin{pmatrix} e^{-4i\pi/5} & 0 \\ 0 & -e^{-2i\pi/5} \end{pmatrix}. \quad (3-35)$$

Note that the conjugate eigenvalues are also a solution, these will represent braidings in the opposite direction. We have to define the signs for clockwise and counter-clockwise exchanges, the ones presented above are normally used for clockwise exchanges.

Unfortunately for us this won't be true every time as we see in the following example: Consider the state: $|((\bullet, \bullet)_1, \bullet)_\gamma\rangle$. it is simple enough to exchange the two left-most particles with the R-matrix as it has a block diagonal form. More specifically in this new basis it has the following eigenvalues and eigenvectors:

$$R|((\bullet, \bullet)_1, \bullet)_\gamma\rangle = e^{-4i\pi/5}|((\bullet, \bullet)_1, \bullet)_\gamma\rangle, \quad (3-36a)$$

$$R|((\bullet, \bullet)_\gamma, \bullet)_\gamma\rangle = -e^{-2i\pi/5}|((\bullet, \bullet)_\gamma, \bullet)_\gamma\rangle, \quad (3-36b)$$

$$R|((\bullet, \bullet)_\gamma, \bullet)_1\rangle = -e^{-2i\pi/5}|((\bullet, \bullet)_\gamma, \bullet)_1\rangle. \quad (3-36c)$$

So the matrix becomes:

$$R = \begin{pmatrix} e^{-4i\pi/5} & 0 & 0 \\ 0 & -e^{-2i\pi/5} & 0 \\ 0 & 0 & -e^{-2i\pi/5} \end{pmatrix}. \quad (3-37)$$

Let us now try to exchange the two rightmost particles. The new R-matrix no longer has a block diagonal form as $|((\bullet, \bullet)_1, \bullet)_\gamma\rangle$ is no longer one of the eigenvectors. The easiest approach then is to write our state in the eigenbasis for the new R-matrix which we do with the F-matrix and equation

(3-27):

$$|((\bullet, \bullet)_1, \bullet)_\gamma\rangle = F_{11}|(\bullet, (\bullet, \bullet)_1)_\gamma\rangle + F_{\gamma 1}|(\bullet, (\bullet, \bullet)_\gamma)_\gamma\rangle. \quad (3-38)$$

We can write this basis change as:

$$\begin{pmatrix} |((\bullet, \bullet)_1, \bullet)_\gamma\rangle \\ |((\bullet, \bullet)_\gamma, \bullet)_\gamma\rangle \\ |((\bullet, \bullet)_\gamma, \bullet)_1\rangle \end{pmatrix} = \begin{pmatrix} \phi^{-1} & \sqrt{\phi^{-1}} & 0 \\ \sqrt{\phi^{-1}} & -\phi^{-1} & 0 \\ 0 & 0 & 1 \end{pmatrix} \begin{pmatrix} |(\bullet, (\bullet, \bullet)_1)_\gamma\rangle \\ |(\bullet, (\bullet, \bullet)_\gamma)_\gamma\rangle \\ |(\bullet, (\bullet, \bullet)_\gamma)_1\rangle \end{pmatrix}. \quad (3-39)$$

Note that our third basis vector fuses to 1, so relation (3-28) applies and the two-by-two block is the $F_{\gamma\gamma\gamma}^\gamma$ we presented in equation (3-31).

We then fall back to the previous case where the R -matrix is diagonal which finally takes us to the last step: Undo the basis change. This is done by the matrix F^{-1} . The final state then becomes:

$$F^{-1}RF|((\bullet, \bullet)_1, \bullet)_\gamma\rangle = -\frac{e^{-i\pi/5}}{\phi}|((\bullet, \bullet)_1, \bullet)_\gamma\rangle - \frac{ie^{-i\pi/10}}{\sqrt{\phi}}|((\bullet, \bullet)_\gamma, \bullet)_\gamma\rangle. \quad (3-40)$$

Operation $F^{-1}RF$ is the one responsible for realizing the braidings so it would be interesting to write it in matrix form. We can then repeat these calculations for the remaining basis vectors $|((\bullet, \bullet)_\gamma, \bullet)_\gamma\rangle$ and $|((\bullet, \bullet)_\gamma, \bullet)_1\rangle$ so operator $F^{-1}RF$ becomes:

$$F^{-1}RF = \begin{pmatrix} -\frac{e^{-i\pi/5}}{\phi} & -\frac{ie^{-i\pi/10}}{\sqrt{\phi}} & 0 \\ -\frac{ie^{-i\pi/10}}{\sqrt{\phi}} & -\frac{1}{\phi} & 0 \\ 0 & 0 & -e^{-2i\pi/5} \end{pmatrix}. \quad (3-41)$$

What we have in the above example is a Hilbert space of three dimensions created by fusions of three anyons with label γ . We proceeded then to use two different bases (or fusion orders) that are connected via F -matrix to execute any braiding between these three particles. Going back to the discussion in section 3.1.1 we have just defined the generators of our group called σ_1 (exchanges between the left most particles) and σ_2 (exchanges between the righthmost particles), they are respectively the R -matrix and the $F^{-1}RF$ -matrix. As expected the Yang-Baxter relation in equation (3-7) still holds:

$$\begin{aligned} \sigma_1\sigma_2\sigma_1 &= \sigma_2\sigma_1\sigma_2 \rightarrow \\ &\rightarrow RF^{-1}RFR = F^{-1}RFRF^{-1}RF \rightarrow \\ &\rightarrow \begin{pmatrix} \frac{e^{-6i\pi/5}}{\phi} & \frac{ie^{-13i\pi/10}}{\sqrt{\phi}} & 0 \\ \frac{ie^{-13i\pi/10}}{\sqrt{\phi}} & -\frac{e^{-4i\pi/5}}{\phi} & 0 \\ 0 & 0 & -e^{-6i\pi/5} \end{pmatrix} = \begin{pmatrix} \frac{e^{-6i\pi/5}}{\phi} & \frac{ie^{-13i\pi/10}}{\sqrt{\phi}} & 0 \\ \frac{ie^{-13i\pi/10}}{\sqrt{\phi}} & -\frac{e^{-4i\pi/5}}{\phi} & 0 \\ 0 & 0 & -e^{-6i\pi/5} \end{pmatrix}. \end{aligned} \quad (3-42)$$

The example we discussed is extremely important because it also is the most commonly used to show that this model of anyons is capable of creating

a universal quantum computer [31].

To use this model in a quantum computer we must define what our logical qubits are going to be in a system of Fibonacci anyons, the most common definition uses the base we were already working with:

$$|((\bullet, \bullet)_1, \bullet)_\gamma\rangle = |0\rangle, \quad (3-43a)$$

$$|((\bullet, \bullet)_\gamma, \bullet)_\gamma\rangle = |1\rangle, \quad (3-43b)$$

$$|((\bullet, \bullet)_\gamma, \bullet)_1\rangle = |N\rangle. \quad (3-43c)$$

Where $|0\rangle$ and $|1\rangle$ are our logical states and $|N\rangle$ is a noncomputational state. This is necessary as the Hilbert space for these three Fibonacci anyons trios is 3-dimensional but we require two level systems to create a quantum computer. Then in this model we have to be careful so as to not use $|N\rangle$ for any logical operations as it holds no logical value. In this arrangement trios of anyons will represent our qubits and even more relevant, note that this automatically gives us a consistent way to measure the qubits of our computer: If we want to know the result of a computation we must only fuse the first anyon pair of a qubit and look to the results. If it fuses to γ the qubit is $|1\rangle$, if it fuses to 1 the qubit is $|0\rangle$.

For this to work we have to arrange our computation in such a way that the amplitude for state $|N\rangle$ is zero at the beginning and end of every operation, in the cases where this state acquires amplitude it is normally said that a "leakage error" occurred. Fortunately for us the matrices R and $F^{-1}RF$ are block diagonal, which means we do not mix our logical states with the noncomputational one during braiding operations. This is exceptionally useful as it allows us to execute single qubit operations (such as a bit flip or Hadamard gate) without worrying about the state $|N\rangle$.

We won't delve deep into the reason as to why this allows for universal quantum computation as we are more interested in implementing our NOON-like interferometer, but explicit details can be found in Nayak et al., Kitaev et al. and Dawson et al. [6, 23, 33]. The important idea is the fact that we can find a braiding that corresponds to a unitary operation arbitrarily close to any desired operation. To do so we can simply increase the braid to get closer to the target operation. In an effort to be more precise we claim that the braid increases logarithmically with respect to the error distance from the operation.

Then if we want to execute a computation in this model we first need to find the braiding that corresponds to our desired operation. Doing so might seem hard at first as the difficulty would seem to grow exponentially with the braid length [30, 29]. On the other hand there are other, more efficient ways

to do find such braiding.

The Solovay-Kitaev algorithm allows us to concatenate shorter braids in order to get closer to the target operation in a much more efficient manner. It constructs a braiding that is polylogarithmically long for a given error distance and even more impressively it is completely possible to run such an algorithm in a classical computer [33].

As we have mentioned before then executing single-qubit operations shouldn't be a problem in this model, but we need to go further to create a universal quantum computer. We need at least one "entangling gate", meaning we need to recreate two-qubit gates by braiding particles from different qubits [23]. This becomes a much more difficult task as we are now dealing with six anyons in a 13 dimensional Hilbert space, our braiding matrices become 13x13 block diagonal matrices with one 5x5 block (for total label 1) and another 8x8 block (for total label γ) [30]. Fortunately though we know from Freedman et al. [31] that there is a solution to our problem, we can safely assume that there exists a braiding that corresponds to any operation we might want to replicate in a two-qubit space.

Again we will not enter into specifics of finding such gates, but braidings for more common gates such as the CNOT have already been designed in two separate research papers [30, 29]. We shall only focus on one those bellow, specifically a design from Bonesteel et al. [30]. It works exactly as expected, when the control qubit is in state $|((\bullet, \bullet)_1, \bullet)_\gamma\rangle = |0\rangle$ the target is left alone and when the control is in state $|((\bullet, \bullet)_\gamma, \bullet)_\gamma\rangle = |1\rangle$ the target flips value.

Doing so requires two basic ideas. First, a pair of anyons from the control qubit will be braided across the target as an immutable pair, if that pair fuses to 1 then no transition occurs, but if the pair fuse to γ then a transition occurs. This means that if the control pair we choose determines the value of the control qubit, as is the case, we automatically get a controlled operation. Second, we do not do exchanges with more than two target particles at a time. The only non-trivial case is when the control pair fuses to γ , which is equivalent to one anyon, meaning the problem reduces to the previous one of finding 3-anyon braidings.

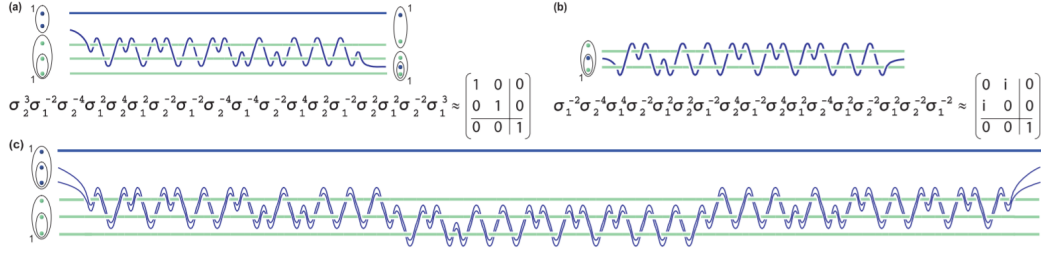


Figure 3.6: Figure and values taken from Bonesteel et al. [30]. (a) A braiding that injects one anyon from one qubit into another qubit. It approximates the identity to a distance of $\epsilon = 1.5 \times 10^{-3}$. The products of σ_1 and σ_2 represent the correspondent unitary operation and are products of matrices R and $F^{-1}RF$ respectively in accordance to equation (3-43). (b) A braiding that approximates a NOT gate with error distance $\epsilon = 8.5 \times 10^{-4}$. (c) A braiding that approximates a CNOT gate utilizing braidings a and b. First it injects two particles from the control qubit into the target, then it executes a NOT-gate and finally it ejects the particles back to the control qubit. The errors distance from a real CNOT-gate are $\epsilon = 1.8 \times 10^{-3}$ and $\epsilon = 1.2 \times 10^{-3}$ when the total label of the six anyon system is 1 or γ , respectively. it is important to note that one could reduce the error distances even further by utilizing the Solovay-Kitaev algorithm on braidings (a) and (b).

At this point we can recall our last discussion in the previous chapter about the logical interferometer constructed for NOON-like states. The CNOT is especially interesting to us as it is integral to executing our circuit presented in figure 2.12 as is the Hadamard gate and the phase gate. Both of those are single qubit operations and approximations can be easily found with the Solovay-Kitaev algorithm. For illustration purposes we present a braiding that approximates the CNOT gate in figure 3.6 and the Hadamard gate in figure 3.7:

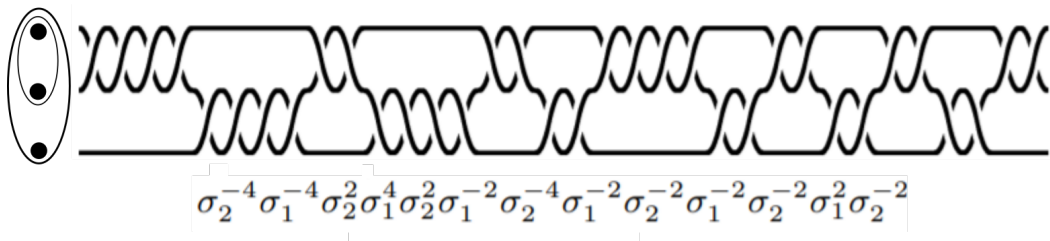


Figure 3.7: Braiding that approximates a Hadamard gate with error distance of $\epsilon = 3 \times 10^{-3}$. σ_1 and σ_2 are the braiding matrices for our model shown previously. Braiding and values taken from Field et al.[34]

It is important to note that those braidings are not necessarily the smallest or most precise ones, again, with the Solovay-Kitaev algorithm one can grow those braidings to obtain better precision.

Our purpose here is to show that we can utilize Fibonacci anyons to recreate not only our logical beamsplitter but any computation. Doing so requires the following steps:

1. Writing the computation as a quantum circuit.
2. Decomposing the circuit in one-qubit and two-qubit gates.
3. Utilizing the Solovay-Kitaev algorithm to write the braidings that correspond to the target gates with the required precision.
4. Use simple substitution to write the computation as concatenated braidings of however many anyons are required.

Following the steps above we can write our logical interferometer with arbitrary precision as a braiding of anyons as long as we can implement the Solovay-Kitaev algorithm. We shall not do it here so as to not extend this discussion too much. The most important point to make is that one can create an anyon interferometer by simply executing computations on a universal quantum computer based on Fibonacci anyons.

4

Anyon interferometry

In Chapter 2 we explored linear optics and interferometry from the perspective of quantum computing. Chapter 3 dealt with anyons and universal quantum computation. In the present chapter we combine those ideas and explore how a universal quantum computer based on anyonic linear optics can be used to perform interferometry at the Heisenberg limit.

Tosta et al. [7] have presented a universal quantum computer model based on linear optics for "fermionic anyons" which we shall go over here. Here is a definition for fermionic anyons: One dimensional particles defined from the creation and annihilation operators a_i^\dagger and a_i that follow these anti-commutation relations:

$$a_i a_j^\dagger + e^{-i\theta\epsilon_{ij}} a_j^\dagger a_i = \delta_{ij}, \quad (4-1a)$$

$$a_i a_j + e^{i\theta\epsilon_{ij}} a_j a_i = 0, \quad (4-1b)$$

where θ is the exchange phase of the particles and ϵ_{ij} is given by:

$$\epsilon_{ij} = \begin{cases} 1, & \text{if } i < j \\ 0, & \text{if } i = j \\ -1, & \text{if } i > j \end{cases}. \quad (4-2)$$

Note that these are remarkably similar to equations (2-42a) and (2-42b) but now account for an anyon exchange phase, hence the name fermionic anyons.

4.1

Linear optics and operator representation

On the interferometry chapter we learned that bosons and fermions follow specific commutation and anti-commutation relations expressed in equations (2-1a), (2-1b), (2-42a) and (2-42b). We also have used a representation of multi-mode states of the type $|n_1\rangle|n_2\rangle\dots|n_m\rangle$ where m represents each mode and n_m the number of particles in a mode. This was good enough at that moment but now we wish to switch to a more general notation. For bosons:

$$|n_1, n_2, \dots, n_m\rangle = \frac{(a_1^\dagger)^{n_1} (a_2^\dagger)^{n_2} \dots (a_m^\dagger)^{n_m}}{\sqrt{n_1! n_2! \dots n_m!}} |0\rangle, \quad (4-3)$$

where the state is normalized, as seen by the denominator, $|0\rangle$ represents the vacuum, a_i^\dagger the appropriate creation operator and n_m the number of particles on mode m .

For fermions:

$$|n_1, n_2, \dots, n_m\rangle = (a_1^\dagger)^{n_1} (a_2^\dagger)^{n_2} \dots (a_m^\dagger)^{n_m} |0\rangle. \quad (4-4)$$

Remember that we can no longer have more than one particle per mode when dealing with fermions, which means that in this context $n_i = i$, $i = \{0, 1\}$. This will also be the case for fermionic anyons.

Let us then describe the optical elements we used in Chapter 2 in a different manner. A phase-shifter and a beamsplitter are both passive devices, meaning they require no power, feedback or user input to work, but the phase-shifter is a one mode device and the beamsplitter a two-mode device.

We have already explained the action of a phase-shifter in a quantum state. In this new notation, if shifting the phase by ϕ , it takes the form:

$$PS_i(\phi)|n_1, n_2, \dots, n_m\rangle = e^{i\phi n_i}|n_1, n_2, \dots, n_m\rangle. \quad (4-5)$$

where i is the mode the phase-shifter acts upon. The phase-shifter is now an evolution operator $PS_i = e^{i\phi H_i}$ where $H_i = a_i^\dagger a_i = N_i$ is the Hamiltonian. We can change perspectives and see how the phase-shifter acts on the creation operators:

$$PS_i(\phi)a_j^\dagger PS_i(-\phi) = e^{i\phi \delta_{ij}} a_j^\dagger. \quad (4-6)$$

The beamsplitter is now going to be an evolution operator $BS_{ij} = e^{i\phi H_{ij}}$ where $H_{ij} = a_i^\dagger a_j + a_j^\dagger a_i$ is the hopping Hamiltonian. We can then act on the creation operators:

$$BS_{ij}(\phi) \begin{pmatrix} a_i^\dagger \\ a_j^\dagger \end{pmatrix} BS_{ij}(-\phi) = \begin{pmatrix} \cos \phi & i \sin \phi \\ i \sin \phi & \cos \theta \end{pmatrix} \begin{pmatrix} a_i^\dagger \\ a_j^\dagger \end{pmatrix}. \quad (4-7)$$

These optical element Hamiltonians are the same independent of the particle type, so we can use them for the fermionic anyons mentioned before and calculate their evolution.

4.2

Linear optics for fermionic anyons

Despite the optical elements remaining the same the evolution might change, meaning we have to solve the Heisenberg equation of motion for these new particles.

For the phase-shifters we have that:

$$i \frac{da_j^\dagger}{d\phi} = [H_i, a_j^\dagger] = [a_i^\dagger a_i, a_j^\dagger] = a_i^\dagger a_i a_j^\dagger - a_j^\dagger a_i^\dagger a_i. \quad (4-8)$$

Then for $i = j$ we simply recover the fermionic results:

$$PS_i(\phi)a_i^\dagger PS_i(-\phi) = e^{i\phi} a_i^\dagger. \quad (4-9)$$

This is expected as the anti-commutation relations transform into the fermion relations. For $i \neq j$:

$$\begin{aligned} a_i^\dagger a_i a_j^\dagger - a_j^\dagger a_i^\dagger a_i &= -a_i^\dagger e^{-i\theta\epsilon_{ij}} a_j^\dagger a_i - a_j^\dagger a_i^\dagger a_i = \\ &= e^{i\theta\epsilon_{ij}} e^{-i\theta\epsilon_{ij}} a_j^\dagger a_i^\dagger a_i - a_j^\dagger a_i^\dagger a_i = 0. \end{aligned} \quad (4-10)$$

Then the complete result becomes:

$$PS_i(\phi) a_j^\dagger PS_i(-\phi) = e^{i\phi\delta_{ij}} a_j^\dagger. \quad (4-11)$$

Let us now take a look at the beamsplitters. The equations we need to solve are:

$$i \frac{da_i^\dagger}{d\phi} = [H_{ij}, a_i^\dagger], \quad (4-12a)$$

$$i \frac{da_j^\dagger}{d\phi} = [H_{ij}, a_j^\dagger]. \quad (4-12b)$$

The commutators are calculated with the anti-commutation relations:

$$[H_{ij}, a_i^\dagger] = a_j^\dagger \{1 - (1 - e^{i\theta}) N_i\}, \quad (4-13a)$$

$$[H_{ij}, a_j^\dagger] = a_i^\dagger \{1 - (1 - e^{-i\theta}) N_j\}. \quad (4-13b)$$

To simplify the calculations we do a direct substitution:

$$i \frac{da_i^\dagger}{d\phi} = a_j^\dagger \{1 - (1 - e^{i\theta}) N_i\} = a_j^\dagger W_i^{(\theta)}. \quad (4-14)$$

We have two variables a_i^\dagger and a_j^\dagger and two equations, meaning we could try to solve the system as is, but we opt for a different method that gives us a new system that is easier to solve. By computing $[H_{ij}, a_j^\dagger W_i^{(\theta)}]$ we can write the Heisenberg equation of motion for this operator:

$$i \frac{d(a_j^\dagger W_i^{(\theta)})}{d\phi} = a_i^\dagger. \quad (4-15)$$

we then have two new equation systems between operators a_i and $a_j^\dagger W_i^{(\theta)}$ and, analogously, between operators a_j and $a_i^\dagger W_j^{(\theta)}$. The systems take the form:

$$i \frac{d(a_i^\dagger W_j^{(\theta)})}{d\phi} = a_j^\dagger, \quad (4-16a)$$

$$i \frac{da_j^\dagger}{d\phi} = a_i^\dagger W_j^{(\theta)}. \quad (4-16b)$$

From which we can find the solutions:

$$BS_{ij}(\phi)a_i^\dagger BS_{ij}(-\phi) = \cos \phi a_i^\dagger + i \sin \phi a_j^\dagger W_i^{(\theta)}, \quad (4-17a)$$

$$BS_{ij}(\phi)a_j^\dagger BS_{ij}(-\phi) = \cos \phi a_j^\dagger + i \sin \phi a_i^\dagger W_i^{\dagger(\theta)}. \quad (4-17b)$$

At this point our solution would be complete if it were not for another problem. In fermionic and bosonic modes that do not appear in the beamsplitter hamiltonian there are creation operators that commute with H_{ij} but in this model of fermionic anyons this is no longer true. For creation operator a_k^\dagger for $i < k < j$ we have:

$$[H_{ij}, a_k^\dagger] = e^{i\phi(a_i^\dagger a_j + a_j^\dagger a_i)} a_k^\dagger - a_k^\dagger e^{i\phi(e^{i2\theta} a_i^\dagger a_j + e^{-i2\theta} a_j^\dagger a_i)}. \quad (4-18)$$

This is treated as an "effective beamsplitter" that creates a phase based on the number of occupied modes between i and j . Accordingly we define a new operator:

$$BS_{ij}^{(\alpha)}(\phi) = e^{i\phi(e^{i\alpha} a_i^\dagger a_j + e^{-i\alpha} a_j^\dagger a_i)}. \quad (4-19)$$

And modify the solutions to:

$$BS_{ij}^{(\alpha)}(\phi)a_i^\dagger BS_{ij}^{(\alpha)}(-\phi) = \cos \phi a_i^\dagger + ie^{i\alpha} \sin \phi a_j^\dagger W_i^{(\theta)}, \quad (4-20a)$$

$$BS_{ij}^{(\alpha)}(\phi)a_j^\dagger BS_{ij}^{(\alpha)}(-\phi) = \cos \phi a_j^\dagger - ie^{-i\alpha} \sin \phi a_i^\dagger W_i^{\dagger(\theta)}. \quad (4-20b)$$

Let us consider an example on a three mode system and a balanced beamsplitter ($\phi = \frac{\pi}{4}$) acting on modes 1 and 3. Consider the state $|1, 1, 0\rangle$, we can rewrite it as $a_1^\dagger a_2^\dagger |0\rangle = -ie^{i\theta} a_2^\dagger a_1^\dagger |0\rangle$. The first thing we do is commute the beamsplitter operator with the creation operator on mode 2 using equation (4-19):

$$-ie^{i\theta} BS_{13} \left(\frac{\pi}{4} \right) a_2^\dagger a_1^\dagger |0\rangle = -ie^{i\theta} a_2^\dagger \left[BS_{13}^{(2\theta)} \left(\frac{\pi}{4} \right) \right] a_1^\dagger |0\rangle. \quad (4-21)$$

Now we just need to evolve the operator on a_1^\dagger using equations (4-20a), (4-20b) and the fact that $W_i^{(\theta)} |0\rangle = |0\rangle$:

$$-ie^{i\theta} a_2^\dagger \left[BS_{13}^{(2\theta)} \left(\frac{\pi}{4} \right) \right] a_1^\dagger |0\rangle = -\frac{ie^{i\theta}}{\sqrt{2}} a_2^\dagger (a_1^\dagger + ie^{i2\theta} a_3^\dagger) |0\rangle. \quad (4-22)$$

Using then the commutation relation $a_2^\dagger a_1^\dagger = -e^{-i\theta} a_1^\dagger a_2^\dagger$ again and we get:

$$-\frac{ie^{i\theta}}{\sqrt{2}} a_2^\dagger (a_1^\dagger + ie^{-i2\theta} a_3^\dagger) |0\rangle = \frac{1}{\sqrt{2}} (a_1^\dagger a_2^\dagger - ie^{-i\theta} a_2^\dagger a_3^\dagger) |0\rangle. \quad (4-23)$$

Then the effect of the beamsplitter becomes:

$$BS_{13} \left(\frac{\pi}{4} \right) |1, 1, 0\rangle = \frac{1}{\sqrt{2}} (|1, 1, 0\rangle - ie^{-i\theta} |0, 1, 1\rangle). \quad (4-24)$$

Such a result is remarkable because it shows that if an anyon switches from mode 1 to 3 while another occupies mode 2 then a relative phase appears,

which would not happen if mode 2 was unoccupied. We have seen a similar behaviour before on the Aharonov-Bohm effect we mentioned in the last section but now this is taking place over one dimensional space.

This closes our discussion of fermionic anyon linear optics. Now, we want to show one can do computation by exploiting this, but before we do so it is important to introduce a similar model but now based on "bosonic anyons". We want to consider what happens when there are no restrictions on the amount of particles per mode.

4.3

Bosonic anyons and the Houg-Ou-Mandel Effect

As we have just mentioned working with bosonic anyons is interesting because we no longer have the limitation of one particle per mode and this might open up new opportunities in realizing "optical" setups. The following discussion is again based Tosta's work in unpublished notes [35].

Bosonic anyons will follow similar relations to fermionic anyons. They are as follows:

$$a_i a_j^\dagger - e^{-i\theta\epsilon_{ij}} a_j^\dagger a_i = \delta_{ij}, \quad (4-25a)$$

$$a_i a_j - e^{i\theta\epsilon_{ij}} a_j a_i = 0. \quad (4-25b)$$

Where θ is the exchange phase of the particles and ϵ_{ij} is given by:

$$\epsilon_{ij} = \begin{cases} 1, & \text{if } i < j \\ 0, & \text{if } i = j \\ -1, & \text{if } i > j \end{cases}. \quad (4-26)$$

The linear optics operators won't change as expected:

$$PS_i = e^{i\phi H_i}, \quad (4-27a)$$

$$BS_{ij} = e^{i\phi H_{ij}}. \quad (4-27b)$$

For $H_i = a_i^\dagger a_i = N_i$ and $H_{ij} = a_i^\dagger a_j + a_j^\dagger a_i$. On the other hand, now the states and the actions of the creation and annihilation operators will be defined as such:

$$|n_1, n_2, \dots, n_m\rangle = \frac{(a_1^\dagger)^{n_1} (a_2^\dagger)^{n_2} \dots (a_m^\dagger)^{n_m}}{\sqrt{n_1! n_2! \dots n_m!}} |0\rangle, \quad (4-28a)$$

$$a_i^\dagger |n_1, n_2, \dots, n_i, \dots, n_m\rangle = e^{i\theta \sum_{k=1}^{i-1} n_k} \sqrt{n_i + 1} |n_1, n_2, \dots, n_i + 1, \dots, n_m\rangle, \quad (4-28b)$$

$$a_i |n_1, n_2, \dots, n_i, \dots, n_m\rangle = e^{-i\theta \sum_{k=1}^{i-1} n_k} \sqrt{n_i} |n_1, n_2, \dots, n_i - 1, \dots, n_m\rangle. \quad (4-28c)$$

Note that creation and annihilation generate exchange phases.

To solve the dynamics of this system we run into some issues, but we can use the discussion on section 2.1.3 to visualize how the number operator evolves when acted upon by the beamsplitter operator.

First let us recall the following operators from section 2.1.3:

$$J_1 = \frac{1}{2}(a_i^\dagger a_j + a_j^\dagger a_i), \quad (4-29a)$$

$$J_2 = \frac{i}{2}(a_i a_j^\dagger - a_i^\dagger a_j), \quad (4-29b)$$

$$J_3 = \frac{1}{2}(N_i - N_j). \quad (4-29c)$$

Where N_i and N_j are the number operators.

On that same section we calculated the commutator $[J_1, J_3] = iJ_2$, we will refrain from calculating the remaining relations, but know that this result generalizes to:

$$[J_i, J_j] = 2i\epsilon_{ijk}J_k, \quad i, j, k = \{1, 2, 3\}. \quad (4-30)$$

where ϵ_{ijk} is the Levi-Civita symbol.

Fisrt, note that $BS(\phi) = e^{i(2\phi)J_1}$ and:

$$N_i = \frac{1}{2}N + J_3, \quad (4-31a)$$

$$N_j = \frac{1}{2}N - J_3. \quad (4-31b)$$

where $N = N_i + N_j$ is the total number operator.

So to find out the action of the beamsplitter on the number operators we do:

$$e^{i\phi J_1} \begin{pmatrix} J_1 \\ J_2 \\ J_3 \end{pmatrix} e^{-i\phi J_1} = \begin{pmatrix} 1 & 0 & 0 \\ 0 & \cos \phi & -\sin \phi \\ 0 & \sin \phi & \cos \phi \end{pmatrix} \begin{pmatrix} J_1 \\ J_2 \\ J_3 \end{pmatrix}. \quad (4-32)$$

Doing the appropriate substitutions from the previous equations and isolating for N_i and N_j we get:

$$N_i(\phi) = \frac{1 + \cos 2\phi}{2}a_i^\dagger a_i + \frac{1 - \cos 2\phi}{2}a_j^\dagger a_j - \frac{i \sin 2\phi}{2}(a_i^\dagger a_j - a_j^\dagger a_i), \quad (4-33a)$$

$$N_j(\phi) = \frac{1 - \cos 2\phi}{2}a_i^\dagger a_i + \frac{1 + \cos 2\phi}{2}a_j^\dagger a_j + \frac{i \sin 2\phi}{2}(a_i^\dagger a_j - a_j^\dagger a_i). \quad (4-33b)$$

Our next step to solve the dynamics of this problem then is to exploit the algebra between the relevant operators. We do so because the previous method of solving the coupled Heisenberg equations is no longer optimal.

Let us calculate $[H_{ij}, a_i^\dagger] = [2J_1, a_i^\dagger]$ and $[2J_1, a_j^\dagger]$:

$$[(2J_1), a_i^\dagger] = a_i^\dagger ((\cos \theta - 1)(2J_1) - \sin \theta (2J_2)) + a_j^\dagger, \quad (4-34a)$$

$$[(2J_1), a_j^\dagger] = a_j^\dagger ((\cos \theta - 1)(2J_1) - \sin \theta (2J_2)) + a_i^\dagger. \quad (4-34b)$$

Which implies:

$$(2J_1) a_i^\dagger = a_i^\dagger (2(\cos \theta J_1 - \sin \theta J_2)) + a_j^\dagger, \quad (4-35a)$$

$$(2J_1) a_j^\dagger = a_j^\dagger (2(\cos \theta J_1 - \sin \theta J_2)) + a_i^\dagger. \quad (4-35b)$$

Then we sum and subtract the above equations:

$$(2J_1) (a_i^\dagger + a_j^\dagger) = (a_i^\dagger + a_j^\dagger) (2(\cos \theta J_1 - \sin \theta J_2) + 1), \quad (4-36a)$$

$$(2J_1) (a_i^\dagger - a_j^\dagger) = (a_i^\dagger - a_j^\dagger) (2(\cos \theta J_1 - \sin \theta J_2) - 1). \quad (4-36b)$$

Now we can multiply the above equations by powers of $2J_1$ to get an expanded taylor series of the exponetial function which we contract to:

$$e^{i\phi(2J_1)} (a_i^\dagger + a_j^\dagger) = (a_i^\dagger + a_j^\dagger) e^{i\phi(2(\cos \theta J_1 - \sin \theta J_2) + 1)}, \quad (4-37a)$$

$$e^{i\phi(2J_1)} (a_i^\dagger - a_j^\dagger) = (a_i^\dagger - a_j^\dagger) e^{i\phi(2(\cos \theta J_1 - \sin \theta J_2) - 1)}. \quad (4-37b)$$

Which leads us to:

$$e^{i\phi(2J_1)} a_i^\dagger = (\cos \phi a_i^\dagger + i \sin \phi a_j^\dagger) e^{i\phi(2(\cos \theta J_1 - \sin \theta J_2))}, \quad (4-38a)$$

$$e^{i\phi(2J_1)} a_j^\dagger = (i \sin \phi a_i^\dagger + \cos \phi a_j^\dagger) e^{i\phi(2(\cos \theta J_1 - \sin \theta J_2))}. \quad (4-38b)$$

To simplify we do the following substitution:

$$\begin{aligned} \cos \theta J_1 - \sin \theta J_2 &= e^{i\theta J_3} J_1 e^{-i\theta J_3} \rightarrow \\ \rightarrow e^{i\phi(2(\cos \theta J_1 - \sin \theta J_2))} &= e^{i\theta J_3} e^{i\phi(2J_1)} e^{-i\theta J_3}. \end{aligned} \quad (4-39)$$

Finally, we have:

$$a_i^\dagger(\phi) = (\cos \phi a_i^\dagger + i \sin \phi a_j^\dagger) e^{i\theta J_3} e^{i\phi(2J_1)} e^{-i\theta J_3} e^{-i\phi(2J_1)}, \quad (4-40a)$$

$$a_j^\dagger(\phi) = (i \sin \phi a_i^\dagger + \cos \phi a_j^\dagger) e^{i\theta J_3} e^{i\phi(2J_1)} e^{-i\theta J_3} e^{-i\phi(2J_1)}. \quad (4-40b)$$

Observe that we can commute the operator $G(\theta, \phi) = e^{i\theta J_3} e^{i\phi(2J_1)} e^{-i\theta J_3}$

with creation operators by using the following relations:

$$G(n\theta, \phi)a_i^\dagger = (\cos \phi a_i^\dagger + ie^{-in\theta} \sin \phi a_j^\dagger)G((n+1)\theta, \phi), \quad (4-41a)$$

$$G(n\theta, \phi)a_j^\dagger = (\cos \phi a_j^\dagger + ie^{in\theta} \sin \phi a_i^\dagger)G((n+1)\theta, \phi). \quad (4-41b)$$

This means we can finally calculate the effect of a beamsplitter on a general state.

Let us consider an example. We will repeat our calculations in section 2.1.1 for the Hong-Ou-Mandel effect but this time for the bosonic anyons we just described. We will be working with a balanced beamsplitter acting on modes 1 and 2 on the state $|1, 1\rangle$. The unitary that describes the beamsplitter is: $e^{i(\pi/2)J_1}$. This gives us:

$$\begin{aligned} (a_i^\dagger a_j^\dagger)_{out}|0\rangle &= e^{i(\pi/2)J_1} a_i^\dagger a_j^\dagger |0\rangle = \\ &= \left(\frac{1}{\sqrt{2}}a_i^\dagger + i\frac{1}{\sqrt{2}}a_j^\dagger\right)G(\theta, \pi/4)a_j^\dagger |0\rangle = \\ &= \left(\frac{1}{\sqrt{2}}a_i^\dagger + i\frac{1}{\sqrt{2}}a_j^\dagger\right)\left(\frac{1}{\sqrt{2}}ie^{i\theta}a_i^\dagger + \frac{1}{\sqrt{2}}a_j^\dagger\right)G(2\theta, \pi/4)|0\rangle = \\ &= \frac{1}{2}(e^{i\theta}(a_i^\dagger)^2 + a_i^\dagger a_j^\dagger - e^{i\theta}a_j^\dagger a_i^\dagger + i(a_j^\dagger)^2)|0\rangle = \\ &= \frac{i}{2}(e^{i\theta}(a_i^\dagger)^2 + (a_j^\dagger)^2)|0\rangle = \frac{i}{\sqrt{2}}(e^{i\theta}|2, 0\rangle + |0, 2\rangle). \end{aligned} \quad (4-42)$$

As expected for $\theta = 0$ we recover the usual result on equation (2-8) for $T = 1/2$

4.4

Computing with fermionic anyons

Now we switch back to our discussion of fermionic anyons. We have completely defined two optical elements and their action on our particles, the next step is to show how we can exploit this to create a universal quantum computer based on linear optics according to Tosta et al. [7].

We need three things to realize this model:

- **1. An encoding.** We need to devise a system of fermionic anyons that is ideal to represent logical qubits $|0\rangle$ and $|1\rangle$ and be able to execute logical operations on the qubits by utilizing unitary operators on the system.
- **2. Universal computation.** The unitaries that we can use need to be able to realize every logical operation a computer might need. As we have mentioned before in section 2.3 this means we need a set of operators we can mix and match so as to build the operations we want.

- **3. Measurements.** If we can't take data out of our system then the computation is useless as we can't access its results.

The reader might realize that we concluded Chapter 3 by presenting these same things for Fibonacci anyons:

- **1.** We presented a basis that encodes our qubits into trios of anyons that fuse a certain way.
- **2.** We encountered braidings on those systems that represent logical operations on the qubits and we made sure that we could not only arbitrarily approximate any one-qubit gate through Solovay-Kitaev, but also reproduce the most common entangling gate, the CNOT.
- **3.** We defined our measurements as fusing the first anyon pair of a trio that forms a qubit.

We must repeat this here for the new model.

4.4.1

Encoding

To encode n qubits we use $2n$ modes. This way we have:

$$|0\rangle = |1, 0\rangle, \quad (4-43a)$$

$$|1\rangle = |0, 1\rangle. \quad (4-43b)$$

Then a 2-qubit system is of the form:

$$|00\rangle = |1, 0, 1, 0\rangle, \quad (4-44a)$$

$$|01\rangle = |1, 0, 0, 1\rangle, \quad (4-44b)$$

$$|10\rangle = |0, 1, 1, 0\rangle, \quad (4-44c)$$

$$|11\rangle = |0, 1, 0, 1\rangle. \quad (4-44d)$$

We need not worry about the exchange phase θ as these anyons obey the Pauli Exclusion Principle. If we were dealing with the bosonic anyons of the previous section we would need to take that into account.

4.4.2

Universal Computation

The next step is to show that we are capable of universal quantum computation. As previously said, to do so we need to be able to create a set of gates that can construct every other possible gate. Just like we did for

Fibonacci anyons, we want a set of one-qubit gates and one entangling two-qubit gate. The encoding we just defined comes into play to help us with this task as it allows us to use any logical one-qubit gate with just phase-shifters and beamsplitters. The action of a phase-shifter on the logical basis is as follows:

$$PS_2(\phi)|\mathbf{0}\rangle = PS_2(\phi)|1, 0\rangle = |1, 0\rangle = |\mathbf{0}\rangle, \quad (4-45a)$$

$$PS_2(\phi)|\mathbf{1}\rangle = PS_2(\phi)|0, 1\rangle = e^{i\phi}|0, 1\rangle = e^{i\phi}|\mathbf{1}\rangle. \quad (4-45b)$$

Note that this is just a rotation around the Z axis in the Bloch sphere by ϕ degrees.

The beamsplitter acts as:

$$BS_{12}(\phi)|\mathbf{0}\rangle = BS_{12}(\phi)|1, 0\rangle = \quad (4-46a)$$

$$= \cos \phi |1, 0\rangle + i \sin \phi |0, 1\rangle = \cos \phi |\mathbf{0}\rangle + i \sin \phi |\mathbf{1}\rangle,$$

$$BS_{12}(\phi)|\mathbf{1}\rangle = BS_{12}(\phi)|0, 1\rangle = \quad (4-46b)$$

$$= \cos \phi |0, 1\rangle + i \sin \phi |1, 0\rangle = \cos \phi |\mathbf{1}\rangle + i \sin \phi |\mathbf{0}\rangle.$$

Note as well that this is equivalent to rotating the logical states around the X axis in the Bloch sphere. This shows us we can execute any one-qubit gate, given we can do arbitrary rotations around two different axes in the Bloch Sphere. The operation $R_z R_x R_z$, or, in this model, $e^{i\alpha} PS_1(\beta) BS_{12}(\gamma) PS_2(\delta)$ allows us to build any unitary by varying parameters α , β , γ and δ . The first operator acts as global phase. We can see this operation represented on figure 4.1.

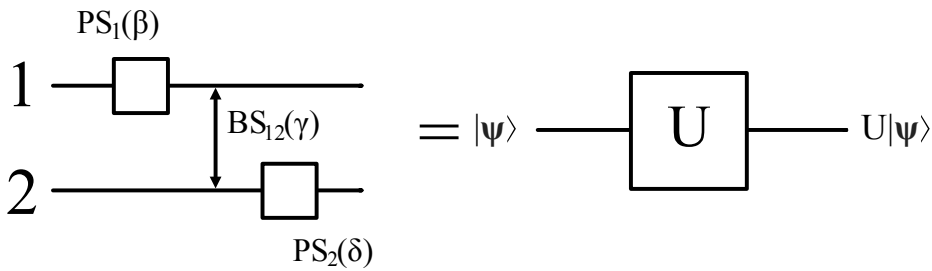


Figure 4.1: General unitary one-qubit gate built from phase-shifters and beamsplitters on the fermionic anyons computational model. On the left we have the two modes that anyons can occupy and on the right the qubit $|\psi\rangle$ before and after general unitary U . The parameters α , β , γ and δ can be chosen so as to create a general unitary.

Now that single-qubit gates are no longer an issue we switch our focus to try and create an entangling two-qubit gate. The operation as presented by

Tosta [7] is: $BS_{12}(\pi/4)BS_{23}(\pi/2)BS_{13}(-\pi/4)BS_{23}(-\pi/2)BS_{12}(-\pi/4)$ which is explicit in figure 4.2.

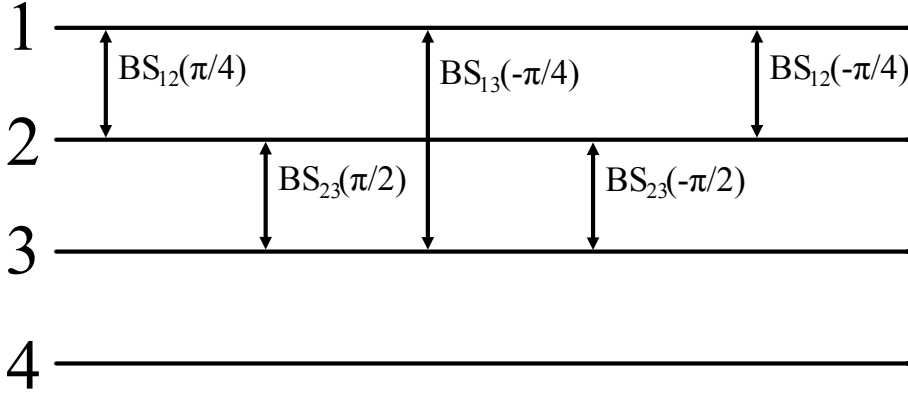


Figure 4.2: Unitary 2-qubit gate built from beamsplitters on the fermionic anyons computational model. On the left we have the four modes that anyons can occupy, which is equivalent to two qubits.

In matrix form, in the encoding basis, this translates to:

$$\begin{aligned}
 C(\theta) &= R_{\hat{z}}\left(\frac{\pi}{2}\right) \otimes |0\rangle\langle 0| + R_{\hat{n}}\left(\frac{\pi}{2}\right) \otimes |1\rangle\langle 1| = \\
 &= \begin{pmatrix} e^{-i\frac{\pi}{4}} & 0 & 0 & 0 \\ 0 & \frac{1-i\cos\theta}{\sqrt{2}} & 0 & \frac{i\sin\theta}{\sqrt{2}} \\ 0 & 0 & e^{i\frac{\pi}{4}} & 0 \\ 0 & \frac{i\sin\theta}{\sqrt{2}} & 0 & \frac{1+i\cos\theta}{\sqrt{2}} \end{pmatrix}.
 \end{aligned} \tag{4-47}$$

where $\hat{n} = (\sin\theta, 0, \cos\theta)$. From this matrix we can see that this is, in fact, entangling.

In order to be thorough one should check how much the unitary above is entangling, meaning we should exhibit its *entangling power*. Entangling power is defined by Zanardi et al. as the average amount of entanglement produced by any unitary operation U over a distribution of unentangled states [36]. To quantify entanglement Zanardi et al. defines an *entanglement measure* of state $|\psi\rangle$ in a Hilbert space by:

$$E(|\psi\rangle) = 1 - Tr_1(\rho^2), \quad \rho = Tr_2(|\psi\rangle\langle\psi|), \tag{4-48}$$

which quantifies the purity of the reduced density matrix ρ of a bipartite system.

We shall not do these calculations for $C(\theta)$ here but they are provided by Tosta in the original source [7] and the entangling power has the following expression:

$$e_p(C(\theta)) = 1 - \cos^4 \frac{\theta}{2}. \tag{4-49}$$

This means we have maximal entangling power for $\theta = \pi$ and minimal for $\theta = 0$. In fact, $C(\theta)$ is no longer an entangling gate for the minimum value of entangling power, so this computational model relies on the fact that $\theta \neq 0$.

What is most interesting about this is not that $C(\theta)$ is entangling only for $\theta \neq 0$, but that, according to Bremner et al. [37], one can construct CNOT gates with any two-qubit entangling gate and some one-qubit gates where the number of necessary entangling gates will be given by their entangling power.

4.4.3

Measurement

All that is left for us to define this model is understanding how to extract information at the end of a computation. As the model is based on linear optics and the logical qubits are defined by occupied and unoccupied modes this task becomes extremely simple: We add detectors at the end of the "optical path" our fermionic anyons have followed. If the first detector of the pair clicks then that qubit is $|0\rangle$, and if the second detector of the pair clicks that qubit is $|1\rangle$.

4.5

NOON-like interferometer

At this point we have completely defined a new model based on linear optics for 1D fermionic anyons. Next we discuss the possibilities of our NOON-like interferometer from section 2.3 in this new model. This is specially relevant as it would allow us to build such a device by exploiting linear optics systems, but as we will see we are limited by specific values of the anyonic phase in our current implementation.

It is not always possible to work with the original circuit we devised. In this new model it is not obvious how to decompose the CNOT gate in terms of the new elementary gates. However, it is clear that such a decomposition is possible. For example, we could apply the Solovay-Kitaev algorithm to approximate a CNOT using the new C^2 operation and other one-qubit gates. Another idea would be to use the work of Bremner et al. [37] mentioned above to find a decomposition. Despite that, we will take an alternative route of not using the CNOT at all and devise a new circuit that also reaches the Heisenberg limit, but uses the elementary operations of the fermionic model. This approach while not as general as those other two is a lot easier and is a good starting point to understand our options in the new model.

First, consider the gate $C^2(\theta)$:

$$C^2(\theta) = \begin{pmatrix} e^{-2i\frac{\pi}{4}} & 0 & 0 & 0 \\ 0 & -i \cos \theta & 0 & i \sin \theta \\ 0 & 0 & e^{2i\frac{\pi}{4}} & 0 \\ 0 & i \sin \theta & 0 & i \cos \theta \end{pmatrix}. \quad (4-50)$$

Observe how it acts on the basis states:

$$C^2(\theta)|\mathbf{00}\rangle = -i|\mathbf{00}\rangle, \quad (4-51a)$$

$$C^2(\theta)|\mathbf{01}\rangle = -i \cos \theta |\mathbf{01}\rangle + i \sin \theta |\mathbf{11}\rangle, \quad (4-51b)$$

$$C^2(\theta)|\mathbf{10}\rangle = i|\mathbf{10}\rangle, \quad (4-51c)$$

$$C^2(\theta)|\mathbf{11}\rangle = i \sin \theta |\mathbf{01}\rangle + i \cos \theta |\mathbf{11}\rangle. \quad (4-51d)$$

This behaves like a controlled operation where the first qubit is the target and the second qubit the control. In case the control is $|\mathbf{1}\rangle$ it creates a superposition according to θ and the value of the target, if the control is $|\mathbf{0}\rangle$ it adds a global phase to the original state.

We can attempt to build a beamsplitter by constructing an analogous circuit with $C^2(\theta)$ taking the place of the CNOTs (See figure 4.3). It is important to also move the Hadamard gate to the last qubit as that will now act as the control. We refer to the unitary that represents our beamsplitter as $LBS(\theta)$. For two qubits in matrix form it becomes:

$$\begin{aligned} LBS(\theta) &= C^2(\theta) \times (I \otimes H) \times C^2(\theta) = \\ &= \frac{1}{\sqrt{2}} \begin{pmatrix} -1 & -\cos \theta & 0 & \sin \theta \\ -\cos \theta & 1 & -\sin \theta & 0 \\ 0 & -\sin \theta & -1 & -\cos \theta \\ \sin \theta & 0 & -\cos \theta & 1 \end{pmatrix}. \end{aligned} \quad (4-52)$$

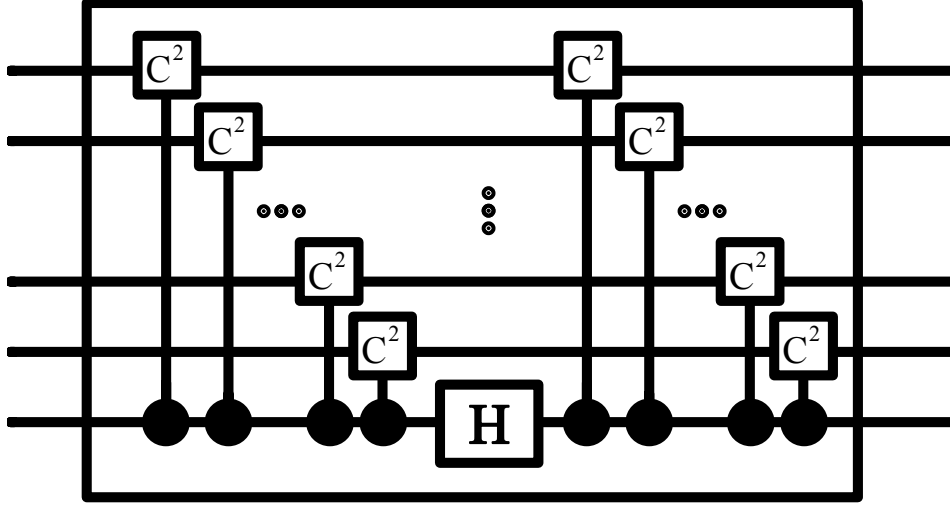


Figure 4.3: New beamsplitter $LBS(\theta)$ for N qubits with $C^2(\theta)$ taking the place of the CNOTs and the Hadamard in a different qubit.

Note that for $\theta = \pi/2$ we get a form that is remarkably similar to the LBS in equation (2-58) in section 2.3 with the exception of some signs. We then focus on both $C^2(\pi/2)$ and $LBS(\pi/2)$, interestingly the value of θ stands in the middle ground between bosons and fermions. These operators act on the basis states in the following way:

$$C^2\left(\frac{\pi}{2}\right)|00\rangle = -i|00\rangle, \quad (4-53a)$$

$$C^2\left(\frac{\pi}{2}\right)|01\rangle = i|11\rangle, \quad (4-53b)$$

$$C^2\left(\frac{\pi}{2}\right)|10\rangle = i|10\rangle, \quad (4-53c)$$

$$C^2\left(\frac{\pi}{2}\right)|11\rangle = i|01\rangle. \quad (4-53d)$$

For this value of θ , C^2 becomes especially significant. When the control qubit is $|1\rangle$ it now flips the target qubit and adds a global phase, if the control is $|0\rangle$ it just adds the global phase to the state.

As for $LBS(\pi/2)$, its action on the basis states is:

$$LBS\left(\frac{\pi}{2}\right)|00\rangle = \frac{|00\rangle - |11\rangle}{\sqrt{2}}, \quad (4-54a)$$

$$LBS\left(\frac{\pi}{2}\right)|01\rangle = \frac{|01\rangle - |10\rangle}{\sqrt{2}}, \quad (4-54b)$$

$$LBS\left(\frac{\pi}{2}\right)|10\rangle = \frac{|01\rangle + |10\rangle}{\sqrt{2}}, \quad (4-54c)$$

$$LBS\left(\frac{\pi}{2}\right)|11\rangle = \frac{|00\rangle + |11\rangle}{\sqrt{2}}. \quad (4-54d)$$

This relation still holds for N qubits, is remarkably similar to our previous logical beamsplitter and we end up with maximally entangled states at the end.

To see this we can perform a Schmidt decomposition to get the Schmidt coefficients. These coefficients must all have the same value for maximally entangled states, while for separable states we have different coefficients [15, 25]. First calculate the density matrix for each state:

$$\rho_1 = \left(\frac{|\mathbf{00}\rangle - |\mathbf{11}\rangle}{\sqrt{2}} \right) \left(\frac{\langle\mathbf{00}| - \langle\mathbf{11}|}{\sqrt{2}} \right) = \frac{1}{2} \begin{pmatrix} 1 & 0 & 0 & -1 \\ 0 & 0 & 0 & 0 \\ 0 & 0 & 0 & 0 \\ -1 & 0 & 0 & 1 \end{pmatrix}, \quad (4-55a)$$

$$\rho_2 = \left(\frac{|\mathbf{01}\rangle - |\mathbf{10}\rangle}{\sqrt{2}} \right) \left(\frac{\langle\mathbf{01}| - \langle\mathbf{10}|}{\sqrt{2}} \right) = \frac{1}{2} \begin{pmatrix} 0 & 0 & 0 & 0 \\ 0 & 1 & -1 & 0 \\ 0 & -1 & 1 & 0 \\ 0 & 0 & 0 & 0 \end{pmatrix}, \quad (4-55b)$$

$$\rho_3 = \left(\frac{|\mathbf{01}\rangle + |\mathbf{10}\rangle}{\sqrt{2}} \right) \left(\frac{\langle\mathbf{01}| + \langle\mathbf{10}|}{\sqrt{2}} \right) = \frac{1}{2} \begin{pmatrix} 0 & 0 & 0 & 0 \\ 0 & 1 & 1 & 0 \\ 0 & 1 & 1 & 0 \\ 0 & 0 & 0 & 0 \end{pmatrix}, \quad (4-55c)$$

$$\rho_4 = \left(\frac{|\mathbf{00}\rangle + |\mathbf{11}\rangle}{\sqrt{2}} \right) \left(\frac{\langle\mathbf{00}| + \langle\mathbf{11}|}{\sqrt{2}} \right) = \frac{1}{2} \begin{pmatrix} 1 & 0 & 0 & 1 \\ 0 & 0 & 0 & 0 \\ 0 & 0 & 0 & 0 \\ 1 & 0 & 0 & 1 \end{pmatrix}. \quad (4-55d)$$

Then we can calculate the partial traces:

$$Tr_B[\rho_1] = Tr_B[\rho_2] = Tr_B[\rho_3] = Tr_B[\rho_4] = \frac{1}{2} \begin{pmatrix} 1 & 0 \\ 0 & 1 \end{pmatrix} = \frac{1}{2} \mathbf{I}. \quad (4-56)$$

Where, the sub-index B means we are "tracing out" the second subspace.

The partial traces are all $\frac{1}{2}\mathbf{I}$ and the Schmidt coefficients can be found by doing the square root of the eigenvalues. In doing so we get $\frac{1}{\sqrt{2}}$ with multiplicity two. This proves that these are all, in fact, maximally entangled states.

As we have said before for N qubits we still have the basis states taken to maximally entangled states. To keep it short we shall omit the complete demonstration here but it can be reached by direct use of mathematical induction. Instead we want to present an argument that should be enough to understand this.

$C^2(\pi/2)$ acts in a similar way to a CNOT, the second qubit acts as the

control and, if it is $|1\rangle$, flips the target (the first qubit). Then for N qubits the first wave of $C^2(\pi/2)$ operations will have two outcomes dependent on the value of the last qubit:

- **1. Control $|0\rangle$:** Leave the state untouched with the exception of a new global phase. Either $-i$, -1 , i or 1 .
- **2. Control $|1\rangle$:** Flip every qubit except for the control and add a new global phase. Either $-i$, -1 , i or 1 .

The Hadamard gate then sets the control qubit to a superposition:

- **1. Control $|0\rangle$:** $\frac{|0\rangle+|1\rangle}{\sqrt{2}}$
- **2. Control $|1\rangle$:** $\frac{|0\rangle-|1\rangle}{\sqrt{2}}$

The second wave of $C^2(\pi/2)$ operations creates a superposition between the original state and one where every qubit is flipped and changes the global phase to either $-i$, -1 , i or 1 :

- **1. Control $|0\rangle$:** $\frac{|0110001\dots 0\rangle \mp |1001110\dots 1\rangle}{\sqrt{2}}$
- **2. Control $|1\rangle$:** $\frac{|0110001\dots 1\rangle \pm |1001110\dots 0\rangle}{\sqrt{2}}$

The sign of the relative phases will be determined by the control qubit and the number of target qubits that share the same value of the control, we will call this N_s . If $N_s = 2m$, for integer m , control qubit $|0\rangle$ leads to $+1$ relative phase and control qubit $|1\rangle$ leads to -1 relative phase. On the other hand if $N_s = 2m + 1$, control qubit $|0\rangle$ leads to -1 relative phase and control qubit $|1\rangle$ leads to $+1$ relative phase.

Figure 4.4 summarizes this argument. The states depicted on the equations and the figure are just for illustration purposes. The argument does not loose generality and works for any basis state with N qubits.

So for any basis state for N qubits the $LBS(\pi/2)$ will take it to a superposition of itself and a state with all qubits flipped. These are always maximally entangled states, we can see that by taking the partial traces and realizing they are always equal to $\frac{1}{2}\mathbf{I}$.

For N qubits we are only interested in two basis elements:

$$LBS\left(\frac{\pi}{2}\right)|00\dots 0\rangle = \frac{|0\dots 0\rangle \mp |1\dots 1\rangle}{\sqrt{2}} = |GHZ_{\mp}\rangle, \quad (4-57a)$$

$$LBS\left(\frac{\pi}{2}\right)|11\dots 1\rangle = \frac{|0\dots 0\rangle \pm |1\dots 1\rangle}{\sqrt{2}} = |GHZ_{\pm}\rangle. \quad (4-57b)$$

which is the same result from equations (2-57a) and (2-57b), except the GHZ states can be switched around. This means that the same result for phase

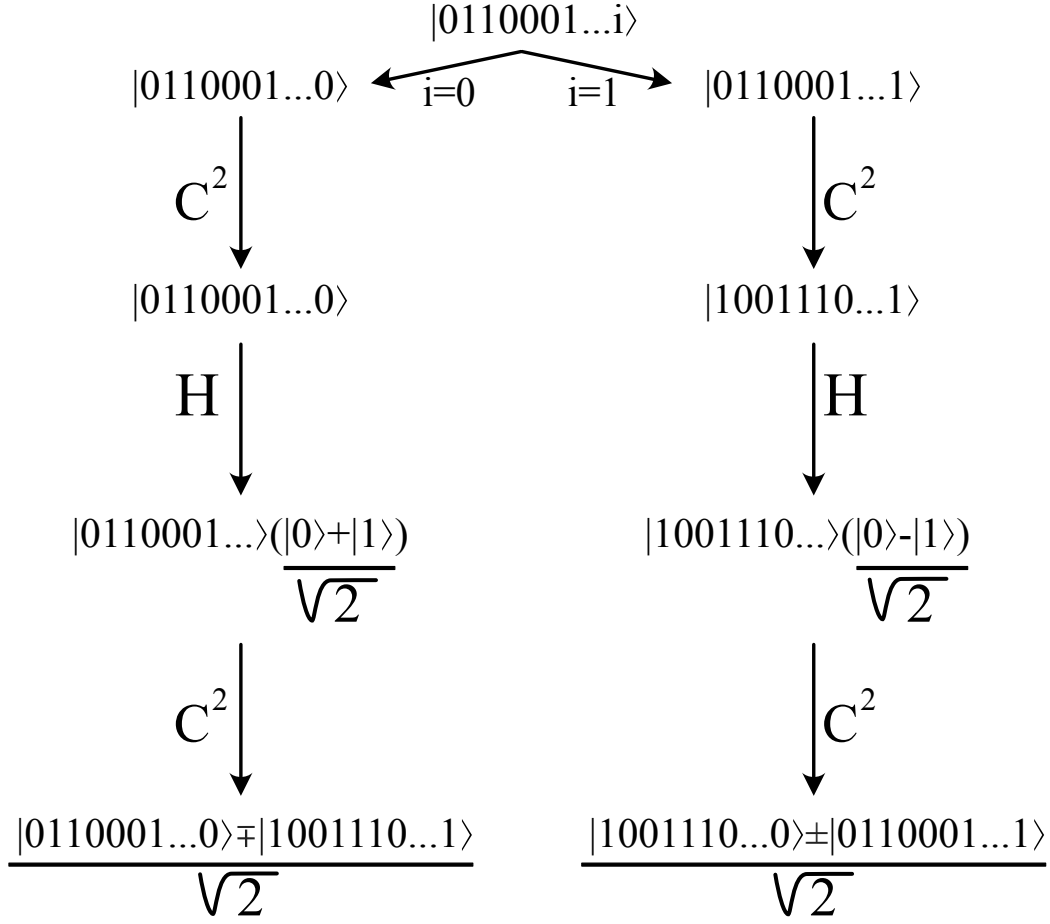


Figure 4.4: This figure summarizes the argument we used to generalize the action of $LBS(\pi/2)$ on the basis states for N qubits. We begin with an arbitrary state filled randomly with 1s and 0s and execute the operations to recreate the $LBS(\pi/2)$. Equations (4-53) tell us how to use $C^2(\pi/2)$ and the action of the Hadamard was explained on section 2.3. The states depicted are just for illustration purposes.

resolution from section 2.1.2 applies here. We have an effective way to achieve the Heisenberg limit in interferometry with fermionic anyons.

For completeness purposes, consider that $LBS(0)$ no longer entangles the basis states:

$$LBS(0)|00\rangle = \frac{|00\rangle + |01\rangle}{\sqrt{2}}, \quad (4-58a)$$

$$LBS(0)|01\rangle = \frac{|00\rangle - |01\rangle}{\sqrt{2}}, \quad (4-58b)$$

$$LBS(0)|10\rangle = \frac{|11\rangle + |10\rangle}{\sqrt{2}}, \quad (4-58c)$$

$$LBS(0)|11\rangle = \frac{|11\rangle - |10\rangle}{\sqrt{2}}. \quad (4-58d)$$

Which also happens for $LBS(\pi)$:

$$LBS(\pi)|00\rangle = \frac{|00\rangle - |01\rangle}{\sqrt{2}}, \quad (4-59a)$$

$$LBS(\pi)|01\rangle = \frac{|00\rangle + |01\rangle}{\sqrt{2}}, \quad (4-59b)$$

$$LBS(\pi)|10\rangle = \frac{|11\rangle - |10\rangle}{\sqrt{2}}, \quad (4-59c)$$

$$LBS(\pi)|11\rangle = \frac{|11\rangle + |10\rangle}{\sqrt{2}}. \quad (4-59d)$$

We can now build our NOON-like interferometer with this new beam-splitter as shown in figure 4.5:

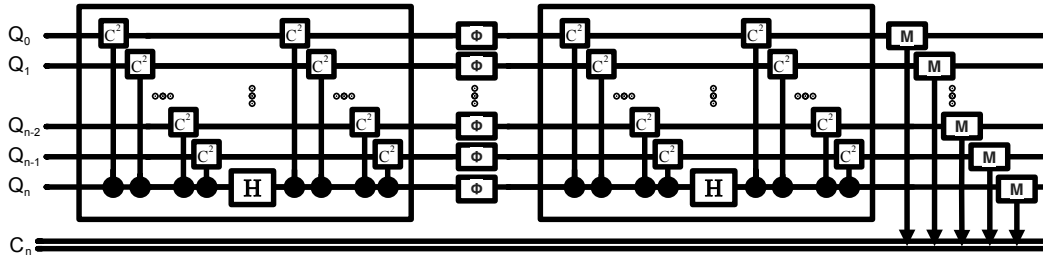


Figure 4.5: New interferometer for N qubits and phase ϕ . $C^2(\pi/2)$ takes the place of the CNOTs. N classical bits are also generated to record the measurements at the end.

Which leads to similar results to what we had in section 2.3: If we apply two LBSs without a phase in the middle we recover the initial state:

$$LBS(\pi/2) \times LBS(\pi/2) = I. \quad (4-60)$$

But, for phase ϕ we get:

$$(LBS(\pi/2))\Phi^N(LBS(\pi/2))|00\dots0\rangle = \frac{1 + e^{Ni\phi}}{2}|00\dots0\rangle \mp \frac{1 - e^{Ni\phi}}{2}|11\dots1\rangle, \quad (4-61a)$$

$$(LBS(\pi/2))\Phi^N(LBS(\pi/2))|11\dots1\rangle = \frac{1 + e^{Ni\phi}}{2}|11\dots1\rangle \pm \frac{1 - e^{Ni\phi}}{2}|00\dots0\rangle, \quad (4-61b)$$

where Φ is a one-qubit phase gate. The same argument for the relative phase after the LBS can be made here, but for these states all target qubits share the value of the control. This way, $N = 2m$, for integer m , leads to -1 phase for control qubit $|0\rangle$ and +1 phase for control qubit $|1\rangle$, and $N = 2m + 1$ leads to +1 phase for control qubit $|0\rangle$ and -1 phase for control qubit $|1\rangle$.

The probabilities are unaffected by the relative phase. For input $|00\dots 0\rangle$ we have:

$$P(|00\dots 0\rangle) = \frac{1 + \cos N\phi}{2}, \quad (4-62a)$$

$$P(|11\dots 1\rangle) = \frac{1 - \cos N\phi}{2}. \quad (4-62b)$$

Again the probabilities are reversed for input $|11\dots 1\rangle$ and we have what we would expect for a NOON state in an interferometer, except for a new relative phase depending on N , which does not affect the probabilities. Once more, to see this remember the mappings we did in sections 2.1.2 and 2.3 respectively: $|N\rangle_{a_i}|0\rangle_{a_j} = |\mathbf{0}\rangle$ and $|0\rangle_{a_i}|N\rangle_{a_j} = |\mathbf{1}\rangle$; $|\mathbf{0}\rangle = |00\dots 0\rangle$ and $|\mathbf{1}\rangle = |11\dots 1\rangle$.

Considering how similar these situations are it would be interesting to repeat the same procedure we have done in Qiskit for the previous interferometer but now on this new circuit with gate $C^2(\pi/2)$.

The same comments from section 2.3 apply and we can switch out the CNOT gates in the code for the new $C^2(\pi/2)$ gate. Again the Transpiler will take care of the job of decomposing the $C^2(\pi/2)$ gate in combinations of gates used by the IBM computer and assigning each logical qubit to a physical one on the device.

We then run the new interferometer for two qubits the same amount of times we did the first one on both the QASM simulator and the IBM Q 5 Yorktown. Afterwards we calculate the probabilities of obtaining state $|00\rangle$ as the final state and exhibit the on figure 4.6. The theoretical prediction remains the same:

$$P(00) = \frac{\cos 2\theta + 1}{2}. \quad (4-63)$$

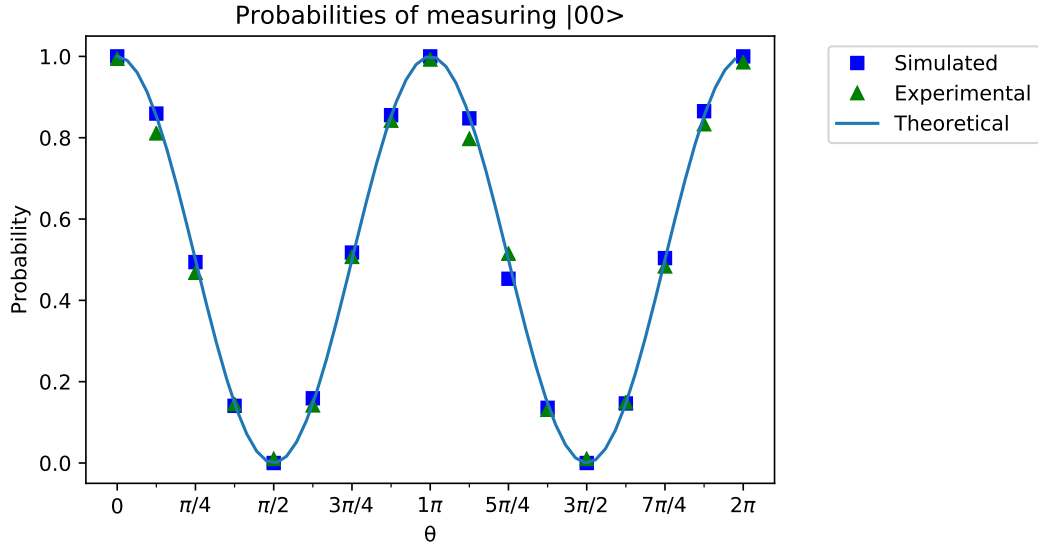


Figure 4.6: Simulated, experimental and theoretical results of the new circuit for two qubits. Probabilities are calculated for one period in steps of $\pi/8$ for θ .

The results are the same from before. This is expected as both the old and the new circuits have depth of six. Let us increase the number of qubits then.

For three qubits the theoretical prediction still remains the same and we can see the plotted results on figure 4.7:

$$P(000) = \frac{\cos 3\theta + 1}{2}. \quad (4-64)$$

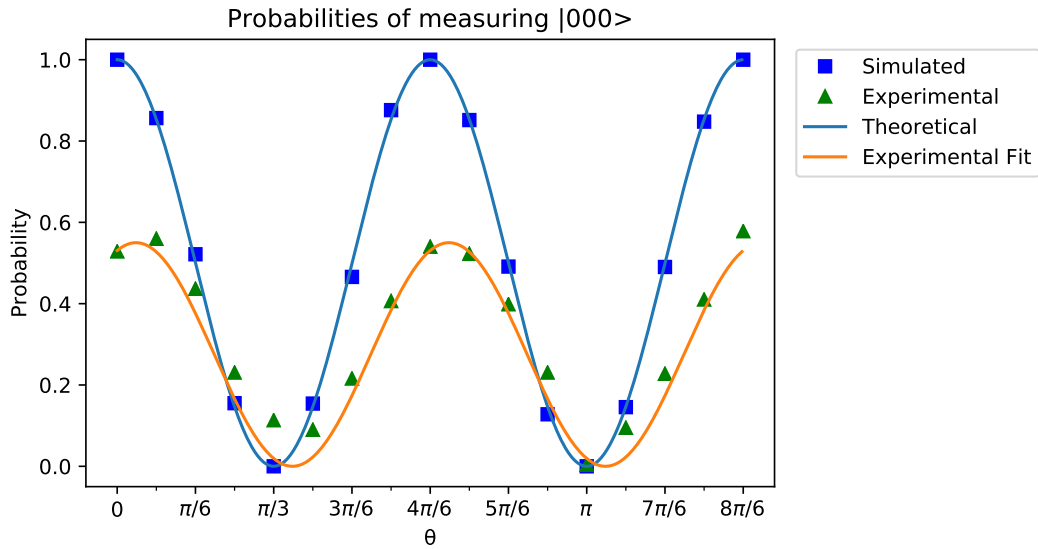


Figure 4.7: Simulated, experimental and theoretical results of the new circuit for three qubits. Probabilities are calculated for one period in steps of $\pi/12$ for θ .

Again our results get considerably worse, this time though they are even worse than the original circuit for three qubits on figure 2.17. This is most likely due to the increase in depth for the new circuit, the original had depth of twelve and this new one has depth seventeen.

The fitted function is:

$$P'(000) = 0.55 \frac{\cos 3(\theta - 0.04\pi) + 1}{2}. \quad (4-65)$$

This means a bigger decrease in amplitude and bigger phase shift. These results are in-between those of figure 2.17 and 2.18, which is expected as this circuit also has a depth value in-between those two.

Finally, let us do it for five qubits. Again the theoretical prediction does not change and the results are plotted on figure 4.8:

$$P(00000) = \frac{\cos 5\theta + 1}{2} \quad (4-66)$$

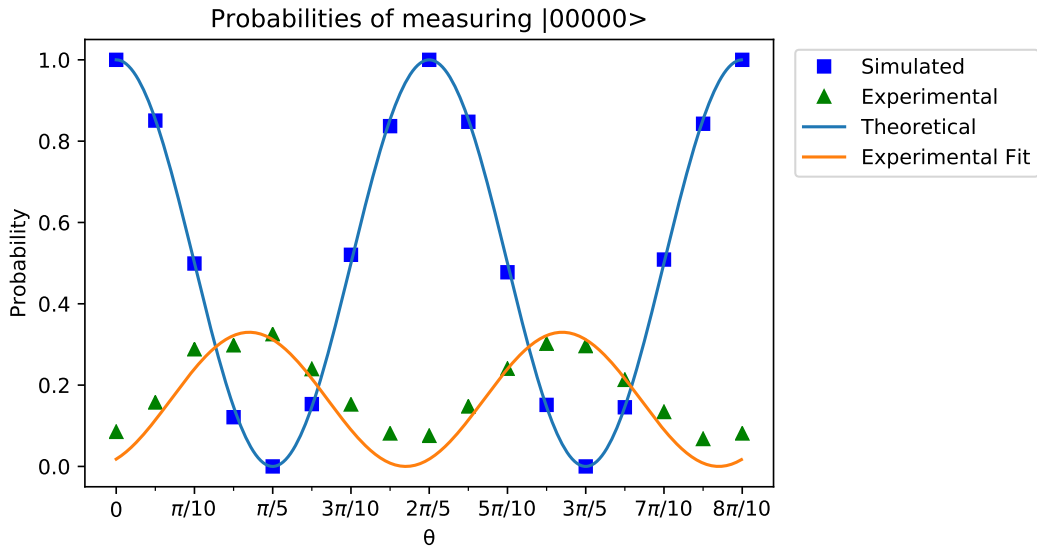


Figure 4.8: Simulated, experimental and theoretical results of the new circuit for five qubits. Probabilities are calculated for one period in steps of $\pi/20$ for θ .

We have an even worse result than that of figure 2.18, again due to the increase in depth. The new circuit has depth of twenty-four versus the twenty depth of the old one which translated to an even lower amplitude and increase in the phase shift. This takes us to the new fitted function:

$$P'(00000) = 0.33 \frac{\cos 5(\theta + 0.23\pi) + 1}{2}. \quad (4-67)$$

As we see this new circuit gives us similar results and any differences should be related to the increased depth due to the fact that $C^2(\pi/2)$ is not part

of the elementary gate set that the IBM computer uses. While not necessarily our main objective we have showed that we can replicate this interferometer with gate $C^2(\pi/2)$ on other quantum computers based on different models and that it in fact produces the same results of the old interferometer on section 2.3 built with CNOT gates. The code used to acquire and plot the data in this section is also available in Appendix A.

The main takeaway we want to end this section on is that we can replicate our NOON-like interferometer without CNOTs by using the operator $C^2(\pi/2)$. This means it is completely plausible to recreate this interferometer using only beamsplitters and phase-shifters for fermionic anyons of exchange phase $\theta = \pi/2$. We have effectively presented a linear optics setup that can produce NOON-like interferometry for any number of anyons.

While for bosons we had that it was non-trivial to produce NOON-like interferometry for $N > 2$ for these fermionic anyons we simply need to scale our setup accordingly. By increasing the number of anyons and the number of optical elements we can achieve NOON-like interferometry in the logical basis for any value of N .

In order to explicitly show it, for two qubits, one must, from figure 4.5:

- 1. Unroll each qubit into an anyon pair.
- 2. Directly substitute the C^2 , Hadamard and phase operators for the appropriate sequences of phase-shifters and beamsplitters presented earlier.

On figure 4.9 we can see the gates and its equivalent setup with beamsplitters and phase shifters:

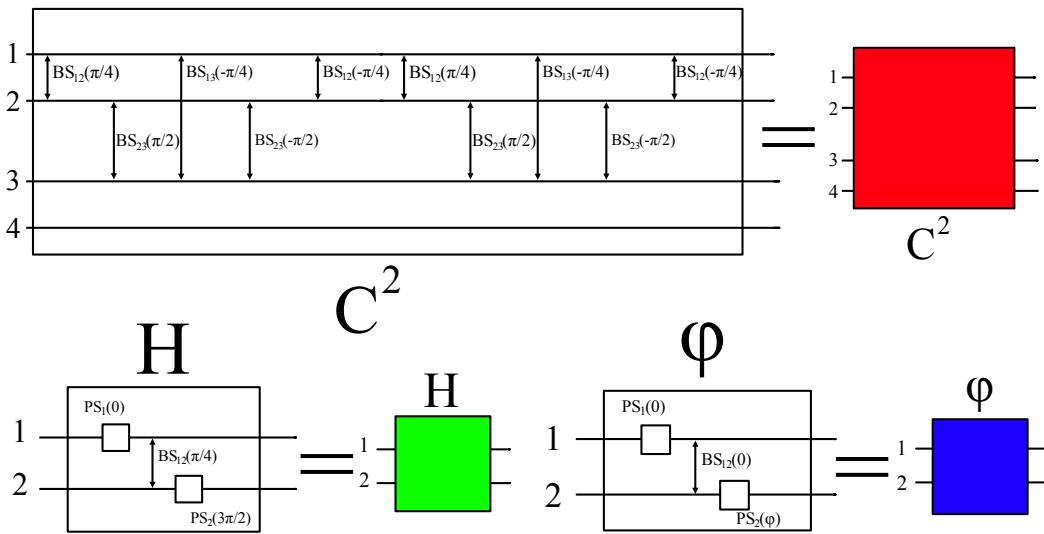


Figure 4.9: The gates used in our NOON-like interferometer for two qubits written in terms of beamsplitters and phase-shifters. We assign colors to each setup in order to be more compact.

Note that to build a Hadamard gate we just need $\alpha = 0$, $\beta = 0$, $\gamma = \pi/4$ and $\delta = 3\pi/2$. A phase gate for phase ϕ can be done by $\alpha = 0$, $\beta = 0$, $\gamma = 0$ and $\delta = \phi$. We can then write the whole setup in figure 4.10 as:

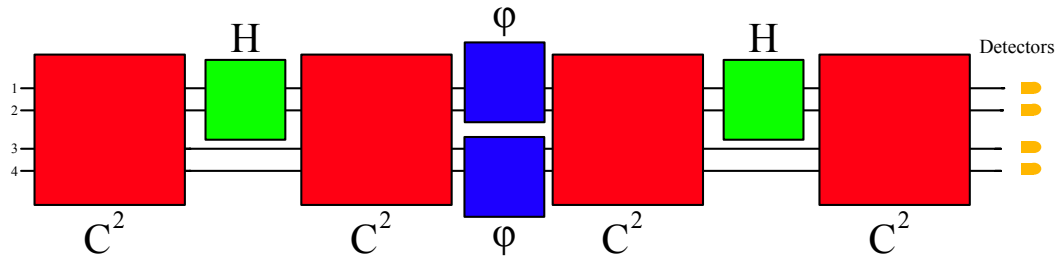


Figure 4.10: The NOON-like interferometer for two qubits written in terms of beamsplitters and phase-shifters using the previously defined color code. Note the detectors at the end to act as measurements.

5

Conclusions and future work

Throughout this work we have presented a review on the most current methods in interferometry as well as a broad perspective on anyons and how they can be exploited to create universal quantum computers. Ultimately we linked those two topics by presenting a computational model that relies on linear optics of anyons and presented an interferometry setup on it.

Firstly, we focused on how particle statistics, either bosonic or fermionic, can affect interferometry experiments while presenting different setups better suited for each scenario. For bosons, we concentrated on the Mach-Zender interferometer and discussed simple interferometry effects such as the Hong-Ou-Mandel. We also took the opportunity to introduce the concept of phase resolution and detailed how it is possible to have better resolution by utilising NOON states to achieve the Heisenberg limit. Furthermore, we presented the Jordan-Schwinger map which allows us to analyze an interferometer through its action on the number operator and easily calculate phase resolution for any setup knowing only the input states.

For fermions, we explained how the Mach-Zender interferometer is no longer viable and how it is impossible to create a NOON state due to the Pauli exclusion principle. To combat this we introduced two new setups, a Ramsey innerferometer and a Non-local interferometer, both of which are capable of producing usable results despite being limited by fermionic statistics.

We ended Chapter 2 by presenting an approach to interferometry in which we treat our setup as a circuit in a quantum computer. We presented a circuit that can perform NOON-like interferometry and not only simulated it but also executed the computation on real devices thanks to the Qiskit software development kit. We concluded that while feasible our circuit cannot scale to a high number of qubits as the amount of errors in the logical operations due to decoherence effects start to grow alongside the depth of the circuit.

Our review of anyons on Chapter 3 began by giving a broad definition of these particles and explaining that our interest in them is due to their unique generalized statistics. We presented them in the light of a familiar effect, the Aharonov-Bohm, and proceeded to describe the quasi-particles in both abelian and non-abelian variants. We introduced the braiding group and the concept of anyon fusion and later generalized it for non-abelian and abelian anyons by introducing the R-matrix and the F-matrix.

The end of the chapter focused on a specific model of non-abelian anyons

that is relevant for quantum computation, Fibonacci anyons. We presented the R-matrix and the F-matrix for such model and explained how it can be exploited for computation by exhibiting an encoding, showing how to obtain a basis of gates capable of universal computation and explaining how measurements would be done on such a computer. Lastly we suggest how to reconstruct our NOON-like interferometer in a quantum computer based on Fibonacci-anyons.

In Chapter 4 we concentrated on uniting the previous two. We presented a computational model based on linear optics for anyons in which we could replicate our NOON-like interferometer with known optical instruments, such as beamsplitters and phase-shifters.

We began by introducing fermionic anyons and their unique commutation relations, afterwards we presented an operator representation of the optical elements that we utilized on chapter 2 and utilized them to describe linear optics for the fermionic anyons. Furthermore, we introduced bosonic anyons and re-described the Hong-Ou-Mandel effect for these new particles.

Lastly, we discussed how to create a universal quantum computer utilizing linear optics for fermionic anyons. In doing so we encountered a new entangling gate we called $C^2(\theta)$ that is dependent on the anyonic exchange phase and with it we managed to construct a scalable version of our NOON-like interferometer that requires only beamsplitters, phase-shifters and anyonic exchange phase $\pi/2$.

Considering the similarities between the original and the new interferometer we saw fit to repeat the same analysis we did with Qiskit on the new one to check that we were in fact executing the same operation. We obtained similar results on both interferometers and attributed any differences to an increase in logical errors introduced due to higher depth.

A good next step would be to generalize our interferometer for any exchange phase. While we have not done so we can safely say that this is possible based on the work done by Bremner et al. [37]. It is possible to rewrite the CNOT gates in the original interferometer with combinations of the $C(\theta)$ and other one qubit gates. Such combinations would depend on the entangling power of $C(\theta)$, which is to say that they would depend on the exchange phase θ .

Another idea would be to look at how we can expand on section 4.3 and suggest a new computational model but now based on bosonic anyons. This might open up the possibilities of working with the "standard" NOON state $\frac{|N,0\rangle + e^{iN\theta}|0,N\rangle}{\sqrt{2}}$ as we would no longer be limited by the Pauli exclusion principle.

6

References

- [1] MICHELSON, A.; MORLEY, E.. **On the relative motion of the earth and the luminiferous ether.** American Journal of Science, (203):333–345, 1887. 1
- [2] THE LIGO SCIENTIFIC COLLABORATION. **A gravitational wave observatory operating beyond the quantum shot-noise limit.** Nature Physics, 7(12):962–965, Dec. 2011. 1
- [3] KOK, P.; LEE, H. ; DOWLING, J. P.. **Creation of large-photon-number path entanglement conditioned on photodetection.** Physical Review A, 65(5), Apr 2002. 1
- [4] WILCZEK, F.. **Magnetic flux, angular momentum, and statistics.** Phys. Rev. Lett., 48:1144–1146, Apr 1982. 1, 3.0.1
- [5] KITAEV, A. Y.. **Fault-tolerant quantum computation by anyons.** Annals of Physics, 303(1):2–30, Jan. 2003. arXiv: quant-ph/9707021. 1, 2.3.1
- [6] NAYAK, C.; SIMON, S. H.; STERN, A.; FREEDMAN, M. ; DAS SARMA, S.. **Non-abelian anyons and topological quantum computation.** Reviews of Modern Physics, 80(3):1083–1159, Sep 2008. 1, 3.3, 3.3, 3.3
- [7] TOSTA, A. D. C.; BROD, D. J. ; GALVÃO, E. F.. **Quantum computation from fermionic anyons on a one-dimensional lattice.** Physical Review A, 99(6), Jun 2019. 1, 4, 4.4, 4.4.2, 4.4.2
- [8] SCHWABL, F.. **Advanced Quantum Mechanics.** Springer, Berlin, 4th ed. 2008 edition edition, Sept. 2008. 2.1, 2.2, 2.2
- [9] ERNST DORN, P.-T. R. G.. **Zeitschrift für Instrumentenkunde.** Berlin [etc.], 1881. 2.1.1
- [10] HONG, C. K.; OU, Z. Y. ; MANDEL, L.. **Measurement of subpicosecond time intervals between two photons by interference.** Phys. Rev. Lett., 59:2044–2046, Nov 1987. 2.1.1
- [11] AASI, J.; ABADIE, J.; ABBOTT, B. P.; ABBOTT, R.; ABBOTT, T. D.; ABERNATHY, M. R.; ADAMS, C.; ADAMS, T.; ADDESSO, P.; ADHIKARI, R. X. ; ET AL.. **Enhanced sensitivity of the ligo gravitational**

- wave detector by using squeezed states of light. *Nature Photonics*, 7(8):613–619, Jul 2013. 2.1.1, 2.1.2
- [12] RISTI, S.. **Flow visualization techniques in wind tunnels – optical methods (Part II)**. 2008. 2.1.1
- [13] HARILAL, S. S.; TILLACK, M. S.. **Laser plasma density measurements using interferometry**. 2004. 2.1.1
- [14] GERRY, C.; KNIGHT, P.. **Introductory Quantum Optics**. Cambridge University Press, Cambridge, UK ; New York, 1 edition edition, Nov. 2004. 2.1.2
- [15] PRESKILL, J.. **Lecture Notes for Physics 219: Quantum Computation**. 2004. 2.1.2, 3, 3.0.1, 3.0.1, 3.2.1, 3.2.2, 3.3, 3.3, 4.5
- [16] AFEK, I.; AMBAR, O. ; SILBERBERG, Y.. **High-noon states by mixing quantum and classical light**. *Science*, 328(5980):879–881, 2010. 2.1.2
- [17] RAMSEY, N. F.. **A Molecular Beam Resonance Method with Separated Oscillating Fields**. *Physical Review*, 78(6):695–699, June 1950. 2.2.1
- [18] DEMKOWICZ-DOBRZAŃSKI, R.; JARZYNA, M. ; KOŁODYŃSKI, J.. **Chapter Four - Quantum Limits in Optical Interferometry**. In: Wolf, E., editor, *PROGRESS IN Optics*, volumen 60, p. 345–435. Elsevier, Jan. 2015. 2.2.1
- [19] DASENBROOK, D.; BOWLES, J.; BRASK, J. B.; HOFER, P. P.; FLINDT, C. ; BRUNNER, N.. **Single-electron entanglement and nonlocality**. *New Journal of Physics*, 18(4):043036, Apr. 2016. arXiv: 1511.04450. 2.2.2, 2.2.2, 2.2.2
- [20] IBM-Q-TEAM. **Qiskit API documentation — Qiskit 0.14.1 documentation**. Retrieved from <https://qiskit.org/documentation/>. 2.3.1
- [21] CROSS, A. W.; BISHOP, L. S.; SMOLIN, J. A. ; GAMBETTA, J. M.. **Open Quantum Assembly Language**. arXiv:1707.03429 [quant-ph], July 2017. arXiv: 1707.03429. 2.3.1
- [22] IBM-Q-TEAM. **Ibm q 5 yorktown backend specification v1.1.0**, 2018. Retrieved from <https://quantum-computing.ibm.com>. (document), 2.3.1, 2.13

- [23] KITAEV, A. Y.; SHEN, A.; VYALYI, M. N. ; VYALYI, M. N.. **Classical and Quantum Computation**. American Mathematical Society, 2002. Google-Books-ID: qYHTvHPvmG8C. 2.3.1, 3.3
- [24] ASFAW, A.; BELLO, L.; BEN-HAIM, Y.; BRAVYI, S.; CAPELLUTO, L.; VAZQUEZ, A. C.; CERONI, J.; HARKINS, F.; GAMBETTA, J.; GARION, S.; GIL, L.; GONZALEZ, S. D. L. P.; MCKAY, D.; MINEV, Z.; NATION, P.; PHAN, A.; RATTEW, A.; SCHAEFER, J.; SHABANI, J.; SMOLIN, J.; TEMME, K.; TOD, M. ; WOOTTON., J.. **Learn quantum computation using qiskit**, 2020. 2.3.1
- [25] NIELSEN, M. A.; CHUANG, I. L.. **Quantum Computation and Quantum Information: 10th Anniversary Edition**. Cambridge University Press, USA, 10th edition, 2011. 2.3.1, 4.5
- [26] AHARONOV, Y.; BOHM, D.. **Significance of electromagnetic potentials in the quantum theory**. Phys. Rev., 115:485–491, Aug 1959. 3.0.1
- [27] WILCZEK, F.. **Quantum mechanics of fractional-spin particles**. Phys. Rev. Lett., 49:957–959, Oct 1982. 3.1
- [28] KHARE, A.. **Fractional Statistics and Quantum Theory**. World Scientific, 2005. 3.1
- [29] HORMOZI, L.; ZIKOS, G.; BONESTEEL, N. E. ; SIMON, S. H.. **Topological quantum compiling**. Physical Review B, 75(16), Apr 2007. 3.3, 3.3
- [30] BONESTEEL, N. E.; HORMOZI, L.; ZIKOS, G. ; SIMON, S. H.. **Braid topologies for quantum computation**. Physical Review Letters, 95(14), Sep 2005. (document), 3.3, 3.3, 3.6
- [31] FREEDMAN, M. H.; LARSEN, M. ; WANG, Z.. **A Modular Functor Which is Universal for Quantum Computation**. Communications in Mathematical Physics, 227(3):605–622, June 2002. 3.3, 3.3, 3.3
- [33] DAWSON, C. M.; NIELSEN, M. A.. **The solovay-kitaev algorithm**. Quantum Info. Comput., 6(1):81–95, Jan. 2006. 3.3
- [34] FIELD, B.; SIMULA, T.. **Introduction to topological quantum computation with non-abelian anyons**. Quantum Science and Technology, 3(4):045004, Jul 2018. (document), 3.7

- [35] TOSTA, A. D. C.; BROD, D. J. ; GALVÃO, E. F.. **Universal quantum computing with one-dimensional bosonic anyons.** In preparation., Oct 2019. 4.3
- [36] ZANARDI, P.; ZALKA, C. ; FAORO, L.. **Entangling power of quantum evolutions.** Physical Review A, 62(3), Aug 2000. 4.4.2
- [37] BREMNER, M. J.; DAWSON, C. M.; DODD, J. L.; GILCHRIST, A.; HARROW, A. W.; MORTIMER, D.; NIELSEN, M. A. ; OSBORNE, T. J.. **Practical scheme for quantum computation with any two-qubit entangling gate.** Physical Review Letters, 89(24), Nov 2002. 4.4.2, 4.5, 5

7

Appendix A: Code used to implement quantum circuits

In sections 2.3 and 4.5 we presented a quantum circuits that implements our NOON-like logical interferometer and proceeded to implement them on simulations and real devices utilizing the Python programming language and the Qiskit software development kit. In this appendix we've collected the code for doing so with some commentary. Note that the code here is for the circuits with five qubits.

First, we begin by loading the necessary modules, setting up the IBM account and initializing global variables such as the number of shots given to the circuits and the arrays where the probabilities of the results will be recorded:

```
1  #Importing necessary modules
2  import numpy as np
3  import matplotlib.pyplot as plt
4  from qiskit import *
5  from qiskit import Aer
6  from qiskit.visualization import plot_histogram, plot_state_city,
   ↪  plot_circuit_layout
7  from math import pi
8  import matplotlib.ticker as tck
9  %matplotlib inline #This is only necessary when working on a Jupyter
   ↪  Notebook.
10 #Loading IBM account and setting up backends
11 IBMQ.load_account()
12 provider = IBMQ.get_provider(group='open')
13 backend_sim = Aer.get_backend('qasm_simulator')
14 backend_exp = provider.get_backend('ibmqx2')
15 #Defining the amount of runs a circuit will undergo.
16 sh=1024
17 #Setting up arrays to record data from runs and
18 #theoretical predictions for plotting.
19 y_exp=np.array([])
20 y_sim=np.array([])
21 x=np.arange(0,(16.5)*pi/(4*5),pi/(4*5))
22 x_th=np.arange(0,4*pi/5,0.01)
23 y_th=((np.cos(x_th*5))+1)/2
```

Next, it's useful to define functions that implement the elements we want in our circuit. The beamsplitter:

```

1 def BeamS(q,qr,c,cr,f):
2     circ=QuantumCircuit(qr,cr)
3     for i in range(q-1):
4         circ.cx(0,i+1)
5     circ.h(0)
6     for i in range(q-1):
7         circ.cx(0,i+1)
8     circ=f+circ
9     return circ
10 # The function receives the amount of qubits, a qubit register, classical
    ↪ bits, a classical bit register and a circuit f to include the BS on.
    ↪ It returns a new circuit with the BS attached.
```

The phasegates:

```

1 def phase(q,qr,c,cr,ph,f):
2     circ=QuantumCircuit(qr,cr)
3     for i in range(q):
4         circ.u1(ph,i)
5     return f+circ
6 # The function receives the amount of qubits, a qubit register, classical
    ↪ bits, a classical bit register, a value for the phase and a circuit f
    ↪ to include the phasegate on. It returns a new circuit with the
    ↪ phasegate attached.
```

The measurements:

```

1 def measu(qr,cr,f):
2     meas=QuantumCircuit(qr,cr)
3     meas.barrier(qr[:])
4     meas.measure(qr[:],cr[:])
5     qc=f+meas
6     return qc
7 # The function receives, a qubit register, a classical bit register and a
    ↪ circuit f to include the measurements on. It returns a new circuit
    ↪ with the measurements attached.
```

And, finally, the logical interferometer:

```

1 def MZI(q,qr,c,cr,ph):
2     MZ=QuantumCircuit(qr,cr)
3     #initialize state:
4     #Uncomment the next three lines to initialize state|1,...,1>
5     #vec=np.zeros(2**q)
6     #vec[(2**q)-1]=1
7     #MZ.initialize(vec, [qr[:]])
8     #BeamSplitter
9     MZ=BeamS(q,qr,c,cr,MZ)
10    #phase
11    MZ=phase(q,qr,c,cr,ph,MZ)
12    #BeamSplitter
13    MZ=BeamS(q,qr,c,cr,MZ)
14    #measurements
15    MZ=measu(qr,cr,MZ)
16    return MZ
17 # The function receives the amount of qubits, a qubit register, classical
   ↪ bits, a classical bit register and a value for the phase. It returns a
   ↪ circuit with our logical interferometer attached.

```

Now that we have defined the function that will build the interferometer we must simply call them to create one with the desired parameters:

```

1 # Define the amount of qubits and classica bits on the circuit
2 q=5
3 c=5
4 #Create the registers
5 qr=QuantumRegister(q)
6 cr=ClassicalRegister(c)
7 #Create the circuit with phase given by elements of array x
8 Mz=MZI(q,qr,c,cr,x[1])
9 #Draw the circuit and check it is correct.
10 Mz.draw()

```

Then we can simulate our circuit:

```

1  #Simulation for phase (Pi/4)
2  #Create circuit
3  MZ=MZI(q,q,c,cr,x[1])
4  #Execute simulation on appropriate backend
5  job_sim = execute(MZ, backend_sim, shots=sh)
6  result_sim=job_sim.result()
7  counts_sim=result_sim.get_counts(MZ)
8  #Exhibit and record results in the appropriate array.
9  y_sim=np.append(y_sim,[counts_sim['00000']/sh])
10 plot_histogram(counts_sim)

```

Also, we run it on the real device:

```

1  #Experimental for phase (Pi/4)
2  #Utilize the transpiler to get the most efficient
3  #representation of the circuit
4  MZ_tp = transpile(MZ, backend=backend_exp, optimization_level=3,
    ↪  initial_layout=[2,0,1,3,4])
5  #check new depth
6  print('Depth:', MZ_tp.depth())
7  #check mapping of real and logical qubits
8  plot_circuit_layout(MZ_tp, backend_exp)
9  #Run the job on the real device and get the job ID
10 job_exp= execute(MZ_tp, backend=backend_exp)
11 id_job=job_exp.job_id()
12 job_exp = backend_exp.retrieve_job(id_job)
13 #Get the results. Save them to the proper array. Plot both experimental
    ↪ and simulation results.
14 result_exp=job_exp.result()
15 counts_exp=result_exp.get_counts()
16 y_exp=np.append(y_exp,[counts_exp['00000']/sh])
17 plot_histogram([counts_sim,counts_exp], legend=['sim', 'exp'])

```

Now we have to repeat this process for every point of data we want to get and finally plot them from the arrays that we are dumping the data. We can automate this loop by doing:

```

1  #Create empty list of circuits.
2  circuits=[]
3  #Create circuits for varying phase and append to circuit list.
4  for i in range(len(x)): #
5      q=5
6      c=5
7      qr=QuantumRegister(q)
8      cr=ClassicalRegister(c)
9      MZ=MZI(q,qr,c,cr,x[i])
10     circuits.append(MZ)
11
12 #Execute the circuits on the list
13 job_sim=execute(circuits,backend=backend_sim, shots=sh)
14 result_sim=job_sim.result()
15
16 #Append results to an array with the probabilities
17 for i in range(len(x)):
18     counts_sim=result_sim.get_counts(circuits[i])
19     try:
20         counts_sim['00000']
21     except KeyError:
22         y_sim=np.append(y_sim,[0])
23     else:
24         y_sim=np.append(y_sim,[counts_sim['00000']/sh]) #Probabilities are
        ↪ give by counts/shots

```

For simulations. And for real experiments:

```

1  #Create empty list of circuits.
2  circuits=[]
3  #Create circuits for varying phase and append to circuit list.
4  for i in range(len(x)): #
5      q=5
6      c=5
7      qr=QuantumRegister(q)
8      cr=ClassicalRegister(c)
9      MZ=MZI(q,qr,c,cr,x[i])
10     circuits.append(MZ)
11 #Transpile every circuit on the list and append to new list
12 circuits_tp=[]
13 for i in range(17):
14     circuits_tp.append( transpile(circuits[i], backend=backend_exp,
        ↪ optimization_level=3, initial_layout=[2,0,1,3,4]))

```



```

15
16 #Execute the list of circuits on the real device
17 job_exp= execute(circuits_tp, backend=backend_exp)
18 #Exhibit job id for retrieving results later
19 job_exp.job_id()
20 #Get results and append them to the appropriate array
21 job_exp = backend_exp.retrieve_job('5e88f6fb063ef70019f0cad4')
22 result_exp=job_exp.result()
23
24 for i in range(len(x)):
25     counts_exp=result_exp.get_counts(i)
26     try:
27         counts_exp['00000']
28     except KeyError:
29         y_exp=np.append(y_exp, [0])
30     else:
31         y_exp=np.append(y_exp, [counts_exp['00000']/sh])

```

And finally we plot the data:

```

1 fig, ax = plt.subplots()
2 #Define the fitting function for the experimental points
3 x_fit=np.arange(0,2*pi/5,0.01)
4 y_fit = 0.65*(np.sin((x_th*5)-(pi/1.6))+1)/2
5 #Plot all the results and the theoretical predication.
6 ax.plot(x,y_sim, 'bs', x,y_exp, 'g^', x_th,y_th,x_th,y_fit)
7 plt.xlabel('$\Theta$')
8 plt.ylabel('Probability')
9 plt.title('Probabilities of measuring |00000>')
10 plt.legend(['Simulated', 'Experimental', 'Theoretical', 'Experimental
    ↪ Fit'],loc=1)

```

The same process has to be repeated for 2 and 3 qubits with the appropriate changes and at the end we get the graphs from section 2.3.

On the section 2.3 we also execute a procedure of measurement error mitigation. The code for doing so follows:

```

1 #Load the necessary modules.
2 from qiskit.ignis.mitigation.measurement import (complete_meas_cal,
    ↪ CompleteMeasFitter)
3 #Create a list with the calibration circuits that represents the basis
    ↪ states.
4 cal_circuits,state_labels=complete_meas_cal(qr=qr,
    ↪ circlabel='measurement_calibration')
5 #Execute the calibration and exhibit the job id.
6 cal_job=execute(cal_circuits, backend=backend_exp,
    ↪ shots=8192,optimization_level=0)

```

```

7 cal_job.job_id()
8 #Use the results to build the change of basis matrix and a filter to apply
  ↪ to the noisy results
9 cal_job = backend_exp.retrieve_job('5e6a5b0dd00f3c00112df76a')
10 cal_results=cal_job.result()
11 meas_fitter=CompleteMeasFitter(cal_results,state_labels)
12 meas_filter=meas_fitter.filter
13 #Retrieve the noisy results
14 job_exp = backend_exp.retrieve_job('5e6a5adce987fe00114c4de5')
15 result_exp=job_exp.result()
16 #Apply the filter
17 mitigated_result=meas_filter.apply(result_exp)
18 #Plot a histogram with both counts for comparison
19 counts=result_exp.get_counts()
20 mitigated_counts=mitigated_result.get_counts()
21 fig, ax=plt.subplots()
22 fig=plot_histogram([counts_sim,counts,mitigated_counts])

```

Finally the last thing we do on Qiskit is run the same interferometer for a different beamsplitter, one that uses C^2 instead of CNOT. So we just change the function that attaches the beamsplitter to the circuit and repeat the rest of the code:

```

1 def C_op(ph): #Set a function that returns C^2 for a given phase
2     C = Operator([[exp(-1j*pi/4)), 0, 0, 0], [0,
  ↪ (1-1j*cos(ph))/(sqrt(2)), 0, (1j*sin(ph))/(sqrt(2))], [0,
  ↪ 0,(exp(1j*pi/4)) , 0], [0, (1j*sin(ph))/(sqrt(2)),0,
  ↪ (1+1j*cos(ph))/(sqrt(2))]])
3     C2=C.power(2)
4     return C2
5
6 C2=C_op(pi/2) #Set the phase we want
7
8 def BeamS(q,qr,c,cr,f):
9     circ=QuantumCircuit(qr,cr)
10    for i in range(q-1):
11        circ.unitary(C2, [0, i+1], label='C2')
12    circ.h(0)
13    for i in range(q-1):
14        circ.unitary(C2, [0, i+1], label='C2')
15    circ=f+circ
16    return circ
17 # The function receives the amount of qubits, a qubit register, classical
  ↪ bits, a classical bit register and a circuit f to include the BS on.
  ↪ It returns a new circuit with the BS attached.

```

All the code on this document was run on the following version of Qiskit:

Qiskit Software	Version
Qiskit	0.17.0
Terra	0.12.0
Aer	0.4.1
Ignis	0.2.0
Aqua	0.6.5
IBM Q Provider	0.6.0

We can recover this information by inputting this command in a Jupyter notebook:

```
%qiskit_version_table
```